THE UNIVERSITY OF CHICAGO

INHIBITION OF FOXP3 BY STAPLED ALPHA-HELICAL PEPTIDES DAMPENS REGULATORY T CELL FUNCTION

A DISSERTATION SUBMITTED TO
THE FACULTY OF THE DIVISION OF THE BIOLOGICAL SCIENCES
AND THE PRITZKER SCHOOL OF MEDICINE
IN CANDIDACY FOR THE DEGREE OF
DOCTOR OF PHILOSOPHY

COMMITTEE ON CANCER BIOLOGY

BY
KATRINA MAXCY HAWLEY

CHICAGO, ILLINOIS
AUGUST 2022

To my family, given and chosen. Thank you for all of your support.

“The future belongs to those who believe in the beauty of their dreams.”

- Eleanor Roosevelt

TABLE OF CONTENTS

LIST OF FIGURES

ACKNOWLEDGMENTS

The list of people who have inspired me, shared their wealth of knowledge, and have contributed not only to the completion of this dissertation but also to shaping my worldview, is long. I'm endlessly grateful for the supportive village I've been fortunate enough to build and know that my future is bright with their continued support.

First, I'd like to thank my PI and mentor, Dr. James LaBelle. Over the years, James and I have navigated the peaks and valleys of graduate school together. James's positive attitude and boundless energy created an environment where I could thrive and his passion for new technologies and impactful science have left an indelible mark on how I will develop my own projects in the future. I'm one of the lucky ones to have you in my corner. I would also like to thank my thesis committee: Dr. Marisa Alegre, Dr. Fed Bernal, Dr. Fotini Gounari, and Dr. Justin Kline. I can't put into words just how much I've appreciated and enjoyed our meetings. I have such respect for each and every one of you and will be forever grateful for the way your unique perspectives have influenced my growth as a scientist, and how your mentorship has been instrumental in getting me to the next stages of my career. I'd also like to acknowledge the leadership and administrators in the Committee on Cancer Biology and in the Department of Pediatrics for running their respective programs smoothly, giving me the time and space needed to dedicate myself to my work. Many thanks go to the staff of the Flow Cytometry Core Facility, Microscopy Core Facility, and Biophysics Core Facility for their guidance and help in collecting and analyzing data. Finally, thank you to my past mentors, especially Dr. Thomas Shenk, Dr. David Sykes, and Dr. David Scadden for inspiring me and believing in me for all these years. It was under your guidance that I began down this path with vigor; I'm so excited to see what the future holds and look forward to our paths crossing again sometime soon.

I'd like to acknowledge all past and present members of the LaBelle Lab. It has been a true pleasure to work with each of you, and I value the friendships built along the way.

A very special thank you goes to fellow CCB graduate student Sravya Tumuluru, who has been there through thick and thin and has always been both a sounding board and at the ready with funny diversions, whichever the situation warranted. I'm incredibly grateful for our friendship; it's rare to find someone that you feel such kinship with and trust implicitly, and I'm grateful that we were able to share this experience together. To my friends outside of the maroon bubble - Olivia Huang, Kelsey Janke, and Lariah Edwards, thank you for always being only a phone call away.

I owe a huge debt of gratitude to my family. My parents instilled a deep curiosity in science from an early age - thank you for looking in microscopes with me and for helping me procure all kinds of hard to find supplies for science fair projects. In addition to fostering inquisitiveness, my family has been there for every major milestone and have always shown such unconditional love whenever things have felt just out of reach and I've needed that love most. Life brings along with it many twists and turns - I'm grateful to have such a strong support system; you've given me the courage to pursue my every dream. Thank you to the extended Hawley/Austin family for loving me like one of your own and for sharing your big, jovial family with me. Finally, I would like to give a very special thank you to my husband, Andrew, for being my everything. He has always been there with a ready ear and pep talk, and most importantly, truly believes in me more strongly at times than I have believed in myself. Together we can accomplish anything and will certainly have so much fun along the way. I can't wait to see what the future has in store for both of us. This past year has been particularly exciting as we've awaited and welcomed our daughter, Celine. Being a mother has brought a whole new sense of purpose and determination to my life; I want to do my part to make the world a better place in every way that I can. As our little family soon ventures to a new city, I remain humbled by the support and friendships we've formed in Chicago and will hold them close for years to come.

ABBREVIATIONS

ADCC: Antibody-dependent cellular cytotoxicity; ADMET: Adsorption, distribution, metabolism, excretion, and toxicity; AKT: Protein kinase B; AML1: Acute myeloid leukemia protein 1; AP-1: Activator protein 1; APC: Antigen presenting cell; AR: Androgen receptor; ATP: Adenosine triphosphate; ATRA: All-trans retinoic acid; BCR: B cell receptor; CCL28: Chemokine ligand 28; CCR4: Chemokine receptor 4; CCR5: Chemokine receptor 5; CCR8: Chemokine receptor 8; CD25: High-affinity IL-2 receptor; CD127: IL-7 receptor alpha-chain; CNS2: Conserved non-coding DNA sequence 2; Co-IP: Co-immunoprecipitation; CTLA-4: Cytotoxic T lympocyte-associated protein 4; DC: Dendritic cell; DCE: 1,2-dichloroethane; DCM: Dichloromethane; DIPEA: N,N-Diisopropylethylamine; DLBCL: Diffuse large B cell lymphoma; DMEM: Dulbecco's modified eagle media; DMF: N,N-Dimethylformamide; DMSO: Dimethyl sulfoxide; EMSA: Electrophoretic mobility shift assay; ER: Estrogen receptor; FBDD: Fragment-based drug discovery; FITC: Fluorescein isothiocyanate; FOXP1: Forkhead box P1; FOXP3: Forkhead box P3; FPA: Fluorescence polarization analysis; GITR: Glucocorticoid-induced TNF receptor-related protein; GR: Glucocorticoid receptor; HATU: 1-[Bis(dimethylamino)methylene]-1H-1,2,3-triazolo[4,5-b]pyridinium 3-oxide hexafluorophosphate; HIF1α: Hypoxia inducible factor 1 subunit alpha; ICB: Immune checkpoint blockade; ICOS: Inducible T cell co-stimulator; IDO: Indoleamine-2,3-dioxygenase; IFNγ: Interferon gamma; IPEX: Immune dysregulation, polyendocrinopathy, enteropathy, X-linked; IL-2: Interleukin 2; IL-7: Interleukin 7; IL-10: Interleukin 10; IL-15: Interleukin 15; IL-17: Interleukin 17; IL-35: Interleukin 35; IRF4: Interferon regulatory factor 4; ITAM: Immunoreceptor tyrosine-based activation motif; ITC: Isothermal titration calorimetry; iTreg: Induced Treg; LAG-3: Lymphocyte-activation gene 3; LBD: Ligand binding domain; LDH: Lactate dehydrogenase; LZCC: Leucine zipper coiled-coil; LZDD: Leucine zipper dimerization domain; mAb: Monoclonal antibody; MDM2: Mouse double minute 2 homolog; MDMX: Mouse double minute X homolog; MHCI: Major histocompatibility complex class

I; MHCII: Major histocompatibility complex class II; MSI-H: Microsatellite instability-high; mTOR: Mammalian target of rapamycin; NFAT: Nuclear factor of activated T cells; NMP: N-Methyl-2-pyrrolidone; NMR: Nuclear magnetic resonance; nTreg: Natural Treg; PD-1: Programmed death protein 1; PD-L1: Programmed death ligand 1; PI3K: Phosphoinositide 3-kinase; PMA: Phorbol myristate acetate; PML: Promyelocytic leukemia protein; PPARγ: Peroxisome proliferator-activated receptor gamma; PPI: Protein-protein interaction; PROTAC: Proteolysis-targeting chimera; PRR: Pattern recognition receptor; pTreg: Peripherally-induced Treg; RORα: Retinoic acid receptor-related orphan receptor alpha; RORγT: Retinoic acid receptor-related orphan receptor gamma T; SAH: Stapled alpha-helical peptide; SPR: Surface plasmon resonance; TAT: Transactivating activator of transcription; TBET: T-box expressed in T cells; Tcon: Conventional T cell; TCR: T cell receptor; TFA: trifluoroacetic acid; TGFβ: Transforming growth factor beta; Th1: T helper cell type 1; Th2: T helper cell type 2; Th17: T helper cell type 17; TIGIT: T cell immunoreceptor with Ig and ITIM domains; TIM-3: T cell immunoglobulin and mucin protein 3; TMB: Tumor mutational burden; TME: Tumor microenvironment; Treg: Regulatory T cell; TSLP: Thymic stromal lymphopoietin; VEGF: Vascular endothelial growth factor

ABSTRACT

Despite continuing advances in the development of novel cellular-, antibody-, and chemotherapeutic-based strategies to enhance immune reactivity, the presence of regulatory T cells (Tregs) remains a complicating factor for their clinical efficacy. To overcome dosing limitations and off-target effects from antibody-based Treg deletional strategies, we investigated the ability of hydrocarbon stapled α-helical (SAH) peptides to target Forkhead box P3 (FOXP3), the master transcription factor regulator of Treg development, maintenance, and suppressive function. Using the crystal structure of FOXP3 homodimers as a guide, we developed SAHs in the likeness of a portion of the native FOXP3 antiparallel coiled-coil homodimerization domain (SAH-FOXP3s) to block this key FOXP3 protein-protein interaction (PPI) through molecular mimicry. We show that lead SAH-FOXP3s bind FOXP3, are cell permeable, non-toxic to T cells, induce dose-dependent transcript and protein level alterations of FOXP3 target genes, impede Treg function, and lead to Treg gene expression changes *in vivo* consistent with FOXP3 dysfunction.

CHAPTER 1

INTRODUCTION

1.1 Project context

The human immune system must be able to perform the opposing functions of protecting the host from a wide range of pathogens while also curtailing excessive inflammation to prevent tissue damage in a context-dependent manner (Figure 1.1). Regulatory T cells (Tregs) play a crucial role in maintaining this immune homeostasis by exerting a variety of suppressive mechanisms that are capable of attenuating effector T cell responses and activity. This is most valuable in the context of auto-antigens and in preventing autoimmunity, but also serves a function in conditions where there is chronic pathogen exposure and inflammation that could ultimately prove deleterious to the host. Tregs are typically defined by their expression of the transcription factor, Forkhead box P3 (FOXP3), considered to be a master regulator of Treg differentiation, maintenance, and function. While Tregs' primary role in the maintenance of dominant tolerance is necessary and critical, many have identified that the suppressive function of Tregs may have the unfortunate byproduct of impeding an effective immune response in some malignancies, including cancers. Further complicating our understanding of this population, Tregs are highly heterogenous, making it crucial that continued efforts are made toward understanding their mechanistic underpinnings in order to identify how best to therapeutically target this population for treatment of a wide range of malignancies.

1.2 Primer of adaptive immunity

The immune system consists of two branches that work cohesively to protect the host from infectious pathogens: the innate immune system and the adaptive immune system. The innate immune system typically is considered a "first responder" as it often exerts its func-

tions on the order of hours, identifying and responding to disruptions to immune homeostasis largely based on pattern recognition of foreign pathogens. Cells of the innate immune system express pattern recognition receptors (PRRs) which signal once bound to ligands with motifs common to pathogens but unique from the host, for example, components of bacterial cell walls like lipopolysaccharides (1). While taking longer to initiate, on the order of days, the adaptive immune response, consisting of B and T lymphocytes, is able to react to and work toward clearing specific pathogens through unique clonally expanded antigen receptors. These specific receptors come to be through a process called V(D)J recombination (2) during lymphocyte development. During V(D)J recombination, DNA segments within either the B or T cell receptors' loci are persistently rearranged with insertion of random nucleotides to produce unique receptors. The end result is the production of individual B and T cells with unique B cell receptors (BCRs) and T cell receptors (TCRs) with the ability to recognize distinct antigens or short peptides, respectively. T cells recognize peptide presented on host-derived major histocompatibility complex (MHC) molecules displayed by antigen presenting cells (APCs). Within the two primary cell populations of the adaptive immune system, B cells produce antibodies in response to activation while T cells vary in function depending upon their final differentiated state. $CD8^+$ T cells perform effector functions based on recognition of MHC class I (MHCI). These functions are typically cytotoxic in nature, often involving the production of granzymes and other mechanisms resulting in target cell lysis. $CD4^+$ cells perform disparate functions following recognition of MHC class II (MHCII); $CD4^+$ conventional T cells (Tcons) aid in production of inflammatory cytokines to bolster immune responses while $CD4^+$ $FOXP3^+$ Tregs perform suppressive functions to prevent autoimmunity and otherwise contribute to the maintenance of immune homeostasis.

$CD4^+$ Tcons and $CD8^+$ T cells work in tandem to eliminate infectious pathogens, undergoing clonal expansion as part of a proliferative burst and ultimately contracting to establish clonal memory populations which are equipped to more efficiently clear repeat infections of

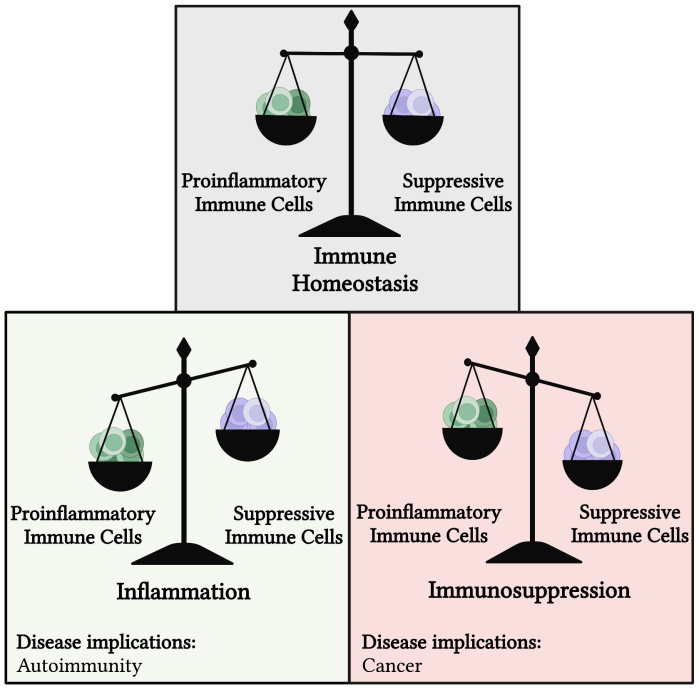

Figure 1.1: **Immune homeostasis and implications on health and disease.** The immune system must be able to maintain homeostatic balance between inflammatory cells, including effector T cells, and suppressive cells, including regulatory T cells. The immune system rapidly alternates between inflammatory and suppressive programs in a context-dependent manner. An excess in strength or duration of either of these responses is associated with disease onset, including autoimmunity in the context of excessive reactivity against host tissues or cancer progression in the event of excessive immunosuppression which consequently dampens endogenous anti-tumor immunity.

the same pathogen. These functions must be performed without excessive damage to the host, a principle called self tolerance (3). Self tolerance is a process initiated very early in thymocyte differentiation. As thymocytes develop and endure TCR iteration during V(D)J recombination, two major steps ensure that only thymocytes that meet two characteristics proceed in differentiation and ultimate release into the periphery (Figure 1.2). The first is based on TCR affinity for self MHC molecules. Thymocytes must be able to recognize MHC molecules, ensuring that there is sufficient specificity to allow for future recognition and engagement with APCs, necessary to initiate activation signaling cascades and an immune response. Thymocytes undergo this positive selection step prior to undergoing negative se-

lection, which requires developing thymocytes to have low reactivity to self-peptide:MHC complexes. This ensures that the relevant TCR-bearing thymocyte is non-reactive against host tissues. These two conditions ensure that only thymocytes with a range of moderate affinities to self-peptide:MHC are able to continue proliferating, leaving thymocytes to three possible outcomes: death by neglect, negative selection, or differentiation to Tregs (4; 5).

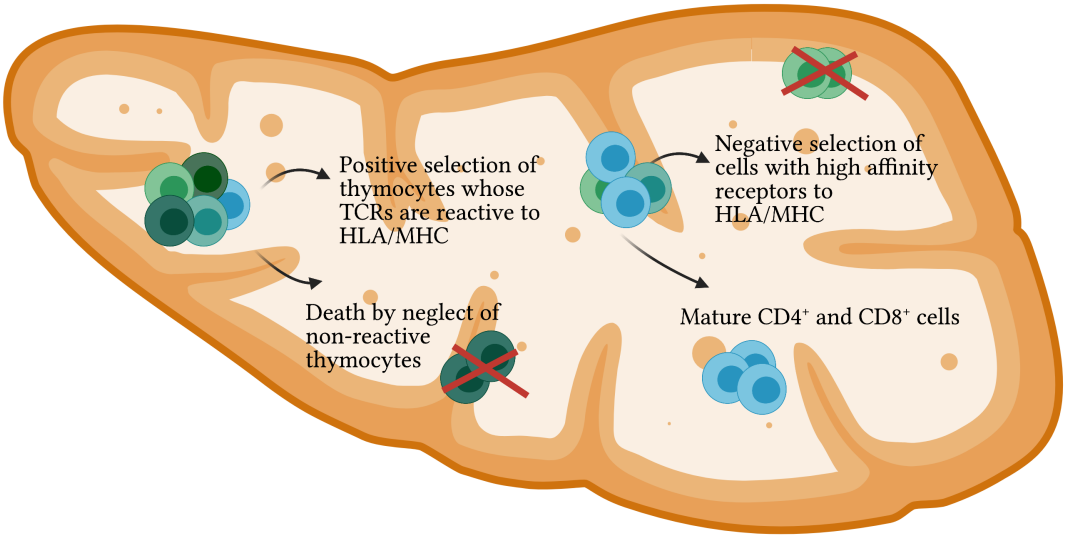

Figure 1.2: **Central tolerance takes place in the thymus.** Thymic selection mechanisms shape TCR repertoire through positive selection of thymocytes able to recognize host MHC, and feasibly mount an immune response. Non-reactive clones die by neglect. Following positive selection, negative selection of clones with high affinity TCRs reactive to self-peptide:MHC occurs to delete auto-reactive thymocytes. These are the major processes that are intended to prevent self-reactivity, but despite being highly efficient, are imperfect, necessitating alternate mechanisms of inducing peripheral tolerance.

1.3 A timeline of regulatory T cell discovery

Work spanning decades has contributed to our current understanding of Treg phenotype and function. In the 1960s, Jacques Miller identified the thymus as the generation site of lymphocytes and observed that neonatal thymectomy results in a wasting disease (6), later clarified to be related to the induction of autoimmunity. Fast forwarding several decades, seminal

discoveries made by Sakaguchi (7) identified a population of $CD4^+CD25^+$ T cells capable of suppressing autoimmunity, bolstered by subsequent discoveries that adoptive transfer of these thymocytes from mature mice could reverse autoimmunity induced by neonatal thymectomy, both proving this population played a major role in preserving immune homeostasis while also indicating that the thymus was a source of T cells capable of preventing autoimmunity. As this population of T cells became more widely recognized, they were named regulatory T cells. For many years thereafter, work focused on establishing whether or not these cells constituted a distinct lineage of T cells, as many of their features were indistinguishable from activated $CD4^+$ conventional T cells, including increased expression of cell surface molecules associated with generalized activation signaling like the high affinity IL-2 receptor (CD25). These common features shared amongst bulk T cells led to skepticism in the field about the relevance of the newly identified Treg population. Efforts to identify mechanisms responsible for Treg-specific immunologic function led to the breakthrough identification of the transcription factor Forkhead box P3, an X chromosome-encoded transcription factor (8; 9; 10) uniquely expressed in Tregs (11; 12; 13). Disease-defining mutations leading to loss of function FOXP3 were found to be the driving force of the multiorgan autoimmunity observed in patients with IPEX (Immune dysregulation, polyendocrinopathy, enteropathy, X-linked) syndrome (14) and in *scurfy* mice (9; 13). Further validating these studies, inactivation of *Foxp3* in murine T cells (15) confirmed the cell-autonomous function of FOXP3. Ectopic expression of *Foxp3* in naïve $CD4^+$ cells was found to induce expression of Treg-associated molecules such as CD25, cytotoxic T lymphocyte antigen 4 (CTLA-4) and glucocorticoid-induced TNF-receptor-related protein (GITR), as well as enable suppressive activity (11; 12; 13). TCR sequencing revealed that despite having similar numbers of $\alpha\beta$TCRs, Treg TCRs are unique from Tcon TCRs, further solidifying the population as distinct (16). Collectively, these data established the role of FOXP3 as a master regulator for Treg differentiation, maintenance, and function; its identification finally provided the unique

molecular marker needed to allow for subsequent studies and characterization of Tregs.

Fate-mapping studies revealed that *Foxp3* expression was heritable and that differentiated Tregs were stable (17). While activated Tcons also upregulate FOXP3, it is done so transiently and at much lower levels than in Tregs (18), suggesting that it is not binary expression of FOXP3 that leads to the suppressive phenotype associated with Treg identity, but rather the overall cumulative expression levels that are most crucial to maintaining their suppressive function. In recent years, the discovery of conserved non-coding DNA sequence 2 (CNS2), an intronic cis-regulatory element, as essential for the heritable maintenance of Treg identity has shone light on the existence of dedicated mechanisms maintaining Treg stability (19; 20). Specifically, demethylation of CpG residues within CNS2 signify an important step toward stable FOXP3 expression in fully differentiated Tregs.

Human Tregs express two isoforms of FOXP3, one of which lacks exon 2, subsequently missing a binding motif required for dimerization with retinoic acid receptor-related orphan receptor alpha (RORα) (21). This same isoform, FOXP3B, also lacks amino-terminal residues that aid in mediating the interaction between FOXP3 and the nuclear factor of activated T cells (NFAT) (22; 23). Both isoforms of FOXP3 are able to confer suppressive function on Tregs when expressed (24; 25). Despite these findings and their implication on FOXP3 stability and requirement for Treg function, recent studies have demonstrated that human Tregs are not homogenous in gene expression and suppressive function, leaving the door open for further delineation and definition of Treg subpopulations, particularly those that may be hyporesponsive. It will be important to elucidate the role of each FOXP3 isoform in driving this heterogeneity.

1.4 Tregs develop and differentiate in the thymus and periphery

Following positive and negative selection in the thymus, $CD4^+$ thymocytes that have high affinity to self-peptide:MHC complexes are either deleted or fated to become Tregs. Natural

Tregs (nTregs) are defined as Tregs that are derived in the thymus. In mice, these Tregs exist under the influence of several other cell types, including Aire-expressing thymic stromal cells, cortical and medullary thymic epithelial cells, and other APCs, which contribute to nTreg differentiation and selection. Thymic development of nTregs requires several signals including high-affinity interactions between their TCR and self-peptide:MHC complexes (26), signaling cascades initiated by elevated levels of cytokines interleukin 2 (IL-2)/interleukin 7 (IL-7)/interleukin 15 (IL-15) in the thymic microenvironment, and co-stimulatory signaling in the form of CD28-dependent engagement with CD80 or CD86 on thymic stromal cells (27). Despite being unable to synthesize IL-2, this cytokine is key to the eventual differentiation and function of Tregs (28; 29). Given established similarities between murine and human thymocyte development, it is likely that these processes occur similarly in humans with one caveat, the existence of a unique thymic medulla structure, Hassall's corpuscules, which may contribute to forming a specialized compartment for nTreg development (30). Hassall's corpuscles secrete thymic stromal lymphopoietin (TSLP), which functions by activating immature migratory dendritic cells (DCs) (31).

In addition to undergoing differentiation in the thymus, Tregs can be generated in the periphery (pTregs) through conversion of mature $CD4^{+}FOXP3^{-}$ T cells under conditions such as chronic stimulation by agonist peptide, subobtimal (anergic) stimulation against agonist peptide, response to homeostatic cues, or response to commensals (though this is specific to pTregs generated in the colon) (32; 33; 34; 35; 36). TCR sequencing has demonstrated that pTregs have some overlapping profiles with Tcons, but are largely distinct (16; 37; 38; 39), suggesting that certain T cell clones may be more amenable to conversion. pTreg induction is most useful toward attenuating the response of $CD4^{+}$ Tcon and $CD8^{+}$ T cell reactivity toward commensals and other benign microbes (36). In this context, $CD4^{+}$ Tcons are sent signals to upregulate FOXP3 and differentiate into Tregs based on the surrounding microenvironment, largely depending upon soluble cues like Transforming growth factor beta

(TGFβ), IL-2, and retinoic acid (33; 40). While these cues induce Tregs easily *in vitro* (41; 42), making the link to physiological relevance has been more challenging. All-trans retinoic acid (ATRA), for example, enhances the activation of the *Foxp3* locus *in vitro*, but its effects *in vivo* are complicated by pleotropic effects on a variety of other cell types (43). Although FOXP3 expression is elevated in these induced Tregs (iTregs), incomplete CpG demethylation at the *Foxp3* locus may in turn make this expression inherently unstable (41; 44; 45). The observed intensity of FOXP3 expression and suppressive functional ability of induced Tregs has been variable, adding to the ambiguity about the role these cells play *in vivo*.

While it is difficult to delineate pTregs and nTregs due to a lack of specific cell-surface markers, pTregs may function only in response to restricted specific cell types, tumors, or foreign antigens, unlike nTregs (46). Over the years, several intracellular markers have been suggested as unique to nTregs, including Helios (*Ikzf2*) (47). This was later debunked following observations that the transcription factor was also expressed in pTregs induced under certain circumstances (48; 49; 50). nTregs and pTregs largely share transcriptional signatures, though fine differences exist and likely reflect differences between thymic selection and peripheral induction (51; 52). Further identification of the different contexts in which nTregs and pTregs exert their functions will be important areas for follow-up study, and may consequently indicate how subtle differences in genetic programs become relevant to phenotype. Studies of thymic pools, peripheral lymphoid organs, and autoimmune lesions demonstrate that these environments are largely composed of recruited nTregs (53), again bringing into question the context in which pTregs function (38; 54; 55). Evaluating the contribution of nTregs versus pTregs in the tumor microenvironment will be important toward interpreting opportunities for therapeutic intervention, particularly if one Treg population over the other is more crucial for observed attenuation of anti-tumor immunity.

1.5 Characterization of Treg subpopulations is dependent on the identification of discrete markers

As the primary marker of Tregs, FOXP3, is intracellular, it has been a challenge over the years to purify and subsequently analyze this cell population through traditional means like FACS sorting. In naïve mice, CD25 expression can be used accurately to isolate Tregs, but this population is not pure in the human population, where some 30% of $CD4^+$ cells express CD25 despite only approximately 1% of the highest expressing cells having suppressive capacity. Adding to this challenge is the fact that expression of CD25 exists along a continuum, making it difficult to demarcate exactly where the boundary might exist between Tregs and other activated T cell populations. To aid in isolating T cell populations, CD127, the IL-7 receptor alpha-chain, has been an addition which notably is expressed anti-correlatively to FOXP3. Thus, $CD127^{low}$ expressing $CD4^+$ T cells correlate strongly with high expression of FOXP3 and suppressive capacity (56). Even this additional marker is complicated by the existence of non-suppressive $CD4^+FOXP3^+$ cells existing in the periphery, leading to the inclusion of CD45RA and CD45RO as additional markers of suppressive potential.

$CD45RA^+CD25^+CD127^{low}$ Tregs with a naïve phenotype exist in peripheral blood and cord blood, and also possess suppressive capacity. Expression of CD45RA in the absence of CD45RO is a marker for T cells that are antigen inexperienced. Tregs must be continuously stimulated by cognate antigen to be maintained (57), therefore $CD45RA^+$ Tregs are not naïve in the same way that other T cell subsets are considered to be naïve. One major observation has been that virtually all Tregs that are $CD45RA^+$ are also $CD31^+$, a marker indicating recent migration from the thymus. This suggests that $CD45RA^+$ Tregs are thymus-derived and quiescent (58; 59).

$CD45RO^+CD25^+CD127^{low}$ Tregs have been identified as potent suppressors with expression of Treg markers and anergic state corresponding most closely to the murine $CD4^+CD25^+$ Tregs. As a result, this population has been labeled 'effector' Tregs that are functionally

differentiated. Contrary to CD45RA$^+$ Tregs, CD45RO$^+$ Tregs exist primarily in adults (60). Though CD45RO positivity is conventionally used to demarcate memory T cells, there is limited evidence to suggest true memory pools of Tregs exist in part due to the rapid turnover of CD45RO$^+$ Tregs which is contrary to many observation of true memory pools of T cells (61). These observations all go to suggest that despite variations in function and cell surface marker expression, the Treg compartment is closely developmentally related (Figure 1.3).

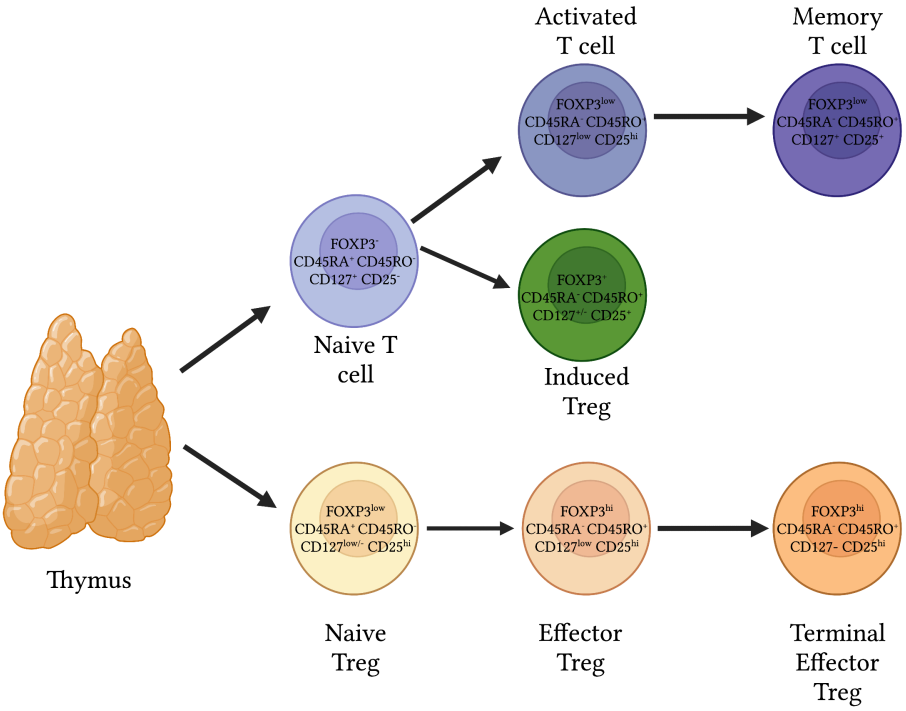

Figure 1.3: **CD4$^+$ T cell activation and lineage commitment.** As CD4$^+$ naïve Tcons and Tregs exit the thymus, their activation is dependent upon antigen encounter and subsequent stimulation following CD28 ligation with CD80/86 on an APC. A proliferative burst post-stimulation is followed by contraction, leaving only a fraction of T cells which remain as part of a memory pool. Tregs can alternately be induced in the periphery if naïve T cells are exposed to certain signaling molecules like TGF-β and ATRA.

1.6 Tregs enforce peripheral tolerance through a variety of suppressive mechanisms

Regulatory T cells exert their suppressive effects as the primary mediators of peripheral tolerance through a variety of mechanisms, both contact-dependent and non-contact-dependent (Figure 1.4). Mechanisms of contact-dependent suppression include inhibition of effector cell activation through increased expression of inhibitory molecules like CTLA-4 and lymphocyte-activation gene 3 (LAG-3). CTLA-4 can suppress the costimulatory functions of dendritic cells through downregulation of CD80/86 and resultant transendocytosis (62). Similarly, LAG-3 inhibits DC maturation through engagement of MHCII and induction of an immunoreceptor tyrosine-based activation motif (ITAM)-mediated inhibitory signaling pathway (63; 64). Non contact-dependent pathways for mediating suppression include mechanisms such as expression of CD39 and CD73 ectoenzymes, which jointly facilitate conversion of adenosine triphosphate (ATP) to adenosine, creating an immunosuppressive local environment (65). High levels of CD25 expression allow Tregs to serve as 'cytokine sinks', adsorbing IL-2 from the surrounding environment, and keeping this crucial cytokine from effector T cells that rely upon it for activation and proliferation. Tregs can also contribute to the initiation of effector T cell death through direct cytolysis following production of granzymes and perforin (66). Finally, Tregs manipulate the cytokine milieu to promote an inhibitory microenvironment through production of suppressive cytokines; TGF-β, interleukin 10 (IL-10), and interleukin 35 (IL-35). These all play roles in inducing FOXP3 expression in conventional T cells, attenuating DC function, and in general are required for maximal suppressive capacity (67).

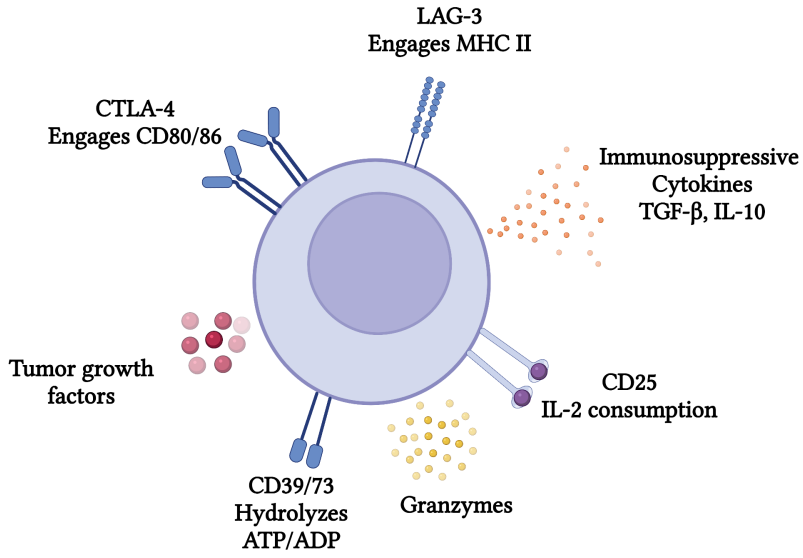

Figure 1.4: **Mechanisms of Treg suppression.** Tregs are able to exert their suppressive effects in order to maintain peripheral tolerance through a variety of mechanisms that are both contact-dependent and non-contact-dependent. This includes the elevated expression of co-inhibitory receptors, production of lytic agents and immunosuppressive cytokines, and modulation of the metabolic microenvironment.

1.7 Diverse functions in Tregs include non-suppressive activity

Additional functional diversity in Treg subpopulations has been identified, either connected to unique activity outside of canonical immunosuppression or related to behavior specific to tissue localization. In some contexts, like under microbial or parasitic infection, Tregs can take on effector functions such as production of proinflammatory cytokines, like as interferon gamma (IFNγ) and interleukin 17 (IL-17) (68). This inherent plasticity and difference in Treg functional outcomes is determined by many of the same programs as are observed in Tcons and other effectors. Interferon regulatory factor 4 (*Irf4*) is crucial for T helper cell type 2 (Th2)/ T helper cell type 17 (Th17) differentiation, and its absence in Tregs impairs their ability to limit Th2 responses (69). In another example, T-box expressed in T cells (*Tbet*) expression can lead to improved suppression of T helper cell type 1 (Th1) and Th17

responses (70). An important takeaway is that Tregs are an important contributor to the specificity and ultimate effectiveness of immune responses, adapting quickly based on the immediate context and signaling cues received. Though playing a crucial role in establishing tolerance, Tregs can paradoxically promote inflammation in some instances, suggesting they may have a more broad role in ensuring tissue homeostasis (71).

Some of the more tissue-specific functions of Tregs include regulating tissue repair and wound healing (72). In skin for example, inflammation following an injury and break in the skin is required to protect against infection, but excess inflammation impairs wound healing, resulting in longer time to heal and increased granulation tissue (73; 74). In muscle tissue repair, Tregs similarly support muscle remodeling by modulating macrophage differentiation (75). In recent years, Tregs have also been identified to be regulators of allergy and interactions with the gut microbiome. These variations in function will have major implications for designing therapies in the context of cancer, where tissue-resident status likely influences immune reactivity.

1.8 Tregs in cancer: cross-talk leading to tumor immune escape

A plethora of evidence has demonstrated that the relationship between the tumor and immune system impact the development and progression of cancers (76). An increased frequency of Tregs in the tumor microenvironment (TME) is associated with poor prognosis in cancer types (77; 78; 79) near universally, with one notable exception being colorectal cancer where Tregs are required to suppress inflammation driven by the gut microbiota (80). Tregs can also be used as a biomarker to predict response to immunotherapy. Higher pretreatment levels of Tregs in the peripheral blood were associated with improved survival in patients treated with ipilimumab, an antibody targeting CTLA-4 (81), and correlations have been observed between improved response to immune checkpoint blockade (ICB) and frequency of programmed death ligand 1 ($PDL1^{+}$) Tregs (82). Importantly, in making these correlations,

it's important to consider proportions of Tregs relative to other effector T cells, as overall immunogenicity of each tumor likely drives responsiveness to ICB and other immunotherapies. Thus many groups look at ratios of $CD8^+$ T cells to $FOXP3^+$ Tregs as a closer proxy for insight into inflamed versus non-inflamed tumor status. Inflamed tumors are considered to be generally more likely to be responsive to immunotherapy. The suppressive mechanisms of Tregs outlined above can prove advantageous to tumor growth, through inhibition of anti-tumor immunity or in plastic response to signals from the tumor driving Treg stability and/or conversion as a means of perpetuating an immunosuppressive environment.

Chemokines play a role in controlling leukocyte recruitment; evidence has suggested that release of chemokines like chemokine ligand 28 (CCL28) in hepatocellular carcinoma (83) promoted recruitment of Tregs to the TME. Upregulation and preferential expression of chemokine receptors like chemokine receptor 4 (CCR4), chemokine receptor 5 (CCR5), and chemokine receptor 8 (CCR8) on Tregs in the TME further promote their trafficking. Membrane-bound TGFβ associated with tumor exosomes (84) along with other immunosuppressive factors like IL-10 and vascular endothelial growth factor (VEGF) can enhance the suppressive function of existing Tregs and can induce the conversion of Tregs from effector cells, often mediated by indoleamine-2-3-dioxygenase (IDO)-expressing APCs within the TME.

In addition to direct recruitment or conversion, the metabolic environment within the TME favors Treg stability. Cancer cells reliant on aerobic glycolysis and fatty acid synthesis (85) contribute to an environment that is nutrient-poor, lactate-rich, and hypoxic. This environment restrains effector T cells (86) which rely heavily on glycolysis, and further play a role in modulating T cell fates to favor lineages such as Treg over Th17 through differential activity of mammalian target of rapamycin (mTOR), hypoxia inducible factor 1 subunit alpha (HIF-1α), and Peroxisome proliferator-activated receptor gamma (PPAR-γ) which drive differential expression of retinoic acid receptor-related orphan receptor gamma

T (RORγT) and FOXP3 (87). Tregs are able to utilize alternate metabolic pathways, like fatty acid oxidation and oxidative phosphorylation, through FOXP3-mediated programs, allowing them to persist and function in the TME (88). These features of the TME not only potentiate Treg suppressive activity at the cost of effector T cells, but ensure repeat propagation through promotion of Treg induction and trafficking (Figure 1.5).

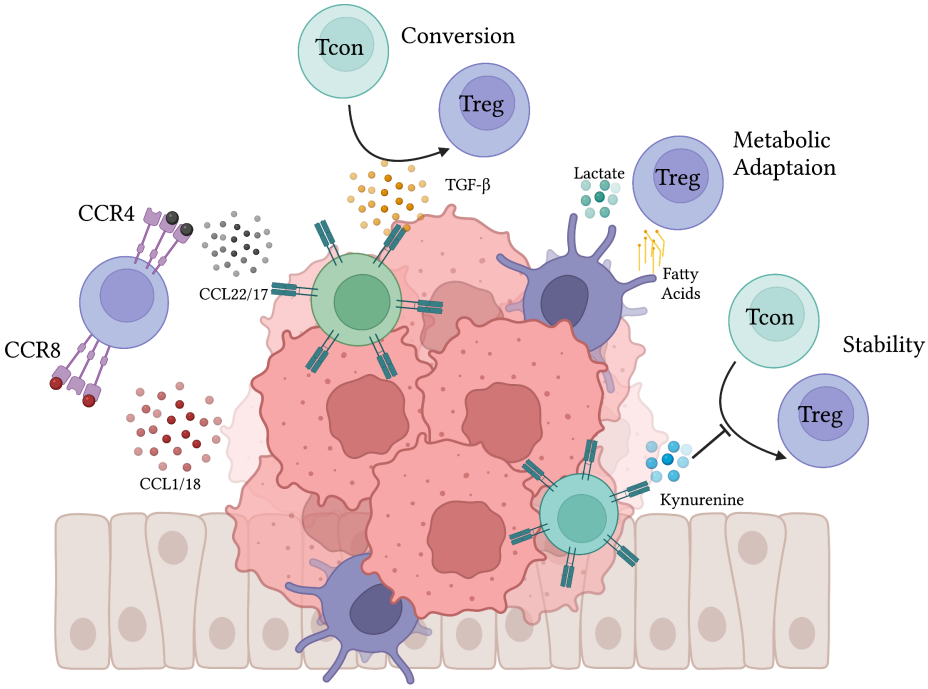

Figure 1.5: **Preferential recruitment and maintainance of Tregs in the TME.** Several factors lead to the preferential recruitment and maintenance of the Treg lineage in the tumor microenvironment. These include release of chemokines, cytokines, and other signaling molecules. The lactate-rich, fatty acid-rich, hypoxic environment of the tumor favors metabolic programs that Tregs are uniquely situated to adapt to through utilization of pathways like fatty acid oxidation and oxidative phosphorylation.

1.9 Therapeutically targeting Tregs

In cancer, nondeleterious mutations accumulate over time in tumor cells, generating neoantigens that increase immunogenicity, which can facilitate antitumor immune reactivity (89). As a result, melanoma and microsatellite instability-high (MSI-H) cancers with among the

highest tumor mutational burden (TMB) respond well to ICB (90; 91). Generally, with the exceptions of these cancer types, fewer than 15% of patients are able to receive this significant level of benefit (92). This has led to continued interest in identifying therapies that can bolster the anti-tumor immune response as a strategy to eradicate tumors.

Regulatory T cells have been a therapeutic target of interest for decades based on early work showing that their depletion amplifies anti-tumor immune reactivity (93). Poor clinical outcomes have been predicted by increased peripheral and intratumoral Tregs in a number of settings, including in patients who receive adoptive cellular therapies and immune checkpoint blockade (77; 94). Although discovering effective approaches to modulate Tregs remains a high priority, clinically meaningful progress has been hampered by small molecule or deletional anti-Treg focused therapies lacking sufficient cellular specificity to avoid inadvertent targeting of other T cell populations. Thus, identification and modulation of intracellular molecular targets unique to Tregs, and associated with their immunosuppressive function, should theoretically find increased success.

Previous indirect approaches to inhibiting Tregs, many times trialed in combination with tumor cell vaccination or checkpoint inhibition, include preventing trafficking to tumors through CCR4 blockade (95), stopping the conversion of peripheral Tregs by blocking IDO (96; 97), and inhibiting the phosphoinositide 3-kinase (PI3K)- Protein kinase B (Akt)-mTOR pathway, an important regulator of Treg stability (NCT02646748). Direct approaches to target Tregs have been through the use of monoclonal antibodies (mAbs) to target their consistently high cell-surface expression of CD25 and CTLA-4. While murine studies suggested that anti-CTLA-4 targeting augmented anti-tumoral T cell-mediated responses through selective depletion of intratumoral FOXP3$^+$ Tregs (98), recent work has determined that anti-CTLA-4 therapies do not deplete FOXP3$^+$ Tregs in human patients (99). Alternatively, modest positive clinical results were measured using a humanized CD25-blocking mAb (daclizumab) (100), but were ultimately unsuccessful because of the simultaneous depletion of

CD25-expressing effector cells. IL-2-diphtheria toxin fusion protein (ONTAK) was developed as an alternative strategy with initial efficacy (101) but ultimately abandoned due to major off-target toxicity, such as vascular leak syndrome (102). While development of second- and third- generation iterations of therapeutics designed to block these and similar molecular targets are underway (103), we currently still lack agents that are specific for Tregs and thereby do not have full clarity on how such targeting would impact anti-tumor immune responsiveness.

1.10 FOXP3 as a target

FOXP3 homodimerization, DNA binding, and its interaction with other co-transcriptional regulators are essential for Treg function. The FOXP3 homodimer serves as a context-specific activator and repressor of expression at target loci of a key set of core Treg genes (104; 105). Several features of FOXP3 make it a potentially favorable drug target (Figure 1.6): 1) FOXP3 is expressed in Tregs with little to no expression in other cells (106); 2) reduction and not absence of FOXP3 leads to dose-dependent non-Treg immune reactivation in mice and humans, suggesting that only a fraction of FOXP3 in a cell needs to be inhibited to alter Treg function (107; 108; 109); 3) naturally occurring mutations within the coding region of FOXP3 in IPEX patients are primarily located in the two distinct protein:protein interaction interfaces highlighting critical structure/function relationships (23; 110); 4) FOXP3 sequence, structure, and overall function are highly conserved in humans and mice reflecting shared mechanisms of action allowing for meaningful pre-clinical testing (10; 14; 111; 112); 5) known FOXP3 crystal structures allow for correlation between structure and drug design (113; 114); and 6) recent evidence has confirmed that the loss of FOXP3 expression in post-thymic Tregs leads to reprogramming of Tregs into a T effector cell-like phenotype (115). Lastly, although Treg loss of any kind could lead to unwanted immune activation, Treg depletion alone in patients and adult mice does not result in rampant autoimmunity,

supporting that transient Treg inhibition remains a clinically viable therapeutic strategy (93; 116; 117). Given these points, we set out to develop a hydrocarbon stapled α-helical peptide that would corrupt Treg activity via disruption of a key PPI domain of FOXP3 through molecular mimicry.

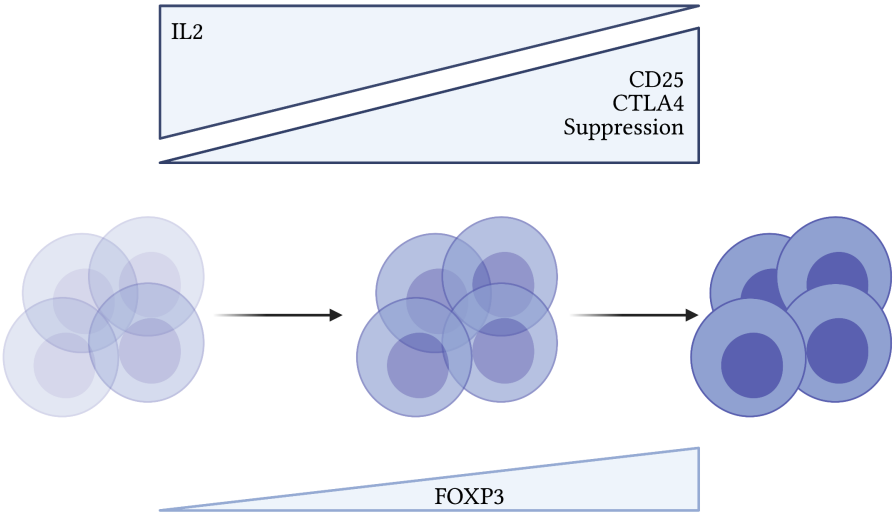

Figure 1.6: **FOXP3 modulation can achieve a change in effector status.** The proportion of dimerized FOXP3 is positively correlated with suppressive capacity and expression of suppressive effector molecules like CD25 and CTLA-4. Attenuating the quantity of FOXP3 existing in a dimer likely will dampen suppressive capacity and push cells away from a suppressive state.

1.11 Classifying and identifying protein-protein interactions

PPIs are either homomeric or heteromeric, and are then labeled either obligate or non-obligate depending upon the strength and duration of the interaction (118). PPI affinities

span many orders of magnitude with interfaces that are generally either hydrophobic with a surrounding region of polar residues (119) or consist of interspersed hydrophobic and polar interactions (120). Most PPIs have been classified into four groups: globular proteins that interact through discontinuous epitopes, globular proteins that undergo a conformation change following binding, a globular protein interacting with a single peptide chain, and bound peptide chains (121) (Figure 1.7). Globular interacting proteins constitute the PPIs that remain the most challenging targets for drug development given their flatter interaction surfaces. Less complex PPIs, like those between two peptide chains while more straightforward to target in theory, are often more intrinsically disordered when not in their native complex, presenting separate challenges in identifying important binding sites at the onset of drug development. As a result, the intermediate between these two extremes and likely most easily targetable PPIs are those between a globular protein and single peptide (122).

New computational methods have improved identification of putative PPIs through sequence similarity and phylogenetic analysis (123). Recent predictions have suggested the existence of some 300,000 - 650,000 interactions in the protein interactome (124). Databases like STRING (125), TIMBAL (126), and PICCOLO (127) provide structural information on predicted and known PPIs, small-molecule inhibition, and others.

1.12 Screening PPI inhibitors

Developing inhibitors of PPIs is a challenging exercise in balancing advantageous and disadvantageous physicochemical properties with on-target function, like minimizing molecular mass and lipophilicity while allowing for access to hot-spot regions on a globular protein (121). High throughput screening is the most conventional approach to discover novel inhibitors of PPIs, but often have a high false hit rate where low or weak hits register as positive. In the past few years, fragment-based drug discovery (FBDD) has been utilized to identify targets by showing strong correlations between protein hot-spots and fragment bind-

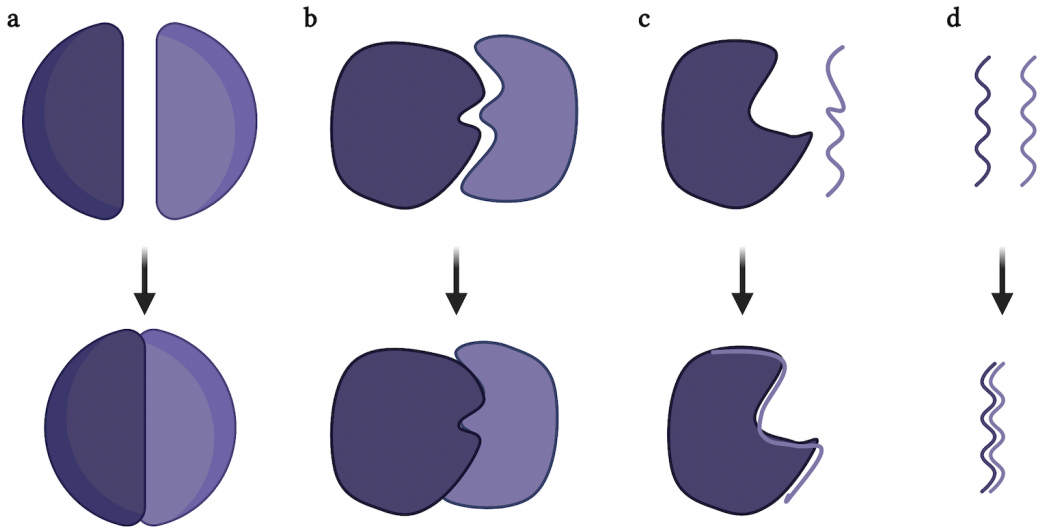

Figure 1.7: **Classifications of PPIs.** Protein-protein interactions generally fall under four structural classifications including (a) pairs of globular proteins that interact through a discontinuous epitope (b) pairs of globular proteins where at least one if not both proteins undergo a conformational change following binding (c) a globular protein interacting with a single peptide chain (d) an interaction between two peptide chains. Figure adapted from Scott *et al* (121)

ing sites (128), and is less likely to be biased towards any one class of molecules (129). Biophysical techniques like thermal shift, X-ray crystallography, protein-based nuclear magnetic resonance (NMR) spectroscopy, surface plasmon resonance (SPR), and isothermal titration calorimetry (ITC) have provided details on likely points of interaction, and thus potential sites to manipulate (130; 131; 132). Though immensely useful, these studies often are facilitated through the use of truncated proteins, leaving a still-incomplete picture of the PPI of interest.

1.13 Designing therapeutics against transcription factors and transcription factor PPIs

Many transcription factors have been identified as crucial in driving various hallmarks of cancer. These include but are not limited to transcription factors that mediate properties like self-renewal (133; 134; 135), replicative immortality (136; 137; 138), epithelial to mesenchymal transition (139; 140), differentiation and/or cell death (141), development of resistance (142; 143), autoregulatory circuits (144; 145), and immune invasion (146; 147). These mutated or dysregulated transcription factors represent a broad array of potential drug targets in cancer – their role in promoting aberrant gene expression can have major consequences in preventing normal cellular activity.

Transcription factor activity has often been found to be altered through a variety of mechanisms including translocations, mutations, and changes in expression. The first transcription factor drivers of cancer were identified in blood cancers, where fusion proteins like promyelocytic leukemia protein (PML) – RORα and acute myeloid leukemia protein 1 (AML1) – ETO, among others, were found to prevent differentiation from myeloblast stages, thus locking cells in a stem cell-like state (148). In subsequent years, identification of transcription factors driving solid tumors has expanded and are implicated in a variety of cancer types including epithelial tumors (149), melanoma (150), and prostate cancer (151). Despite transcription factors being ideal potential targets, they have traditionally been difficult to drug (152; 153), leading to more successful pharmacological inhibition achieved through targeting of upstream kinases or nuclear receptors, or through indirect or direct modulation of expression, all of which lack specificity for the transcription factor itself (154; 155). Groups have attempted several strategies to manipulate transcription factor activity more directly through inhibition of binding between transcription factors and their cognate DNA, decreasing transcription factor availability by targeting them for degradation through ubiquitylation and subsequent proteasomal degradation, and inhibiting the binding between a transcription

factor and its cofactors.

This is not to suggest that there has been no success in targeting transcription factors to date. In fact, small molecule approaches have found success in targeting nuclear hormone receptors like the androgen receptor (AR), estrogen receptor (ER), and glucocorticoid receptor (GR) in breast cancer, prostate cancer, and certain blood cancers (156; 157). However, these are more unique situations in which a natural small molecule (hormone) already binds a pocket in the ligand binding domain (LBD), making development of small molecule therapeutics more feasible.

Work in developing compounds to alter transcription factor interaction with cognate DNA has largely been unsuccessful. Despite immense efforts, particularly in developing polyamide-based DNA minor groove binding compounds (158), the highly positively charged DNA binding interfaces have proven a major obstacle to overcome. Recent efforts to inhibit transcription factor:DNA binding have recently been focused on modulating immune cells. Work from the Hogan group identified a small molecule capable of disrupting NFAT: activator protein 1 (AP-1) complex formation with DNA in a sequence-specific manner; inhibiting IL-2 and other cyclosporin A-sensitive cytokine genes important for effector immune responses (159). To date, no compounds have progressed to clinical trials, bringing into question their potential utility.

Transcription factors are regulated in the cell by ubiquitylation and proteasomal degradation (160) in order to keep their protein levels in check. Heterozygous knockouts and observations of haploinsufficiency suggest that reductions in transcription factor protein can have significant implications on disease onset (161; 162; 163). The proteasome pathway thus provides a means for modulating transcription factor activity through ubiquitylation to drive proteasomal degradation. E3 ubiquitin ligases have been targeted through compounds like thalidomide, which can stabilize E3 ubiquitin ligases and consequently allow for degradation of target proteins (164). A strategy to target transcription factors has been the

development of proteolysis-targeting chimeras (PROTACs), bifunctional molecules with a ligand covalently bound to an E3 ubiquitin ligase (165; 166; 167). PROTACs are able to globally knockdown their target protein, and aren't restricted to limited activity present at a particular active site. Interestingly, PROTACs also act catalytically, whereby each bifunctional molecule can repeat its activity over multiple cycles of binding and degrading their target protein, a stark contrast to many other therapeutics (166). The pharmacokinetic properties and therapeutic qualities of PROTACs are likely complicated - while they should require infrequent dosing, ideally limiting off-target toxicity, their adsorption, distribution, metabolism, excretion, and toxicity (ADMET) properties are likely poorer due to their large size.

Another strategy to target transcription factors is through blocking their ability to interact with specific partner proteins like complement co-activators and co-repressors, which control and determine gene expression at specific loci in a cooperative manner. Three types of modulators have been used to disrupt these interactions: small molecules, antibodies, and peptides. Despite some successes, small molecules with drug-like properties are best at targeting PPIs with concentrated binding foci, such as enzymes, ion-channels, or receptors (168). PPI hot-spots often span a large portion of the target proteins, making it challenging to maintain good ADMET properties on compounds that are often defacto required to be much larger in molecular weight (169). Small molecules often fail to target PPIs, like transcription factor PPIs, mediated by large interfaces where binding is the summation of geographically distinct, relatively flat, or low-affinity interactions and not by pocketed areas or grooves suitable for high-affinity small molecule binding (170). For context, the typical PPI is 1500-3000Å, significantly larger than the typical receptor-ligand contact site (300-1000Å) (171). For PPIs under 2000Å in size, the total interaction surface is generally limited to a single region; as interactions increase in size the number of interaction surfaces correspondingly increases (172). Additionally, amino acid residues participating in PPIs can be both

continuous and discontinuous in their structures, allowing for high affinity binding that is difficult to disrupt with small molecules (173). As a result, 90% of human gene products have been historically deemed 'undruggable' (174). The use of monoclonal antibodies to target PPIs is limited to extracellular proteins, further restricting possible targets. Peptides, the final remaining category, are designed based on hot-spot determination (175) and retain high affinity to their protein targets. In comparing these three modalities of blocking PPIs, peptides have intermediate molecular weight and higher specificity and affinity relative to small molecules and antibodies. The overall success of peptide therapeutics targeting transcription factor PPIs will largely depend upon the identification of hot-spot residues (176), which contribute disproportionately to interaction energy (169). Hot-spot residues can be identified through the use of alanine scanning, which studies the effects of iterative point mutation of amino acid residues to alanines to identify which residues are essential for binding (177; 178). Alanine scanning has implicated certain residues including tryptophan, tyrosine, arginine, asparagine, and histidine as frequently overrepresented as hotspot residues (178); these typically interact in a cooperative manner and tend to packed in discrete foci (179).

1.14 Peptides and peptide mimetics

In contrast to small molecule and antibody approaches, peptides synthesized in the likeness of their native sequence are natural choices to target such PPIs due to the fidelity of structural contact points between binding partners. Furthermore, peptides are systemically absorbed at a fast rate, avoiding first-pass metabolism (180). Peptide design is based on rational design of scaffolds, mimicking three core recognition motifs: α-helices, β-strands, and reverse-turns (175). α-helical interactions largely involve binding at hydrophobic interfaces. Despite the advantages in diversity of peptides that can be produced, the amide backbone of peptides is extremely vulnerable to degradation in vivo (181) and peptides have poor secondary structure in solution, in part because any protein or portion of a protein taken out

of context from the native structure can unfold, reducing potential biological activity (182). In part to overcome these hurdles, hydrocarbon 'stapled' peptides have shown great promise for disrupting α-helical PPIs through stabilization of a protein fragment's natural secondary structure and imparting it with drug-like properties including enhanced target specificity, affinity, protease resistance, and cellular uptake depending upon biophysical features like α-helicity, hydrophobicity, and charge (181; 183; 184; 185; 186).] Hydrocarbon stapling as opposed to other strategies like amide or disulfide cross-linking confers additional chemical and metabolic stability while avoiding complications like hydrolysis or reduction (181). Hydrocarbon stapling utilizes metathesis chemistry to covalently link non-natural amino acid side chains (187) (Figure 1.8). To date, stapled peptides have been used in a wide range of disease applications, with development for both extracellular and intracellular targets like Myc/Max (188), Bcl-2/Bax (189), and mouse double minute 2 homolog (MDM2)/p53 (190).

1.15 Approach

We describe a strategy focusing on using peptide mimicry to target an 'undruggable' coiled-coil α-helical homodimerization domain of FOXP3 to enable pharmacological disruption of FOXP3-mediated Treg transcriptional control. α-helical motifs make up a large proportion of PPIs, including the FOXP3 leucine zipper dimerization domain (LZDD), but their isolation as peptides leads to unfolding, proteolysis, cellular impermeability, and biological impotency (191). Hydrocarbon stapling can address this problem and was developed to investigate and target α-helical interactions while reducing susceptibility to cellular degradation (192). Substitution/insertion of non-natural amino acids with olefin tethers at positions spanning one (i,i+4) or two (i,i+7) turns of an α-helix followed by ruthenium catalyzed metathesis crosslinks, or 'staples' , the inserted residues together. Hydrocarbon stapling endows α-helical peptides with improved pharmacologic properties such as cellular penetration, protease resistance, and increased binding affinity.

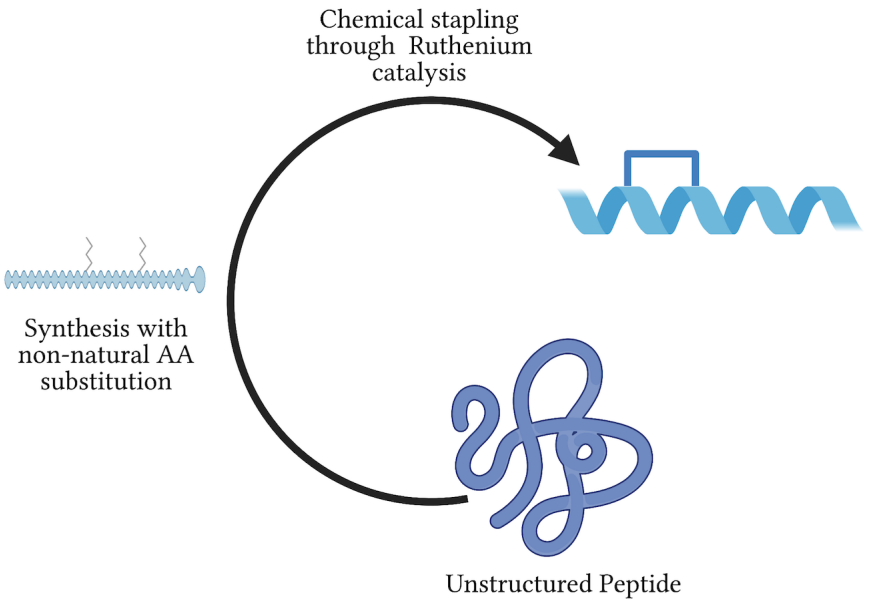

Figure 1.8: **Hydrocarbon-stapling confers benefits to peptide therapeutic design.** Addition of non-natural amino acids stapled through ruthenium catalysis-mediated olefin metathesis promotes resistance to proteolytic degradation and maintenance of protein secondary structure

Our contributions here elucidate the activity of a novel and specific approach to Treg inhibition that targets FOXP3 protein-protein interaction (PPI) domains, specifically that of FOXP3 homodimerization at the leucine zipper coiled-coil (LZCC), using single and double-stapled peptides. We provide proof-of-principle determination of their *ex vivo* and *in vivo* efficacy. This new and substantively different approach to Treg inhibition is expected to overcome cellular specificity limitations and thereby enhance the future transformative promise of modulating Tregs for therapeutic benefit. These findings provide strong scientific justification for continued development of FOXP3 inhibitors and their utility in uncovering previously unknown FOXP3-associated biological mechanisms. Importantly, the clinical feasibility and positive efficacy of using stapled peptides has been validated in patient-derived xenograft

models (193) and in first-in-human phase I and II trials of ALRN-6924 (194), a stapled peptide designed to disrupt the interaction between p53 and its endogenous inhibitors, mouse double minute X homolog (MDMX) and MDM2 (NCT-02264613, 03725436, 02909972, and 03654716). This collectively suggests the viability and promise of our approach.

CHAPTER 2

MATERIALS AND METHODS

2.1 Mice

Ex-vivo treated conventional T cells and regulatory T cells were isolated from Foxp3$^{IRES-GFP}$ or C57BL/6 mice originally purchased from the Jackson Laboratory (C.Cg-Foxp3^{tm2Tch}/J, C57BL/6J). All animal experiments were approved by and performed in accordance with the guidelines and regulations set forth by the Institutional Animal Care and Use Committee of the University of Chicago.

2.2 Murine T cell isolation and expansion

Foxp3$^{IRES-GFP}$ mice were sacrificed and their spleen, thymi and lymph nodes removed. Following organ isolation, cells were put into a single cell suspension by physical disruption of organs through a 40µM filter. CD4$^+$ cells were enriched through negative selection from spleen and lymph nodes of Foxp3$^{IRES-GFP}$ mice using a CD4$^+$ T cell isolation kit following the manufacturer's protocol (Miltenyi Biotec #130-104-454). CD4$^+$ cells were stained with CD4 – PE (BD Biosciences) and CD25 – APC (BD Biosciences) flow cytometric antibodies diluted 1:100 in PBS; Tcons (CD4$^+$CD25$^-$) and Tregs (CD4$^+$CD25$^+$GFP$^+$) were sorted on a BD FACSAria (University of Chicago Flow Cytometry Core). Sorted populations were $>$ 98% pure. *Ex-vivo* sorted Tcons and Tregs were maintained and expanded in Advanced Dulbecco's modified eagle media (DMEM) media supplemented with 10% fetal bovine serum, 100U/mL penicillin/streptomycin, 5µg/mL Gentamicin solution, 2mM L-Glutamine, 1X Non-Essential Amino Acids, 10mM HEPES, human IL-2 (500U/mL Tcons, 2000U/mL Tregs), and CD3/CD28 Dynabeads at a ratio of 1 bead:1 cell (Tcons) or 3 beads:1 cell (Tregs).

2.3 Human T cell isolation and iTreg induction

15mL of blood was drawn from healthy donors (University of Chicago IRB protocol: IRB14-0221). Following collection, blood was diluted with 15mL of PBS. 15mL of the diluted blood was then layered over 15mL of Ficoll-Paque PLUS density gradient media (GE Life Sciences). Following centrifugation for 30 minutes at 400G at 20°C with brakes off, the PBMC layer was removed and $CD4^+$ cells were isolated utilizing the $CD4^+$ T Cell Isolation Kit (Miltenyi Biotec #130-045-101) per manufacturer's protocol. In order to induce Tregs, $CD4^+$ cells were expanded in TEXMACS (Miltenyi Biotec #130-097-196) media containing 1500U IL-2, 100nM ATRA, 2ng/mL TGF-β, and anti-CD28 (Biolegend #302914) at 1:1000 on 6-well plates previously coated with CD3 (Biolegend #317302, 5µg/mL).

2.4 Stapled peptide reagents

Fmoc-protected natural amino acids, N-Methyl-2-pyrrolidone (NMP), dichloromethane (DCM), and N,N-Dimethylformamide (DMF) were purchased from Gyros Protein Technologies. The activating reagent (1-[Bis(dimethylamino)methylene]-1H-1,2,3-triazolo[4,5-b]pyridinium 3-Oxide Hexafluorophosphate; HATU) was purchased from GenScript. The following were obtained from Sigma Aldrich: Rink amide AM resin LL (0.26 mmol/g), Grubbs Catalyst 1st Generation, anhydrous 1,2-dichloroethane (DCE), acetic anhydride (Ac_2O), N,N-Diisopropylethylamine (DIPEA), piperidine, and artificial amino acids Fmoc-(R)-2-(7-octenyl)alanine (R8) paired with S5 to produce i, i+7 staples. Chemical reagents and solvents were used as received.

2.5 Stapled peptide synthesis and purification

Native and hydrocarbon stapled peptides were synthesized by Fmoc-based solid phase peptide synthesis as described (183). Briefly, the solid phase synthesis resin was swollen with DCM followed by DMF. Piperidine (20% vol/vol) in NMP was used for FMOC deprotection

with 2 x 10 minute treatments. To the resin beads, an equal volume was added of a 0.3M solution of amino acid in NMP, followed by a 0.285M solution of HATU coupling agent in NMP, and finally a 0.6M solution of DIPEA in NMP. Typically, for standard couplings, a 10x excess of amino acids relative to resin loading were used, and the reaction was allowed to proceed for 30 minutes. For addition of S5 or R8, a 5x excess of amino acids were used for 1 hour of coupling. For the amino acids immediately following S5 or R8, the N-terminus was deprotected with 4 x 10 minute piperidine treatments followed by 4 x 1 hour coupling reactions. After completion of synthesis, the amino terminus was either acetylated by reaction with capping solution (4:1:0.1 NMP:Ac_2O:DIPEA) or left with an FMOC-protected amine. The olefin metathesis step was carried out by first swelling resin with anhydrous DCE, followed by exposure to 20 mole percent Grubbs' first-generation catalyst in DCE at 4mg/mL for 3 x 2 hours under nitrogen bubbling. For fluorescein isothiocyanate (FITC)-functionalized peptides, the resin was then deprotected, and β-alanine and FITC were added to the N-terminus. The resin was then washed extensively with DCM and dried, and the peptides were then cleaved off the resin and deprotected using 95% trifluoroacetic acid (TFA), 2.5% water, and 2.5% triisopropylsilane. Double-stapled peptides were synthesized similarly as described previously (184). Following synthesis, peptides were purified to $> 95\%$ purity with HPLC/MS using a C18 column with mobile phases of water + 0.1% formic acid and acetonitrile. Acetonitrile was reduced in the pure fractions by rotary evaporation, and the peptides were then lyophilized. Aliquots were quantified by amino acid analysis.

2.6 Circular dichroism spectroscopy

Dimethyl sulfoxide (DMSO) stock solutions of peptide were diluted in Milli-Q water. Each stock was aliquoted to two vials, then lyophilized for two days. Each sample was dissolved in 1mL 5mM sodium acetate buffer, pH 3.6 to bring samples to 2.5-10μM. Each sample was put through 1 hour of heated sonication to assist in dissolution. A blank sample following

the same protocol was prepared to take the blank background reading for all samples. Data were acquired in 5 repetitions at 20°C from 260nm to 190nm in a 1-mm path length quartz cell using 1nm wavelength increments and a response time of 4s on a Jasco J-815 Circular Dichroism Spectropolarimeter (Easton, MD, USA). The data were converted to per-residue molar ellipticity, and percent α-helicity was calculated as described previously (195).

2.7 Proteolytic degradation

In vitro proteolytic degradation was measured by LC/MS (Agilent 1200) as previously described (183). The following parameters were used: 20µl injection, 0.6ml flow rate, 15 minute run time consisting of a gradient of water (0.1% formic acid) to 20%–80% acetonitrile (0.75% formic acid) over 10 minutes, 4 minute wash to revert to starting gradient conditions, and 0.5 minute post-time. The DAD signal was set to 280nm with an 8nm bandwidth and MSD set to scan mode with one channel at (M+2H)/2, ± 1 mass units, and the other at (M+3H)/3, ± 1 mass units. Samples were composed of 5µl peptide in DMSO (1mM stock) and 195µl buffer consisting of 50mM Tris-HCl, pH 7.4, for proteinase K proteolysis. Following injection of the 0-hour time sample, 2.5µl of 4ng/µl proteinase K (New England Biolabs) was added, and intact peptide was quantified by serial injection over time. Plots of MSD area versus time yielded exponential decay curves, and half-lives were calculated by nonlinear regression analysis using Prism 7 software (GraphPad).

2.8 Recombinant protein constructs, expression, and purification

Human FOXP3 regions ΔN (T182-P431) and LZCC (T182-M337) were cloned from FOXP3-pcDNA3.1 kindly provided by Anjana Rao (196) using Taq DNA polymerase (Qiagen) and primers listed below per the manufacturer's protocol. PCR fragments were ligated into pGEX4T1 and the vector's GST tag was changed to a 6x-His tag using His primers (Table

1) and a previously described around the horn PCR amplification scheme. BL21 bacteria expressing His6-LZCC-pGEX4T1 (T182-M337) and His6-ΔN-pGEX4T1 (T182-P431) were induced when OD600 reached 0.6-0.8 with 1mM IPTG for 6 hours at 37°C while shaking. Bacteria were pelleted using an ultracentrifuge and stored for future use in a -80°C freezer. Bacterial pellets were suspended in base buffer (100mM KCL, 20mM HEPES, 10µM EDTA, 10% Glycerol, 20mM imidazole, and 1mM DTT) and lysed with lysozyme (1mg/mL) for 30 minutes. Pellets were then sonicated six times in 10 second on/off pulses at 4°C. Nuclease and protease inhibitors without EDTA were added for 15 min before lysate was clarified by centrifugation at 6000G for 60 minutes. The remaining supernatant was incubated with Ni-NTA resin for 1 hour at 20°C. The Ni-NTA resin was washed with base buffer (+30mM imidazole). Protein was eluted from the Ni-NTA resin with base buffer (+500mM imidazole) and purified by size exclusion on an ATKApure FPLC machine using a Superdex 75 column (GE Lifesciences). Protein production was confirmed by SDS-page separation followed by Coomassie staining to identify appropriately sized protein or by western blot analysis using His antibody (Invitrogen #MA1-21315) and quantified by extinction coefficient at 280nm wavelength using a DeNovix DS-11 Spectrophotometer.

2.9 Primer table

Primer Name	Sequence $5^{'}$ to $3^{'}$	Tm
T182 Forward	TATAGAATTCACCCTTTCGGCTGTGCC	60.5
M337 Reverse	TCGACTCGAGTGTTGTGGAACTTGAAGTAG	61
P431 Reverse	TATACTCGAGAGGTGTAGGGTTGGAACACC	61.8
His forward	CTGGTTCCGCGTGGATCCCCGGAATTC	66.4
His Reverse	ATGGTGATGGTGATGGTGCATGAATACTGTTTCCTGTG	64.7
delE251 SDM Forward	GGAGAAGAAGCTGAGTGCCATGCAGG	63.3
delE251 SDM Reverse	CAGCTGGTGCTGGGGAGAAGAAGCTG	65
Mutant K251D Forward	CTGGAGAAGGAGGATCTGAGTGCCATG	
Mutant K251D Reverse	CATGGCACTCAGATCCTCCTTCTCCAG	
EMSA $A^{'}$GT25	IRDye700	

2.10 Fluorescent polarization analysis

Fluorescence polarization analysis (FPA) was performed to measure binding of FITC-labeled SAHs to serially diluted recombinant ΔN or LZCC FOXP3 (max concentration 4µg/mL) as previously described (183). Protein was incubated with 50nM FITC-labeled native or stapled peptide in 1X PBS, pH 8 (final volume 200µL) for 1-15 minutes at room temperature in a 96-well black flat-bottom plate (Nunc). Polarization values were measured at λem = 492nm and λex = 517nm using a SpectraMax spectrometer (Molecular Devices). Polarization values were determined using the equation: P = (Y-X)/(Y+X), where Y is vertical emission intensity and X is horizontal emission intensity. The fraction of peptide bound to protein was calculated using the equilibrium polarization value obtained for a given protein to which background-subtracted FP values were normalized. Binding curves, K_d values, and 95% confidence intervals were determined utilizing Prism 7 graphing software. The data were fit to a sigmoidal binding curve (4-parameter) which follows the equation: Y=bottom+(top bottom)/(1+10($^{(LogEC50–X)xHillSlope}$) as described on the Prism 7 website.

2.11 Electrophoretic mobility shift assays

Single-stranded oligonucleotides containing FOXP3 binding sites were annealed with their respective complementary strands and purified on 12% polyacrylamide gels as described (196). IR700-labeled FOXP3 probes ($A^{'}$GT25, Table 1) were incubated for 15 minutes at room temperature with 50-100pmoles of recombinant ΔN-FOXP3 along with DMSO, peptide, 200X unlabeled oligo or anti-FOXP3 (Abcam Ab248) antibody. The binding buffer contained: 12mM HEPES at pH 7.5, 100mM NaCl, 1mM DTT, 1mM EDTA, 12% glycerol, and 20µg/mL poly(dI)-poly(dC). DNA-protein complexes were then separated by electrophoresis on a 10% polyacrylamide TBE gel and were imaged using an Odyssey Imager (Li-Cor).

2.12 Surface plasmon resonance

Purified LZCC, ΔN, or full-length FOXP3 (Origene TP317580) was associated to a Series S CM5 chip (Cytiva #29104988) through covalent bonding. 50mM NaOH was used to remove the protective layer on the CM5 chip, followed by protein immobilization with EDC, NHS, and ethanolamine per the manufacturer's directions. The amount of desired protein bound was based on calculating R_{lig} with a target R_{max} of 50 RU. Following peptide immobilization, increasing concentrations of peptides were washed over the chip for a 20s association time and 30s dissociation time. Kinetic curves were calculated using a two-state reaction global fit, and kinetic constants were used to calculate K_D. The reference sample was a buffer only sample flowed over immobilized protein.

2.13 Confocal fluorescent microscopy for peptide pentration

Human iTregs and expanded murine Tcons and Tregs were treated with 0-5µM FITC-peptide for up to 4 hours in OptiMEM, washed twice with PBS, fixed in 2% PFA for 15 minutes at room temperature, and stained with Hoechst 33342 dye in PBS for 10 minutes at room

temperature. The cells were reconstituted in PBS at a concentration of 2 million/mL and 100µL of a single-cell suspension (200,000 cells) was spun onto slides using a Thermo Scientific Cytospin 4 at 400rpm for 2 minutes. Slides were then imaged using a Leica SP5 laser confocal microscope. Post-acquisition processing (multi-channel overlay) was performed using ImageJ software (NIH). The results are representative of images taken from multiple fields across the same slide in at least three biological replicates.

2.14 Viability assays - Lactate dehydrogenase release

Murine thymocytes were freshly isolated and plated at 50,000 cells/well. The cells were incubated with increasing concentrations of SAHs, DMSO, or positive control (1% Triton X-100) in 200µL OptiMEM for 4 hours. Cells were pelleted and media extracted for calorimetric analysis using a cytotoxicity detection kit following the manufacturer's protocol (Roche). Data were background subtracted and normalized to the positive control in order to measure % cytotoxicity.

2.15 Viability assays - Annexin V/PI flow cytometry

To measure apoptosis, cells were stained with Annexin V - APC from an Annexin V Apoptosis Detection Kit following the manufacturer's protocol (eBiosciences). Immediately prior to analysis on a LSRII cytometer (BD Biosciences), 2µL of Propidium iodide (Life Technologies 1µg/mL) was added to each tube in order to determine proportions of thymocytes in early apoptosis, late apoptosis, and necrosis following SAH or DMSO treatment.

2.16 Peptide treatments

T cells were washed in PBS then resuspended in OptiMEM with 100nM to 10µM of peptide or DMSO vehicle control. Cells were then treated for 4-6 hours at 37°C (2 hours without

serum, remaining hours with 10% serum added back), and then either left unstimulated or stimulated with 10ng/µL phorbol myristate acetate (PMA) + 0.5µM Ionomycin (PMA/Iono) in complete media for qRT-PCR. Cells were treated for 24 hours (2 hours without serum, remaining hours with 10% serum added back), and then stimulated with CD3/CD28 Dynabeads in complete media for flow cytometry analysis.

2.17 RNA isolation and cDNA preparation

Following relevant peptide treatments as indicated above, cells were lysed with Trizol (Life Technologies) and total RNA was isolated from each treatment condition using the Direct-zol RNA MiniPrep kit (Zymo Research) per manufacturer's instructions and quantified by DeNovix DS-11 Spectrophotometer. RNA was either saved for RNAseq or converted to cDNA for qRT-PCR. RNA from each biological replicate (1µg) was converted to double-stranded cDNA using the Superscript III first strand synthesis reverse transcription kit (Invitrogen) per the manufacturer's directions.

2.18 Quantitative real-time PCR

qRT-PCR was performed using TaqMan Master Mix and Gene Expression Probes (Applied Biosystems) for each of the following genes: *Foxp3*: Mm00475162 , *Il2rα*: Mm01340213, *Ubc*: Mm02525934. Samples were run on the 7500 Fast Real-Time PCR System (Applied Biosciences). Data was analyzed with the ExpressionSuite software utilizing the ΔΔCT method with *Ubc* as the housekeeping gene and DMSO-treated cells as reference samples. Data shown are means of technical triplicates plotted as a single plot, for three biological replicates.

2.19 Flow cytometric analysis

Cells were acquired and treated as described above. The following antibodies were used for staining at a dilution of 1:100 in PBS in the dark at 4°C for 30 minutes: CD4 - PE (BD #553730), CD25 - APC (BD #557192), Live/Dead - APC-Cy7 (ThermoFisher #L34975). For intracellular staining of FOXP3 and cytokines, cells were fixed and permeabilized with the FOXP3 Fixation/Permeabilization kit (eBioscience) per the manufacturer's protocol. After fixation and permeabilization, cells were stained with a FOXP3-FITC antibody (Invitrogen #11-5773-82) at 1:50 in permeabilization buffer for a minimum of 1 hour on ice. Samples were analyzed using a LSRII cytometer (BD) or FACSAria (BD). Data analysis was performed using FlowJo software (Tree Star).

2.20 *Ex-vivo* suppression assays

C57BL/6 mice were sacrificed and splenocytes were isolated by physical disruption as described above. Splenoctyes were $CD3^+$ T cell-depleted utilizing the CD3ε microbead kit per manufacturer's directions (Miltenyi Biotec #130-094-973). CD3-depleted splenocytes were then irradiated at 3000 rads utilizing a gamma irradiation source. Following Tcon and Treg isolation via FACS sorting as described above, Tcons were labeled with CellTrace Violet (ThermoFisher #C34557) per the manufacturer's protocol. Tregs were then serially diluted down a 96-well U-bottom plate (50,000 cells to 3,125 cells per well) and co-cultured with 50,000 labeled Tcons, 250,000 irradiated splenocytes, and soluble anti-CD3 Antibody at 1µg/mL (BioXCell #BE0002). The cells were stimulated for 3 days before staining with LIVE/DEAD - APC-Cy7 (ThermoFisher #L34975) per the manufacturer's protocol, along with antibodies CD4 – PE (BD #553730) and CD25 – APC (BD #557192) at a 1:100 dilution in PBS. Cells were analyzed via flow cytometry and analyzed on FlowJo software (Tree Star).

2.21 RNA sequencing and data analysis

Library preparation and sequencing were performed by the University of Chicago Genomics Facility. 100bp paired-end reads for each sample were generated using the HiSEQ4000 (Illumina, San Diego, CA). Alignment to the murine genome (mm10) was performed using Tophat and Bowtie. Differential expression analysis was performed using EdgeR, and data was filtered to exclude genes with counts per million (CPM) less than 2 in 3 or more samples. Gene set enrichment analysis (GSEA) was performed using the GSEA portal (http://www.broad.mit.edu/GSEA/) in the following way. Each gene set was queried for enrichment within the expression profile generated by comparing DMSO and SAH-treated cells. GSEA was performed with the following parameters: probe set collapse = false; phenotype = SAH vs. DMSO; permutation: sample, permutations = 1000. Gene set size: 50 - 1000, utilizing diffofclasses. Samples are plotted in columns and the genes in rows.

2.22 Stastistical statements

A one-way ANOVA test with multiple comparisons was used to evaluate statistically significant changes between treatment groups. Plots were created using Prism 7 (GraphPad Software). Expression data was depicted by RQ Min/Max with a 95% confidence level using the ExpressionSuite Software (Thermo Fisher/Life Technologies). Statistical significance was defined as $p < 0.05$ or as otherwise indicated.

2.23 Data availability

The RNAseq data that support the findings in this study are available in the National Center for Biotechnology Information Gene Expression Omnibus (GEO) and are accessible through accession number GSE201116.

CHAPTER 3

RESULTS

3.1 Design and synthesis of stapled α-helical peptides targeting FOXP3

The leucine zipper coiled-coil of FOXP3 is necessary and sufficient for FOXP3 homodimerization, heterodimerization with Forkhead box P1 (FOXP1), and is critical for FOXP3's ability to regulate transcription (197; 198). FOXP3 homodimerization is mediated by a two-stranded anti-parallel α-helical coiled-coil interaction within this domain. Each contiguous helix is made up of the zinc finger and leucine zipper regions of FOXP3 (Figure 3.1a). Within this contiguous helix, only a portion of the leucine zipper constitutes the leucine zipper coiled coil (LZCC). This anti-parallel arrangement produces a generally hydrophobic coiled-coiled core with flanking charged and polar residues necessary for dimer stabilization while solvent-exposed polar residues enhance solubility (114). Sequence alignment of murine and human FOXP3 demonstrate that this helix is highly conserved between species (90%) with only five unique residues spanning the entirety of the contiguous zinc finger and leucine zipper regions (10). Most importantly, key core binding residues, Q235, E249, and K252 are 100% conserved between human and murine sequences, suggesting the ability to target both murine and human FOXP3 by drugging this region. Using the crystal structure of murine FOXP3 zinc finger and leucine zipper regions, additional examination of this portion of the FOXP3 sequence finds, like other coiled-coil interactions, a buried motif with amino acids (a.a.) of a and d resonance (Figure 3.1a). These amino acids are involved in binding to an identical anti-parallel helix, aligned on the hydrophobic interface of each respective helix (Figure 3.2). Within this helix, the terminal end residues that define the homodimer interaction are R229 and Q244 on one helix with Q244 and H259 on the corresponding anti-parallel helix of another FOXP3 monomer. The interface accessible surface area of the

FOXP3 coiled-coil is 966Å2 (16% of total), compared to the average of 1492Å2 in other similar protein dimers, thereby classifying it as a rather flexible and dynamic interaction (114; 199).

To determine the feasibility of blocking FOXP3 homodimerization through peptide-based molecular mimicry, a library of acetyl-capped SAHs incorporating residues within the core coiled-coil domain and N-terminally flanking region corresponding to hFOXP3(214-262) were synthesized with varying peptide length, charge, and staple positioning (Figure 3.1b). Three differently positioned (*i, i*+7) hydrocarbon staples (B, C, and D) were inserted in such a way that they would extend along the peptide's exposed face in an effort to avoid disruption of critical coiled-coil amino acid contact points (Figure 3.1b, Figure 3.3, Figure 3.4). These peptides additionally have a range of isoelectric points (pI) reflecting potential differences in solubility in various settings (e.g. *in vitro* versus *in vivo*, etc.) despite overlapping amino acid usage. Hydrocarbon staples spanning 7 residues (*i, i* + 7) were chosen over shorter staples (*e.g. i, i* + 4) as longer staples have been generally shown to better stabilize α-helicity along long peptide fragments and can allow for increased protection against proteolysis (200). Variation of peptide length and staple positions greatly affected overall α-helicity as measured by circular dichroism spectroscopy (Figure 3.5). Importantly, circular dichroism was performed without addition of organic solvent (e.g. acetonitrile) as this has been shown to enhance the estimated α-helical content of amphipathic helical peptides and in pH 3.6 to allow for escape from acidic compartments like endosomes (201).

Calculated α-helicity amongst these SAHs generally ranged from 10% - 40% in solution and showed only variably improved α-helicity compared to their sequence-matched native unstapled peptide controls (Figure 3.5). One notable exception was SAH(229-259)$_C$, which was 67% α-helical, 2x greater compared to its native, unstapled counterpart, in solution (Figure 3.5). We hypothesized that greater helical stabilization would be advantageous and lead to increased mimicry of the natural FOXP3:FOXP3 PPI, in addition to potential

improvements in cellular permeability and proteolytic resistance. To determine if these assumptions were true, SAHs were next screened to measure how amino acid sequence, peptide length, and staple position variations affected their ability to bind FOXP3 and enter target cells.

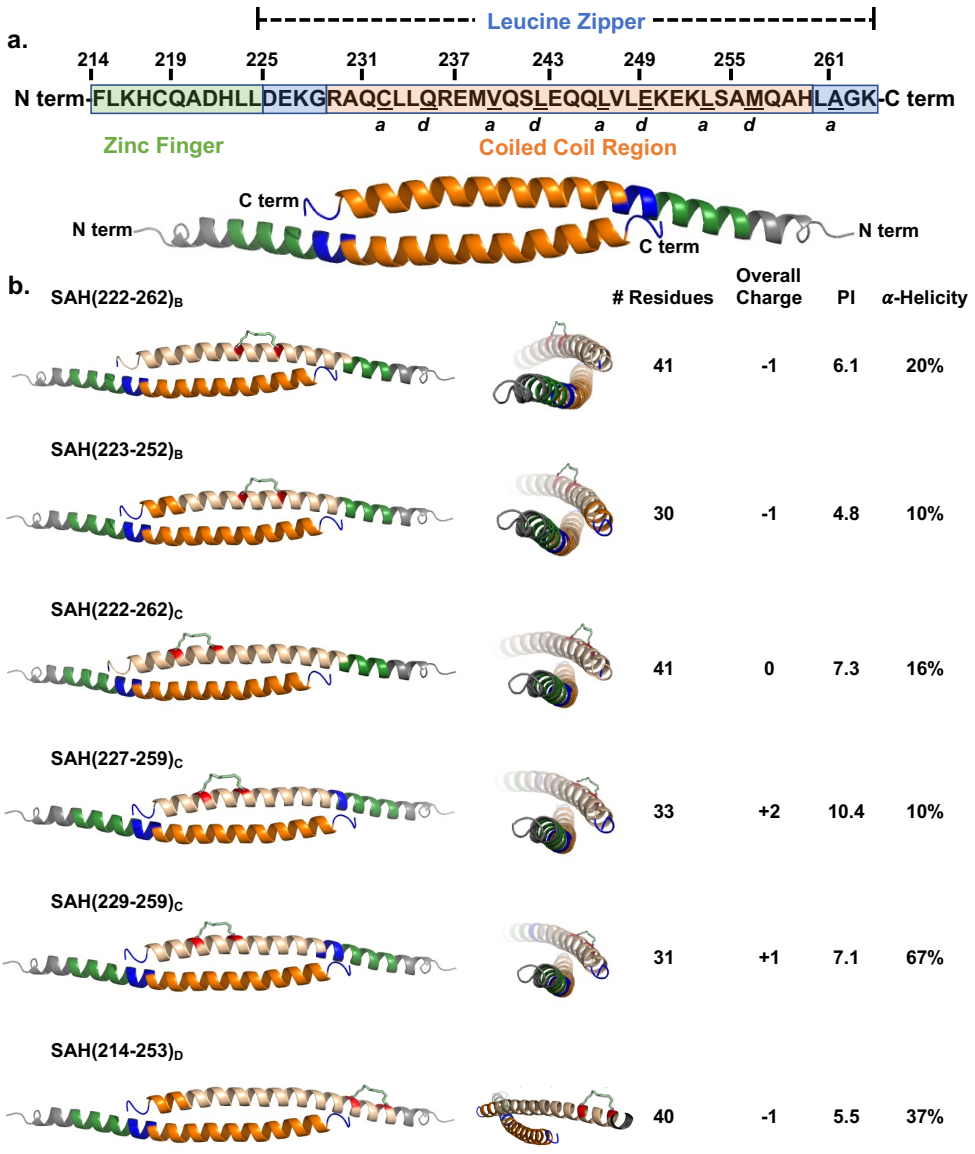

Figure 3.1: **Design and synthesis of stapled α-helical peptides targeting FOXP3.** (a) Human FOXP3 sequence. Residues F214-K263 represent the entirety of a helix constituting the zinc finger (F214-L224; shown in green) and leucine zipper (D225-K263; shown in blue) regions. Within the leucine zipper, the coiled-coil (R229-H259; shown in orange), represents an area that is highly conserved between human and murine FOXP3. Underlined residues indicate a and d core residues, which bind each other on an identical anti-parallel helix, and are key contact points for homodimerization. The homodimerized FOXP3 helix is labeled according to the color codes in the sequence above. (b) Design strategy for SAHs targeting FOXP3. SAHs differing in sequence, length, staple position, overall charge, pI, and α-helicity are represented. Each 3-dimenisional structure shown is based on the crystal structure (PDB: 4I1L); the upper helix represents each SAH (shown in tan) with hydrocarbon staple (end residues shown in red).

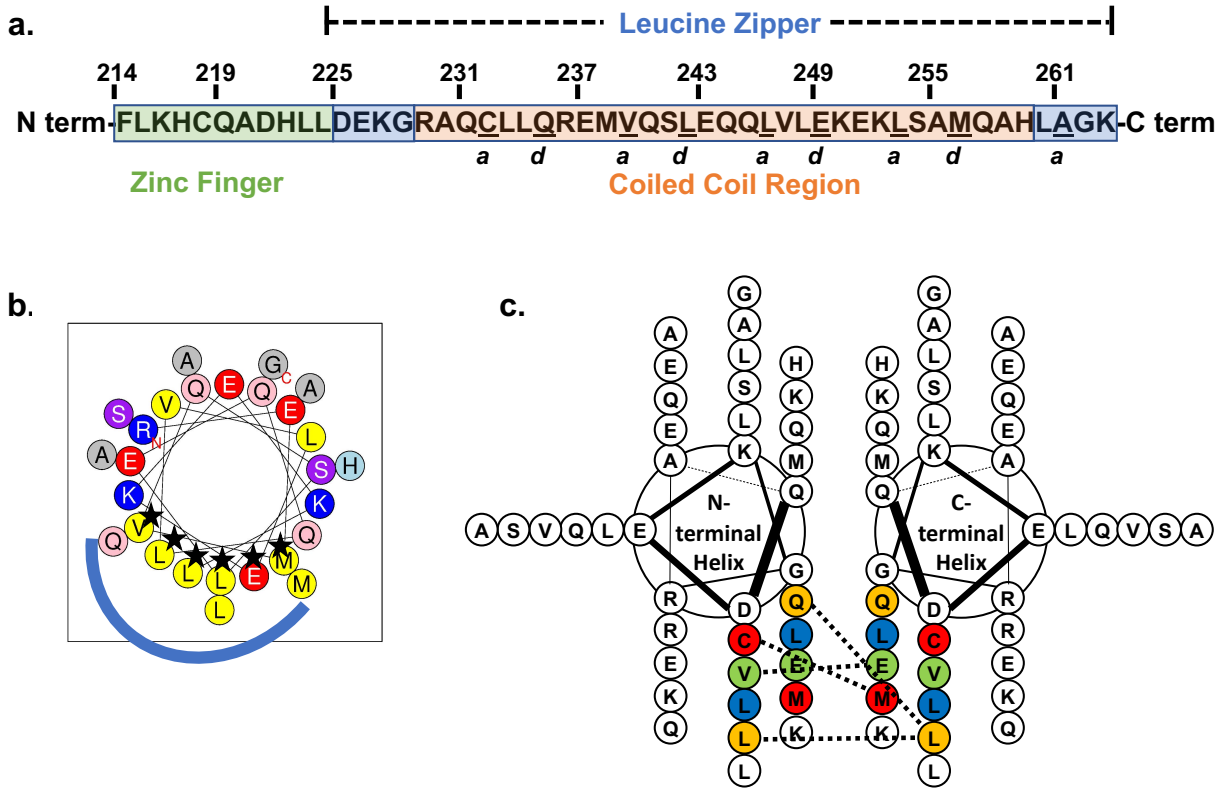

Figure 3.2: **Strategic design of staple positions for FOXP3-targeting SAHs in relation to the FOXP3:FOXP3 interface.** (a) Human FOXP3 sequence. Residues F214-K263 represent the entirety of a helix constituting the zinc finger (F214-L224; shown in green) and leucine zipper (D225-K263; shown in blue) regions. Within the leucine zipper, the coiled-coil (R229-H259; shown in orange), represents an area that is highly conserved between human and murine FOXP3. Underlined residues indicate a and d core residues, which bind each other on an identical anti-parallel helix, and are key contact points for homodimerization. The homodimerized FOXP3 helix is labeled according to the color codes in the sequence above. (b) Helical wheel plot shows the relative position of amino acids looking down the barrel of the helix. Positively charged amino acids (blue), negatively charged amino acids (red), and hydrophobic amino acids (yellow) are indicated. The more hydrophobic side of the helix constitutes the majority of the residues constituting the FOXP3:FOXP3 interacting face (blue half circle). Residues of a and d resonance are starred. (c) Two helical wheel plots are shown with residues of a and d resonance color-coded as defined above. Interactions between individual amino acids on oppositely-oriented FOXP3 helix are indicated by a dotted line.

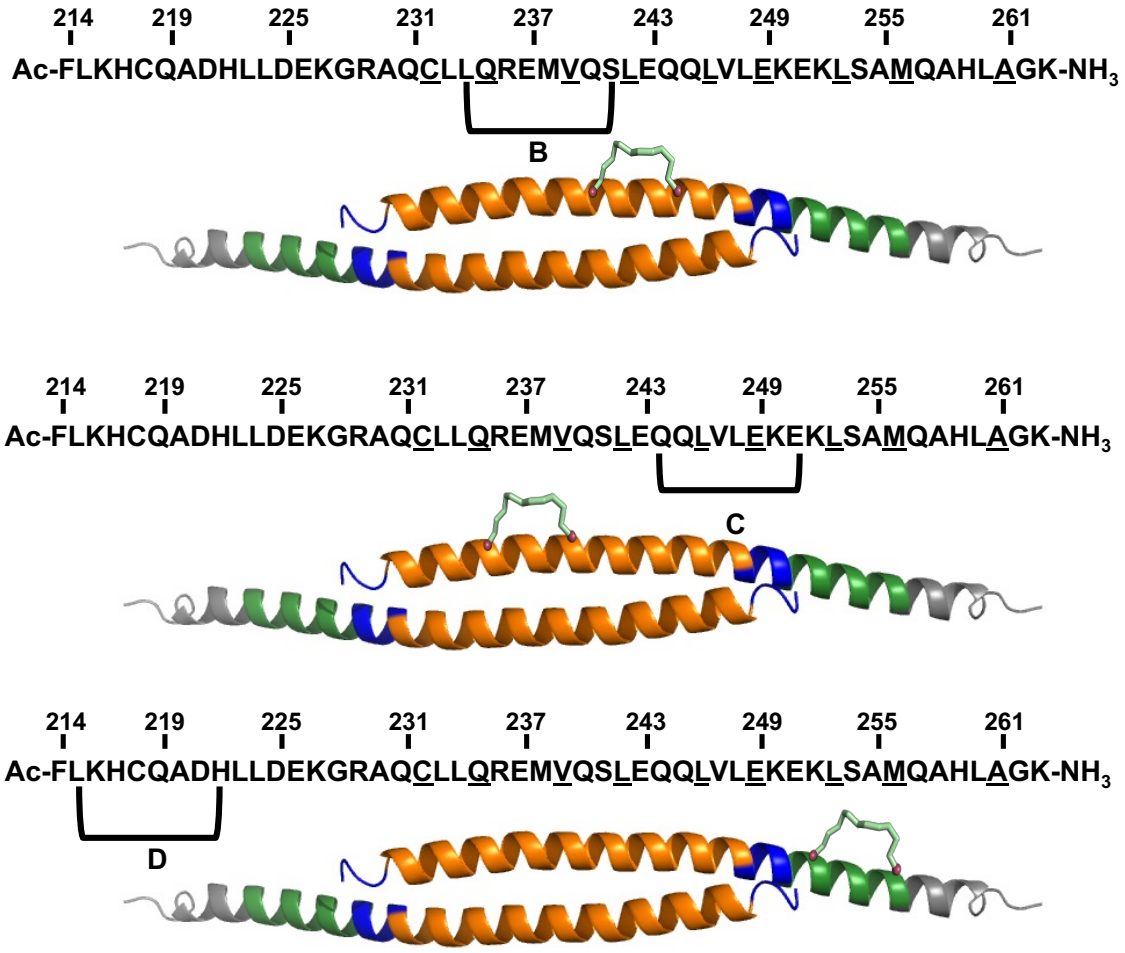

Figure 3.3: **Position of hydrocarbon staples screened in SAH-FOXP3 design.** Three staple positions (B, C, and D) were utilized in initial SAH design. Each of the staples faces away from the FOXP3 dimerization interface and are positioned either N-terminally, C-terminally, or centered with respect to the middle of the peptide length.

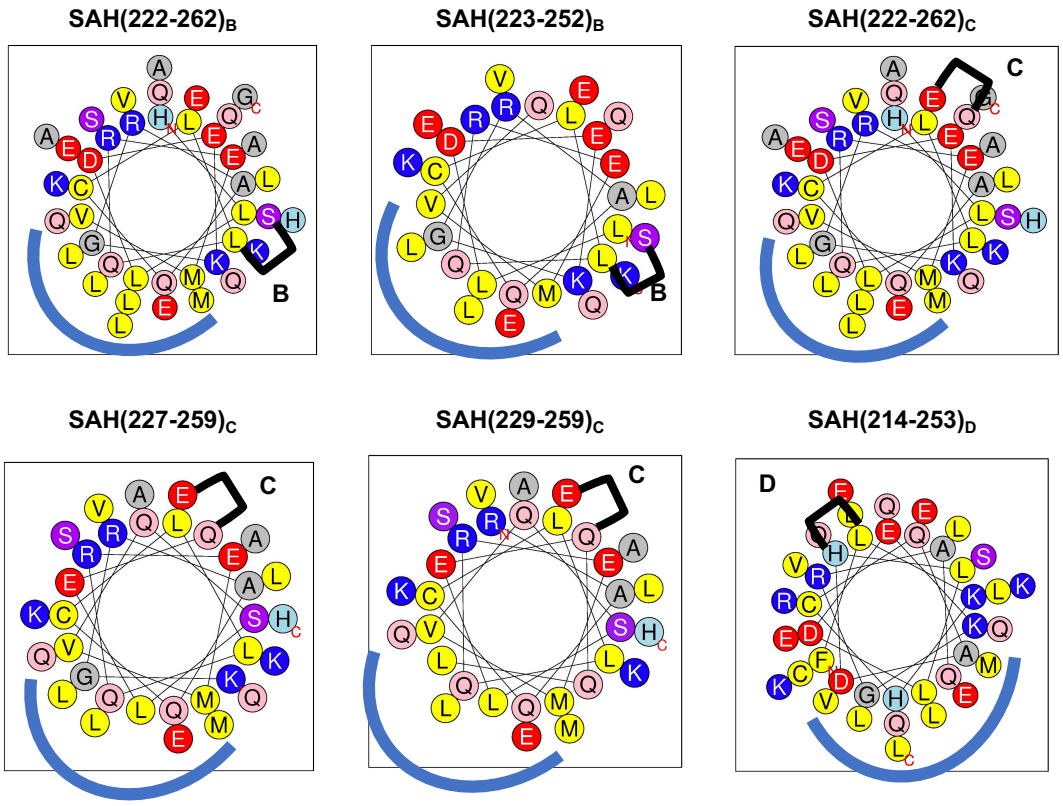

Figure 3.4: **Visualization of staple positions of SAHs targeting FOXP3 in relation to FOXP3:FOXP3 interface.** Helical wheel plots indicate the relative position of amino acids looking down the barrel of the helix. Positively charged amino acids (blue), negatively charged amino acids (red), and hydrophobic amino acids (yellow) are indicated. The more hydrophobic side of the helix constitutes the majority of the residues on the interacting face (blue half circle). Helical wheel plots for screened single-stapled FOXP3-targeting SAHs are shown with staple positions labeled and indicated. Staples are placed either opposite the interacting face to avoid interference, or immediately adjacent to this interacting area in an effort to extend the naturally occurring hydrophobic interface.

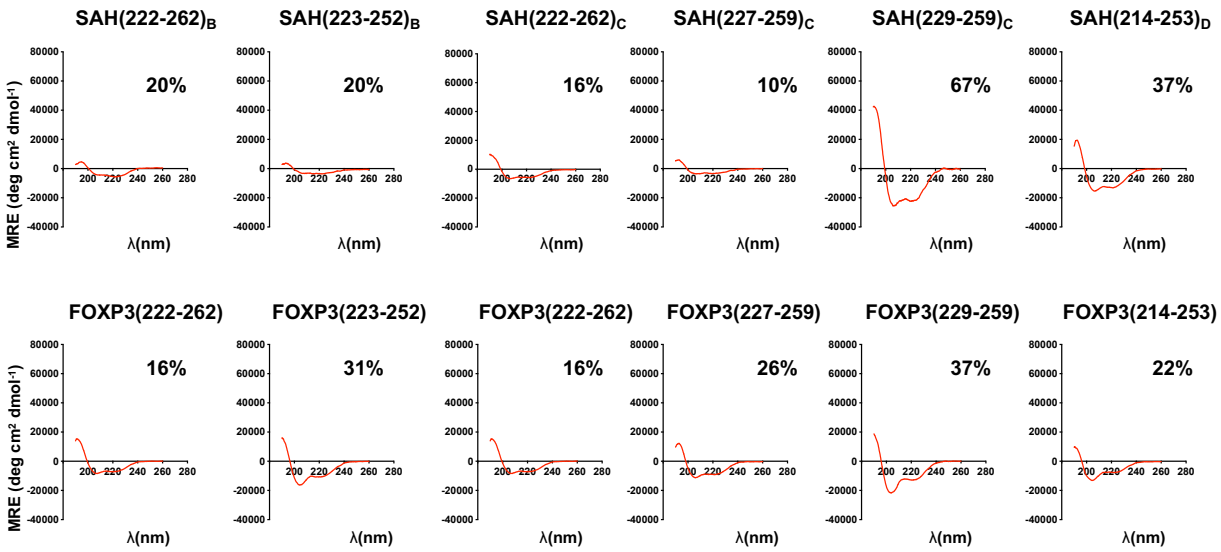

Figure 3.5: **Circular dichroism indicates sequence and staple position differences greatly impact α-helicity of SAHs.** Circular dichroism of FOXP3-targeting SAHs and native unstapled peptides demonstrate that sequence and staple position result in radically different measured α-helicities as calculated by the ratio of peaks at wavelength 208 and 222.

3.2 Helicity, peptide length, and staple position contribute to optimized SAH-FOXP3 target binding

Fluorescence polarization analysis was first used to assess binding affinities to two forms of truncated recombinant FOXP3: LZCC FOXP3 (T182-M337) and ΔN FOXP3 (T182-P431). Here, molecular binding events were measured in solution, allowing for determination of equilibrium constants reflective of specific receptor-target binding of protein and stapled peptide. While none of the native unstapled peptide controls bound LZCC FOXP3 or ΔN FOXP3, all SAHs bound LZCC FOXP3 and ΔN FOXP3 with affinities ranging from 84nM to 226nM (Figure 3.6a). Furthermore, relative affinities were conserved for most SAHs between binding of LZCC FOXP3 and ΔN FOXP3 indicating that the measured specificity was not restricted to the least complex target binding versions of FOXP3. SAHs and their corresponding native peptide controls were next tested for their ability to disrupt FOXP3 binding to cognate DNA using electrophoretic mobility shift assays (EMSAs). FOXP3 homodimerization is required for optimal FOXP3:DNA binding, primarily facilitated by recruitment of cofactors and subsequent formation of supramolecular complexes that enable DNA binding through direct engagement or stabilizing loop formation. Here, a dose titration of individual SAHs were mixed with recombinant ΔN FOXP3 and a well-defined consensus FOXP3 binding oligonucleotide A'GT25 probe (113). Dissociation or prevention of FOXP3 binding to DNA by SAH(229-259)C resulted in a greater dose-responsive inhibition of FOXP3:DNA binding compared to other SAHs (Figure 3.6b). The overall charges of all SAHs ranged from -1 to +2; one possible pitfall of using stapled peptides in EMSAs is the possibility of measuring false positive DNA:target protein dissociation secondary to non-specific binding of stapled peptide to free probe (202). This was not the case at the doses of SAH used in this assay as there were no differences in free probe availability despite charge differences between SAHs (Figure 3.6b). This is particularly interesting given that SAH(227-259)$_C$ has an overall charge of +2 and resulted in no apparent FOXP3:DNA dissociation. Thereby, staple

position rather than overall charge appeared to play are larger role in effective disruption of FOXP3:DNA binding, which also appeared to correlate with more a more stable α-helical secondary structure (Figure 3.5).

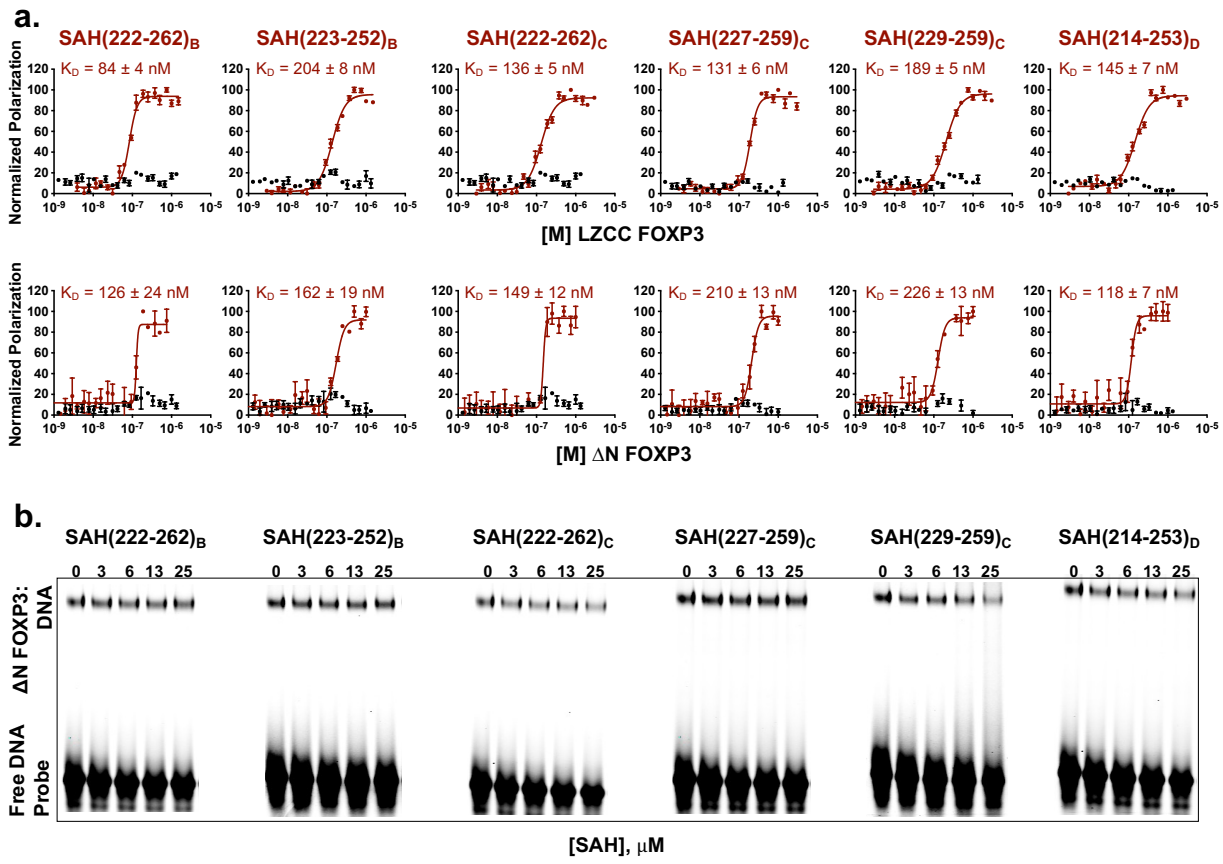

Figure 3.6: **Helicity, peptide length, and staple position contribute to optimized SAH-FOXP3 target binding.** (a) FPA binding curves of SAHs targeting FOXP3 (maroon) and their corresponding native unstapled peptide (black) bound to either LZCC FOXP3 or ΔN FOXP3. SAHs bind truncated FOXP3 with a high degree of specificity (K_D values in the nanomolar range); native unstapled peptides are unable to bind truncated FOXP3 constructs. (b) EMSAs demonstrate that SAHs with staple position 'C' are best able to disrupt FOXP3 binding to cognate DNA. Native unstapled peptides minimally binding even at high concentrations.

Prior to investigating further SAH optimization, all SAHs were next tested to ensure that, despite their amphipathic and helical nature, they could be incubated with cells and

not cause non-specific plasma membrane disruption or induce apoptosis. Indeed, we measured no cytoplasmic lactate dehydrogenase (LDH) release above background for any SAH tested at the 0-10µM dosing range in treated murine thymocytes (Figure 3.7a) nor did we measure increased apoptosis or loss of membrane integrity compared to vehicle-treated cells as measured by annexin V/propidium iodide staining (Figure 3.7b). Cumulatively, these results indicate that a combination of sequence, staple position, and peptide length determine optimal α-helicity, that staple position is critical for on-target binding to FOXP3, and that SAHs are not overtly toxic to T cells.

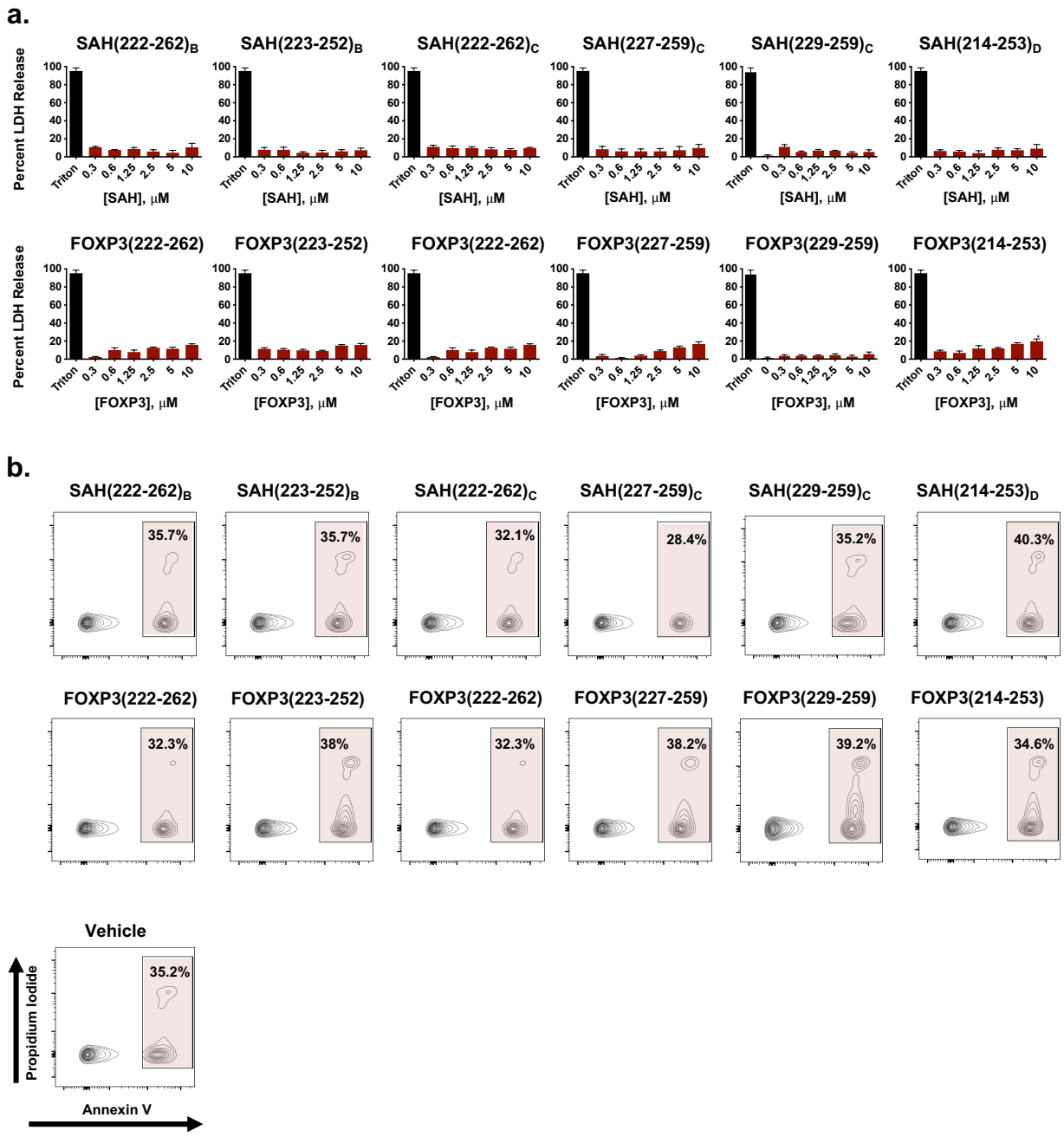

Figure 3.7: **SAHs targeting FOXP3 are non-toxic to T cells.** Absence of nonspecific murine murine thymocyte cell-death as measured by (a) LDH release (normalized to vehicle) and (b) apoptosis as measured by Annexin V (APC) and Propidium Iodide (PE) staining via flow cytometry in T cells treated with 5μM peptide. Vehicle treated controls are shown below their stapled analogs. All compounds exhibited similar levels of apoptosis as vehicle treated controls.

3.3 Double-stapling of peptides modeled after SAH(229-259)$_C$

We selected SAH(229-259)$_C$ for further development based in part on its solubility profile in tissue culture media, overall charge, increased α-helicity compared to its unstapled analog, encouraging binding to recombinant FOXP3 isoforms, and its ability to dose-dependently block the interaction between dimerized FOXP3 and cognate DNA. Additionally, unlike most of the other SAHs tested, SAH(229-259)$_C$ covers more core a and d resonant amino acids and nearly the entire leucine zipper coiled coil region of FOXP3, without approaching the zinc finger region. We next wondered if insertion of additional staples N-terminally to the 'C' position would increase binding to FOXP3 via induction of increased α-helicity or if increased rigidity would decrease its interaction with immobilized FOXP3 (184). We therefore synthesized additional SAHs in the likeness of SAH(229-259)$_C$, namely SAH(229-259)$_{AC}$ and SAH(229-259)$_{BC}$ with second staple positions in the 'A' (a.a. 233 and 240) and 'B' (a.a. 234 and 241) positions (Figure 3.8). We also designed a negative control point mutant that incorporate the single 'C' staple position, SAH(229-259)$_{C(K252D)}$, based on a known IPEX mutation and critical contact point for FOXP3 homodimerization and function (114) (Figure 3.9a,b). Similar to our previous design strategy, staples were placed either opposite or adjacent to, but not within the interaction interface (Figure 3.10a). We observed that SAH(229-259)$_{BC}$ had slightly improved α-helicity (74%) relative to the parent SAH(229-259)$_C$ (67%) as measured by circular dichroism (Figure 3.10b). However, supporting our previous data, all SAH(229-259)$_C$ variants had significantly improved α-helicity relative to previously tested single-stapled SAHs, ranging from 60-80% compared to 10-37% respectively and continued to exhibit greatly improved α-helicity compared to their native, unstapled peptide controls. While the double-stapled SAHs had an identical overall charge compared SAH(229-259)$_C$, they had slightly different PIs. Furthermore, double-stapled peptides had improved resistance to proteinase K in *in vitro* proteolytic degradation assays (Figure 3.11). While it has been reported that singly stapled peptides are monomeric at concentrations used for CD and

FPA, differences in solubility or aggregation of SAH(229-259)$_{AC}$ and SAH(229-259)$_{BC}$ at higher concentrations compared to SAH(229-259)$_{C}$ and SAH(229-259)$_{C(K252D)}$ cannot be ruled out (184).

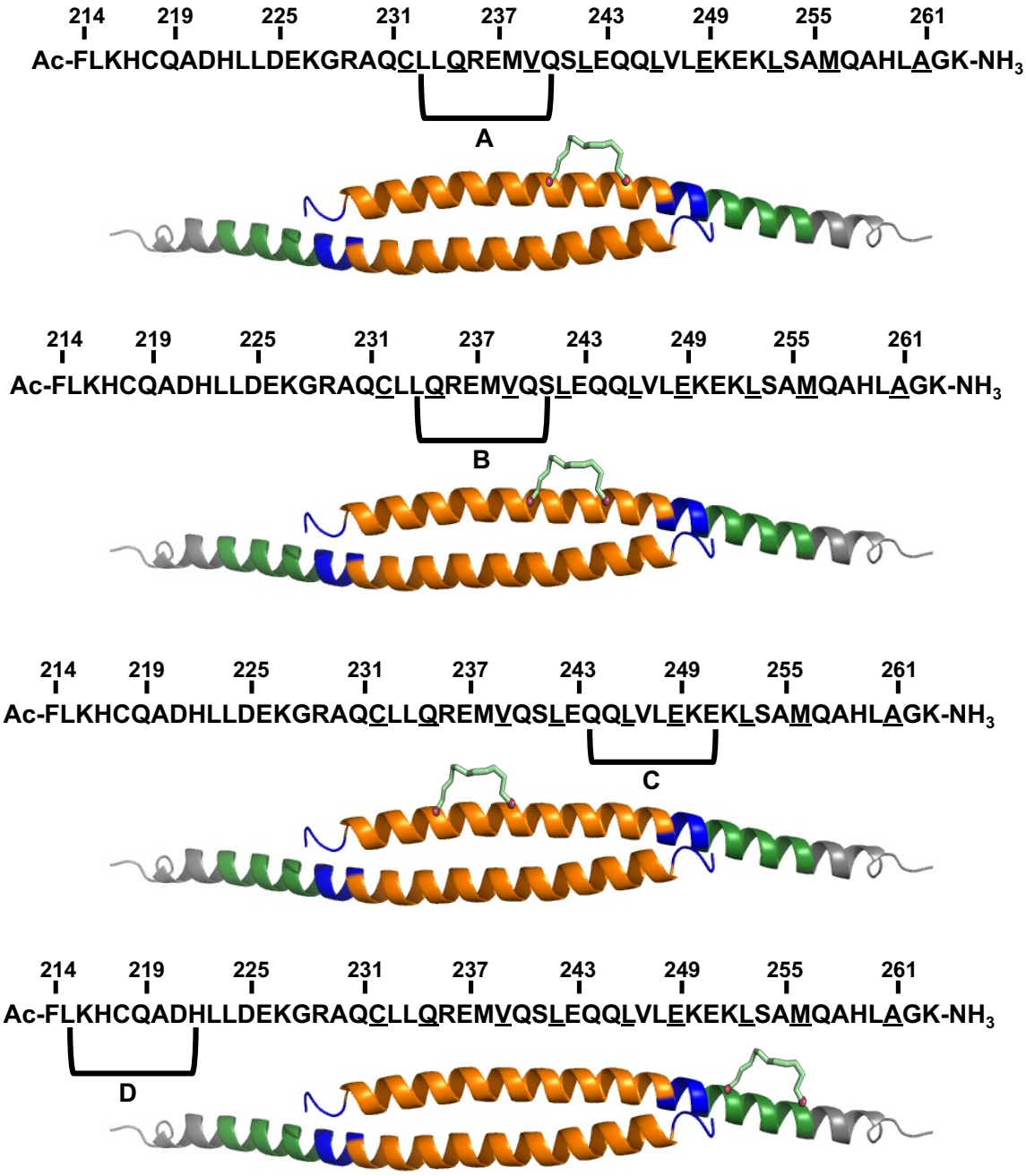

Figure 3.8: **Staple positions tested in analogs of SAH(229-259)$_C$.** Four staple positions (A, B, C, and D) were utilized in SAH design. Each of the staples faces away from the dimerization interface and are positioned either N-terminally, C-terminally, or centered with respect to the middle of the peptide length. A and B staple positions are used specifically in the double-stapled iterations.

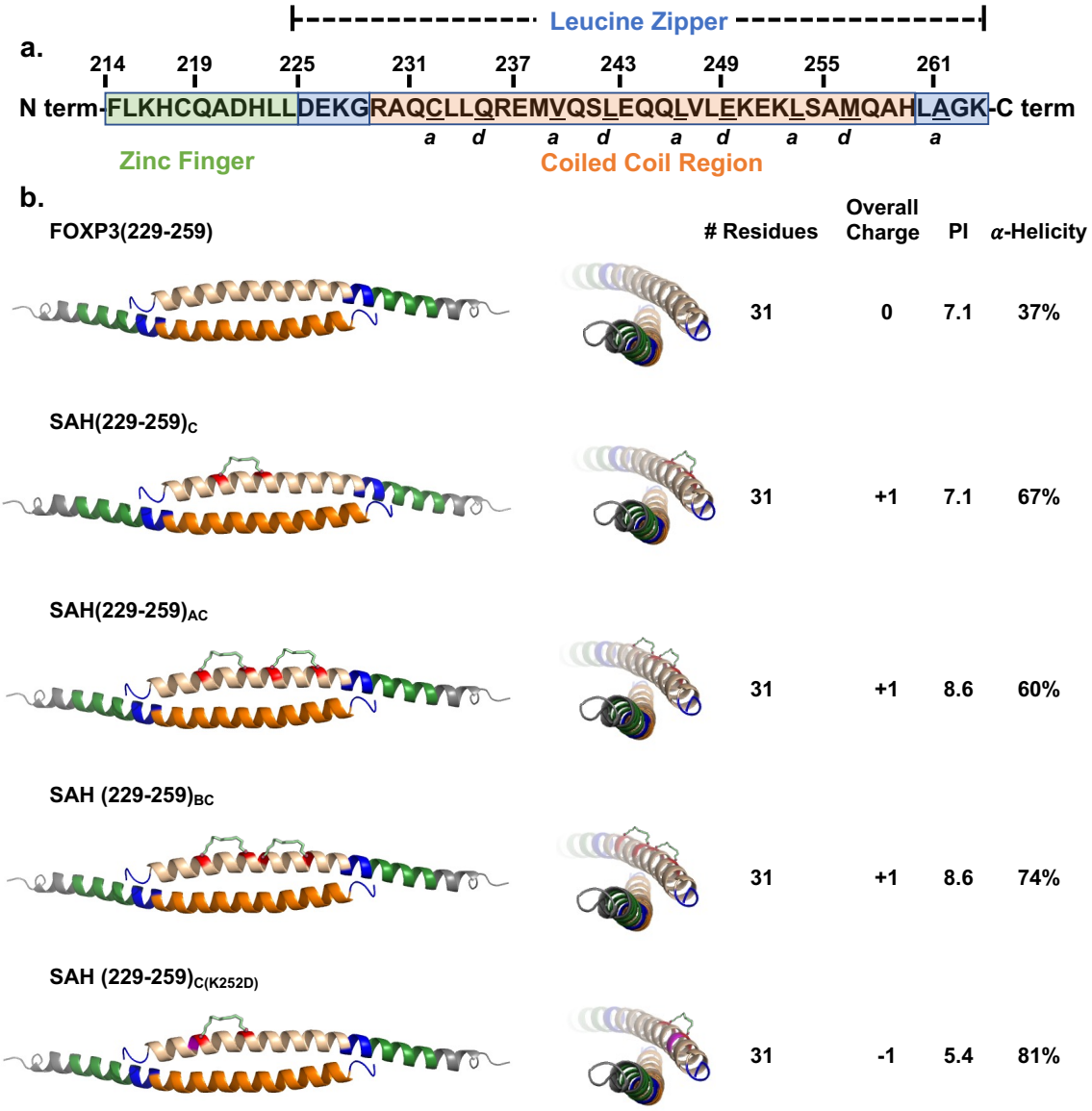

Figure 3.9: **Double stapling of peptides modeled after SAH(229-259)$_C$.** (a) Human FOXP3 sequence. Residues F214-K263 represent the entirety of a helix constituting the zinc finger (F214-L224; shown in green) and leucine zipper (D225-K263; shown in blue) regions. Within the leucine zipper, the coiled-coil (R229-H259; shown in orange), represents an area that is highly conserved between human and murine FOXP3. Underlined residues indicate a and d core residues, which bind each other on an identical anti-parallel helix, and are key contact points for homodimerization. The homodimerized FOXP3 helix is labeled according to the color codes in the sequence above. (b) Design strategy for SAHs modeled after SAH(229-259)$_C$. SAHs share sequence and length, differing in position and number of staples. These changes influence overall charge, PI, and α-helicity. Each 3-dimenisional structure shown is based on the crystal structure (PDB: 4I1L); the upper helix represents each SAH (shown in tan) with hydrocarbon staple (end residues shown in red)

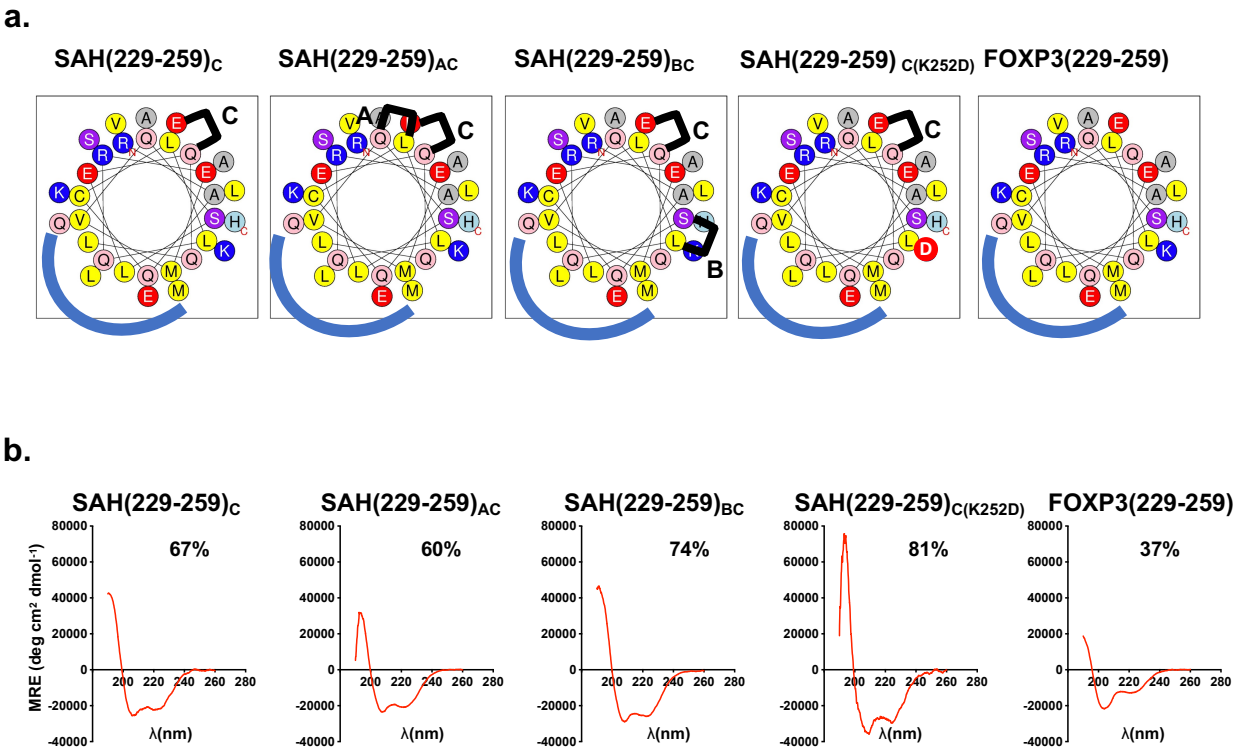

Figure 3.10: **Characterization of SAH(229-259)$_C$ iterations.** (a) Helical wheel plots show the relative position of amino acids looking down the barrel of the helix. Positively charged amino acids (blue), negatively charged amino acids (red), and hydrophobic amino acids (yellow) are indicated. The more hydrophobic side of the helix constitutes the majority of the residues on the interacting face (blue half circle). Helical wheel plots for SAH(229-259)$_C$ analogs are shown with staple positions labeled and indicated. Staples are placed either opposite the interacting face to avoid interference, or immediately adjacent to this interacting area in an effort to extend the naturally occurring hydrophobic interface. (b) Circular dichroism of SAH(229-259)$_C$ iterations demonstrate that double-stapling alone does not necessarily confer improved α-helicity as measured by the ratio of peaks at wavelength 208 and 222.

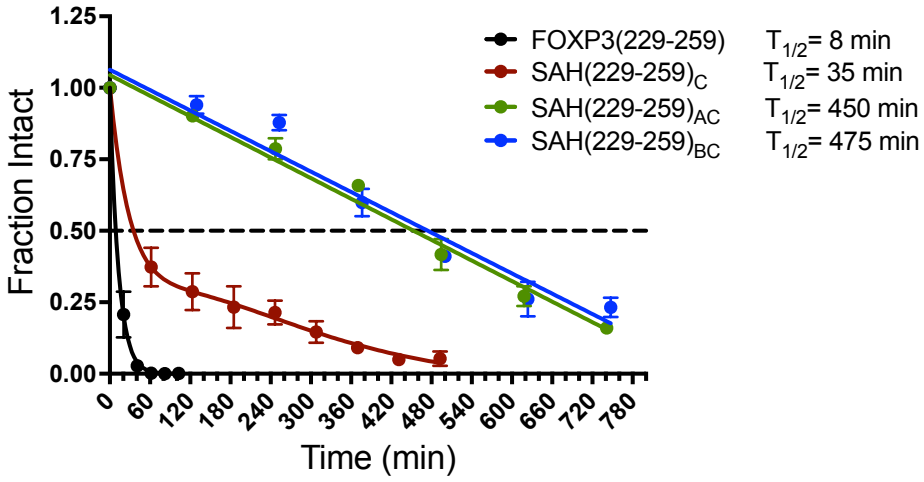

Figure 3.11: **Double stapled peptides are resistant to proteolytic degradation.** Both double stapled peptides SAH(229-259)$_{AC}$ and SAH(229-259)$_{BC}$ have a ∼50 fold increase in resistance to proteinase K degradation compared to native unstapled peptide. Single stapling confers some ∼4 fold improvement in proteolytic degradation, but still has a relatively fast half-life similar to native unstapled peptide.

3.4 Biochemical characterization of SAH(229-259)$_C$ constructs

SAH(229-259)$_C$, SAH(229-259)$_{AC}$, and SAH(229-259)$_{BC}$ bound to LZCC FOXP3 and ΔN FOXP3 with affinities ranging from 98nM – 204nM, as measured by FPA (Figure 3.12a). Unstapled FOXP3(229-259)$_{Native}$ and the point mutant control SAH(229-259)$_{C(K252D)}$ showed no binding to either FOXP3 isoform, reinforcing the importance of inherent helicity and sequence specificity for the SAH:FOXP3 interaction. Here, the addition of two hydrocarbon staples maintained similar high affinity, on-target binding to FOXP3 in solution. Furthermore, SAH(229-259)$_C$ and SAH(229-259)$_{AC}$ dose-dependently inhibited FOXP3 binding to a cognate oligonucleotide, while SAH(229-259)$_{BC}$ resulted in more abrupt blocking of FOXP3:DNA binding. The point mutant and native peptide controls showed no effect (Figure 3.12b). Again, none of the SAH(229-259)$_C$ derivatives, irrespective of overall charge, showed any non-specific binding to the DNA probe. The natural FOXP3:FOXP3 leucine zipper interaction is thought to be rather transient and flexible. This is supported by data

showing that recombinant leucine zippers of FOXP3 must be chemically crosslinked in vitro to observed durable homodimerization (114). Therefore, SPR was next performed to orthogonally determine if the binding of SAHs could be measured using a solid support approach and to determine if double-hydrocarbon stapling limited stepwise, dose-dependent binding to FOXP3 (Figure 3.12c). We hoped that an understanding of binding changes across truncated and full-length immobilized forms of FOXP3 would be additionally informative for advancing candidate SAHs capable of drugging this dynamic PPI in a more biologically-relevant cellular system. Single-stapled SAH(229-259)$_C$ dose-dependently bound to all forms of FOXP3 with the largest dynamic range, reflecting its more stable binding to FOXP3 compared to the double-stapled SAHs. The shape of the response curves to each FOXP3 construct indicated two-step, target specific binding with fast on/off rates as measured by rapid decay in dissociations (Figure 3.12c). Here, double-stapling did not improve the stability of SAH binding to FOXP3. While SAH(229-259)$_{AC}$ also bound all forms of FOXP3, the magnitude of the interaction, as measured in response units, was approximately half that of SAH(229-259)$_C$. The shape of the curves were also more gradual in slope both in ascent and descent suggesting that while less total SAH bound, the SAH(229-259)$_{AC}$ that did bind had stronger avidity when compared to SAH(229-259)$_C$. Despite promising results in EMSA testing, SAH(229-259)$_{BC}$ had no real measurable binding to immobilized FOXP3, similar to unstapled FOXP3(229-259)$_{Native}$. SAH(229-259)$_{C(K252D)}$ dose-dependently bound full-length FOXP3 but had a much lower dose-response compared to that of SAH(229-259)$_C$ (Figure 3.12c). Thus, SAH(229-259)$_C$ appeared to strike an optimal balance of helicity and target binding in vitro and fulfilled a dual requirement for flexibility and specificity for binding as has been measured for other coiled-coil interactions (203; 204; 205).

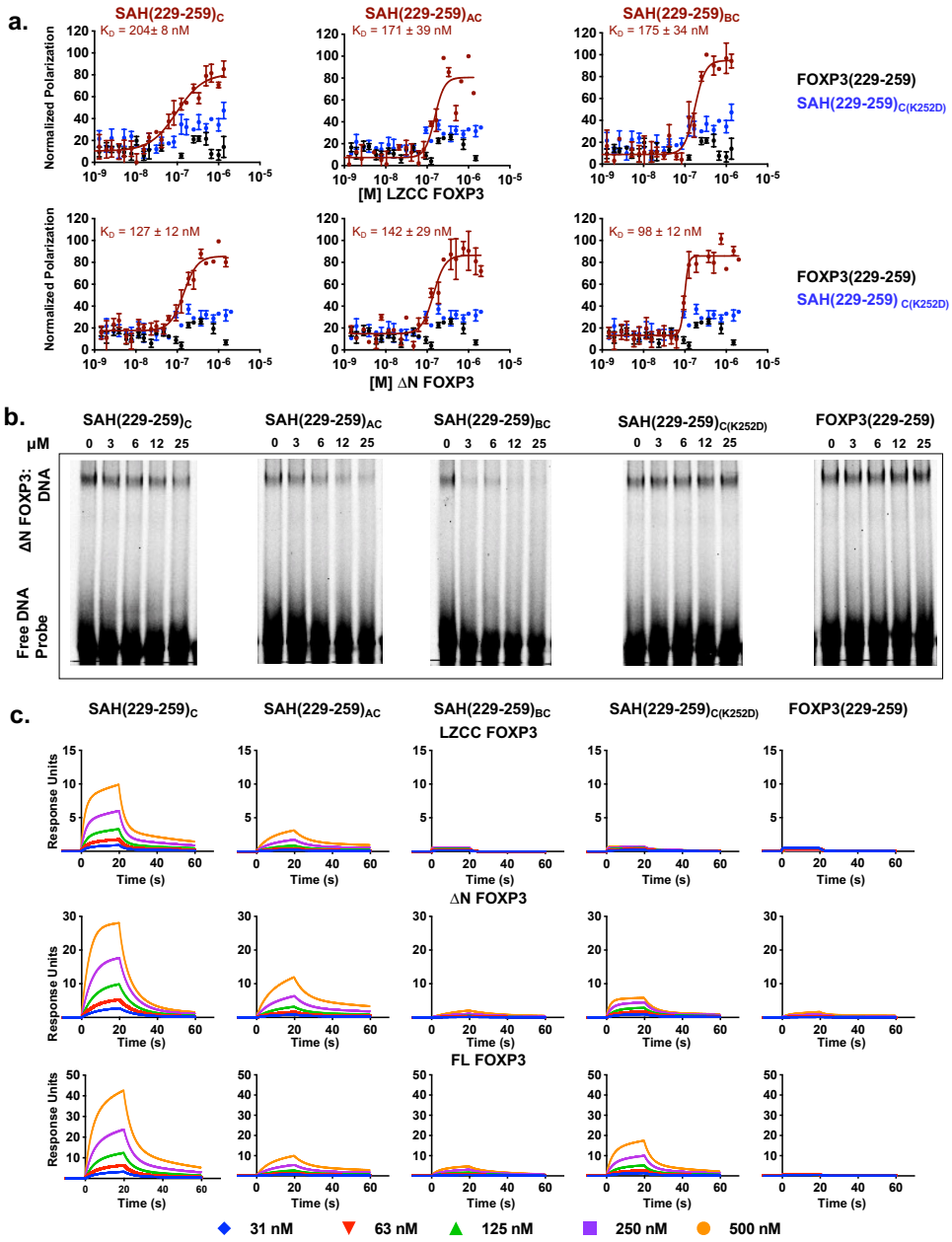

Figure 3.12: **Biochemical characterization of SAH(229-259)$_C$ constructs.** (a) FPA binding curves of SAHs (maroon), their point mutant control (blue), and native unstapled peptide (black) bound to either LZCC FOXP3 or N FOXP3. SAHs show specific binding to protein (K_D in the nanomolar range). Point mutant control and native unstapled peptides are unable to bind either FOXP3 construct. (b) Reduction in ΔN FOXP3 binding to consensus DNA was observed following treatment with SAH(229-259)$_C$ derivatives but not native peptide or point mutant control as measured by EMSAs. (c) SPR of SAHs show variance in affinity and binding kinetics between single- and double- stapled peptides against LZCC FOXP3, ΔN FOXP3, and full-length FOXP3.

3.5 Lead SAH(229-259)$_C$ constructs are cell-permeable and non-toxic to T cells

The ability of SAHs to penetrate cells is well established (202; 206; 207; 208). Staple placement, α-helicity, and charge have been shown to confer differences between stapled peptides in their ability to interact with plasma membranes, directly penetrate cells, and traffic through cells via microvesicles or endosomes (202; 206; 207). Live cell confocal microscopy found that all SAH(229-259)$_C$ compounds localized to the cytosol and nuclei of human *in vitro* induced Tregs (Figure 3.13a) and murine T cells (data not shown). Interestingly, staple position appeared to, at least in part, influence the intracellular patterning of individual SAHs. Treatment of cells with SAH(229-259)$_C$, SAH(229-259)$_{AC}$, and SAH(229-259)$_{C(K252D)}$ resulted in a diffuse cellular staining while SAH(229-259)$_{BC}$ resulted in more punctate patterning, suggesting its cytoplasmic aggregation or vesicular entrapment compared to SAH(229-259)$_C$, SAH(229-259)$_{AC}$, and SAH(229-259)$_{K252D}$. In contrast, unstapled FOXP3(229-259)$_{Native}$ peptide showed no ability to enter or be retained in treated cells. FOXP3 is known to traffic from the cytosol and into the nucleus through binding additional co-factors, making these patterns biologically relevant (209). Importantly, human iTregs were morphologically unaltered following SAH treatment and maintained their round shape and high nuclear to cytoplasmic ratio. Treatment of murine thymocytes with these SAHs at a wide dose titration resulted in no LDH release or apoptotic cell death above background control-treated cells (Figure 3.13b, c).

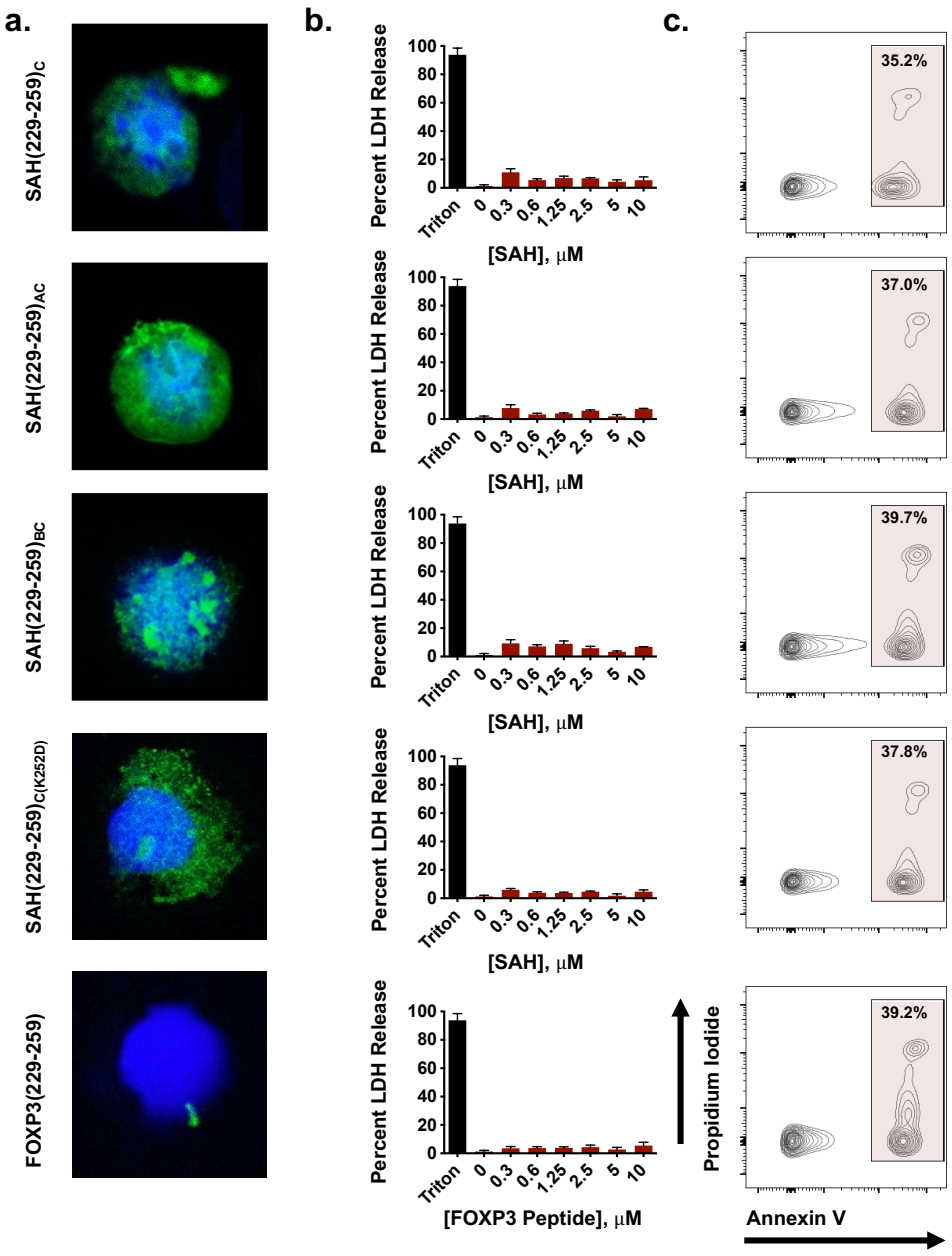

Figure 3.13: **Lead SAH(229-259)$_C$ constructs are cell-permeable and non-toxic to T cells** (a) Cellular uptake by human iTregs incubated with FITC-labeled SAHs. Hoechst 33342 was used as a nuclear dye. SAH uptake exhibits differing patterns, ranging from diffuse to more aggregated throughout the cell, including the nuclei and cytoplasm. Absence of disruptive membrane lysis by (b) lack of non-specific murine thymocyte cell death as measured by LDH release (normalized to vehicle) and (c) apoptosis as measured by Annexin V (APC) and Propidium Iodide (PI) staining as measured by flow cytometry.

3.6 Single-stapled SAH(229-259)$_C$ induces greater gene and protein expression alterations in Tregs compared to double stapled SAHs

We next sought to determine if single- and double-stapled SAH(229-259)$_C$ constructs could perturb normal FOXP3-regulated genetic changes in Tregs through analysis of key FOXP3 transcriptional targets. Consistent with FOXP3 inhibition, SAH (229-259)$_C$ resulted in a dose-dependent decrease in *Il2rα* and increase in *Foxp3* mRNA expression in Tregs but not in conventional CD4$^+$ T cells (Tcons) (Figure 3.14a, b). Treatment with the double-stapled SAH(229-259)$_{AC}$ and SAH(229-259)$_{BC}$ resulted in less significant changes in *Il2rα* and *Foxp3* expression despite their equivalent extracellular ability to bind FOXP3 and incur FOXP3:FOXP:DNA dissociation extra-cellularly, highlighting the importance for multimodal and orthogonal testing of this class of therapeutics (Fig 3.12b). As predicted, no changes were observed in cells treated with the single-stapled SAH(229-259)$_{C(K252D)}$ point mutant control, confirming on-target binding of SAH (229-259)$_C$. These results support superior intracellular on-target efficacy of single-stapled SAH(229-259)$_C$ compared to its double-stapled counterparts. We next wanted to determine if these genetic changes would extend to protein-level alterations in *ex vivo* expanded Tregs. Reflecting our observed transcriptional changes, dose-dependent decreases in IL2Rα and increases in FOXP3 protein expression were measured in SAH(229-259)$_C$ treated Tregs and not in double-stapled or point mutant control peptides (Figure 3.14c). Expanded Tcons showed no changes in IL2Rα or FOXP3 protein levels following treatment with any SAH at equivalent doses (Figure 3.14d). The changes in FOXP3 expression in treated Tregs is particularly intriguing as FOXP3 is known to bind its own promoter and participate in the regulation of its own gene expression (115; 210).

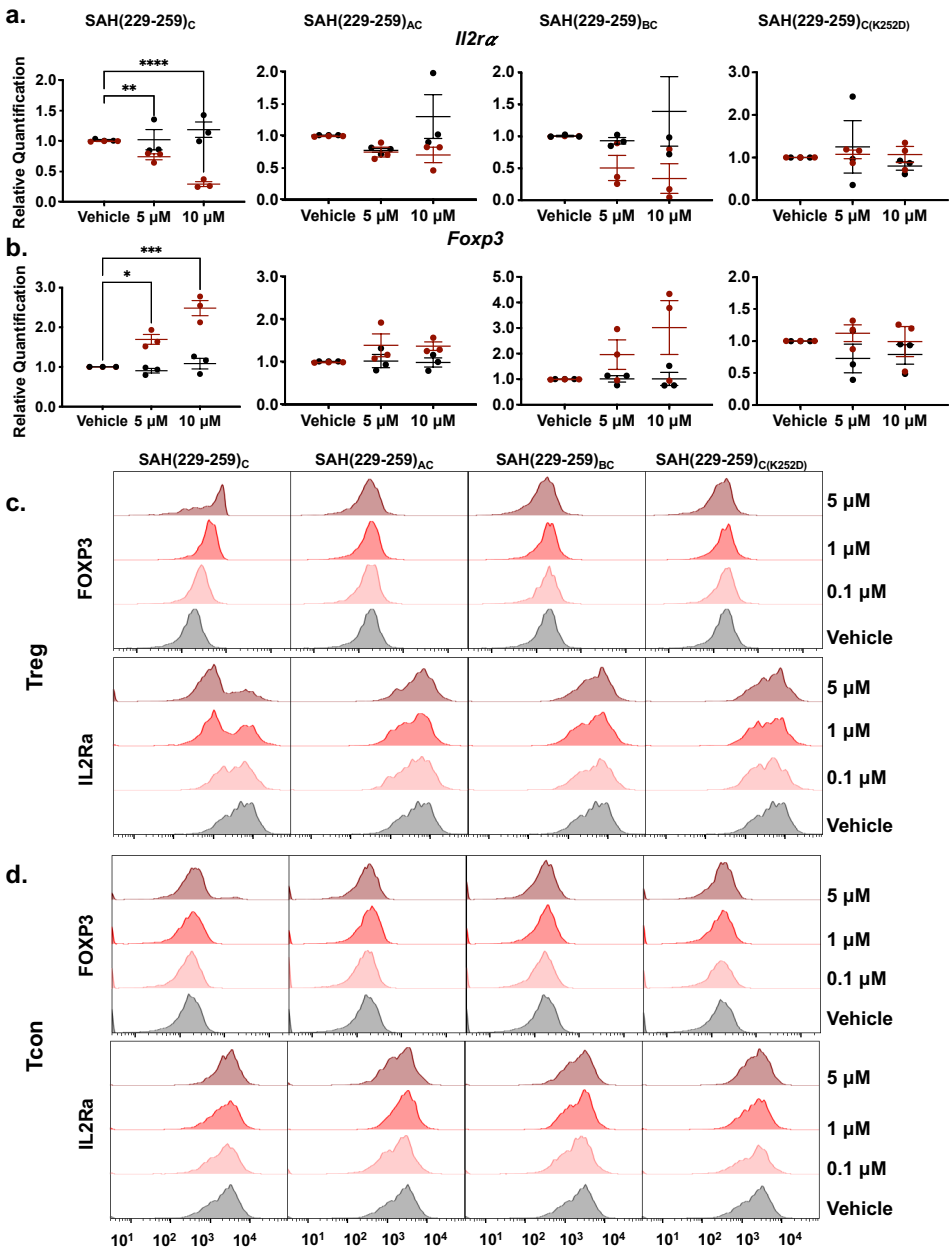

Figure 3.14: **Single-stapled SAH(229-259)$_C$ induces greater gene and protein expression alterations in Tregs compared to double stapled SAHs** SAH(229-259)$_C$ dose dependently altered transcript expression of (a) *Il2rα* and (b) *Foxp3* in Tregs (red) but not Tcons (black) isolated from C57/BL6$^{FOXP3-IRES-GFP}$ mice measured by qRT-PCR. Double stapled SAHs trended toward similar expression patterns while point mutant and native peptide controls didn't alter transcript expression in Tregs or Tcons. SAH(229-259)$_C$ treatment dose-dependently altered IL2Rα and FOXP3 protein in Tregs (c) but not Tcons (d) as measured by flow cytometry. Asterisks indicate p less than 0.05 determined by an ordinary one-way Anova with multiple comparisons. * $p < 0.05$, ** $p < 0.005$, **** $p < 0.0005$

3.7 SAH(229-259)$_C$ results in greater dampening of Treg-mediated immune suppression compared to double-stapled SAHs

Given that SAH(229-259)$_C$ resulted in greater Treg transcript and protein expression compared to its double-stapled iterations, we next assessed whether similar differences would be reflected in their ability to induce dysfunctional Treg-mediated suppression *ex vivo*. To measure this, we assessed whether pre-treatment of Tregs with SAH(229-259)$_C$ constructs would inhibit proliferation of stimulated Tcons in culture. Pre-treatment of Tregs with single and double stapled SAH(229-259)$_C$ peptides dampened Treg-mediated ability to control target proliferation over the course of seven generations of proliferation (represented by individual peaks in each graph) compared to vehicle-treated Tregs during a 72 hour period of stimulation (Figure 3.15). However, SAH(229-259)$_C$ exerted the greatest effect by completely inhibiting Treg-mediated suppression of target proliferation when mixed at a 1:1 ratio. Stark contrasts exist not only when comparing total proliferation relative to a vehicle-treated control, but also in comparing individual generations. SAH(229-259)$_C$ treatment resulted in the greatest proportion of target cells in later generations. Here, Tcon proliferation incubated with SAH-treated Tregs equaled that of Tcons incubated in the absence of Tregs (90.7% and 89.8%, respectively) while Tcons incubated with untreated Tregs had far less proliferation (56.5%) reflecting normal Treg suppressive functioning. While SAH(229-259)$_{AC}$ and SAH(229-259)$_{BC}$ also inhibited Treg-mediated suppression (74.1% and 79.1% proliferation, respectively), they were nearly 13-20% less effective than SAH(229-259)$_C$. Importantly, Tregs pre-treated with SAH(229-259)$_{C(K252D)}$ point mutant control and unstapled peptide showed no ability to prevent Treg-mediated suppression of Tcon proliferation (Figure 3.15). In all cases, the SAH-induced inhibition of Tregs was most measurable when Tregs were co-cultured with Tcons at equal ratios (1:1), though differences between SAH-treated

and vehicle-treated Tregs at higher titrations of Tregs:Tcons, indicated that there was measurable potency and durability to SAH-induced Treg dysfunction. While SAH(229-259)$_{AC}$ and SAH(229-259)$_{BC}$ resulted in less Treg transcriptional and protein expression changes compared to SAH(229-259)$_{C}$ in shorter-term cultures (6 hours), they were able, albeit to a lesser degree, to still negatively impact Treg-mediated suppressive function following longer-term incubation (72 hours). This corresponded positively to our previous data showing that double-stapled SAHs resulted in muted trends in transcript expression compared to SAH(229-259)$_{C}$ at equivalent doses. Collectively, these data indicate that specific inhibition of FOXP3 is feasible using stapled peptides resulting in reduced acute Treg suppressive function. These results also highlight the importance of vetting candidate SAHs in a wide range of biochemical and functional assays to advance the most promising compounds.

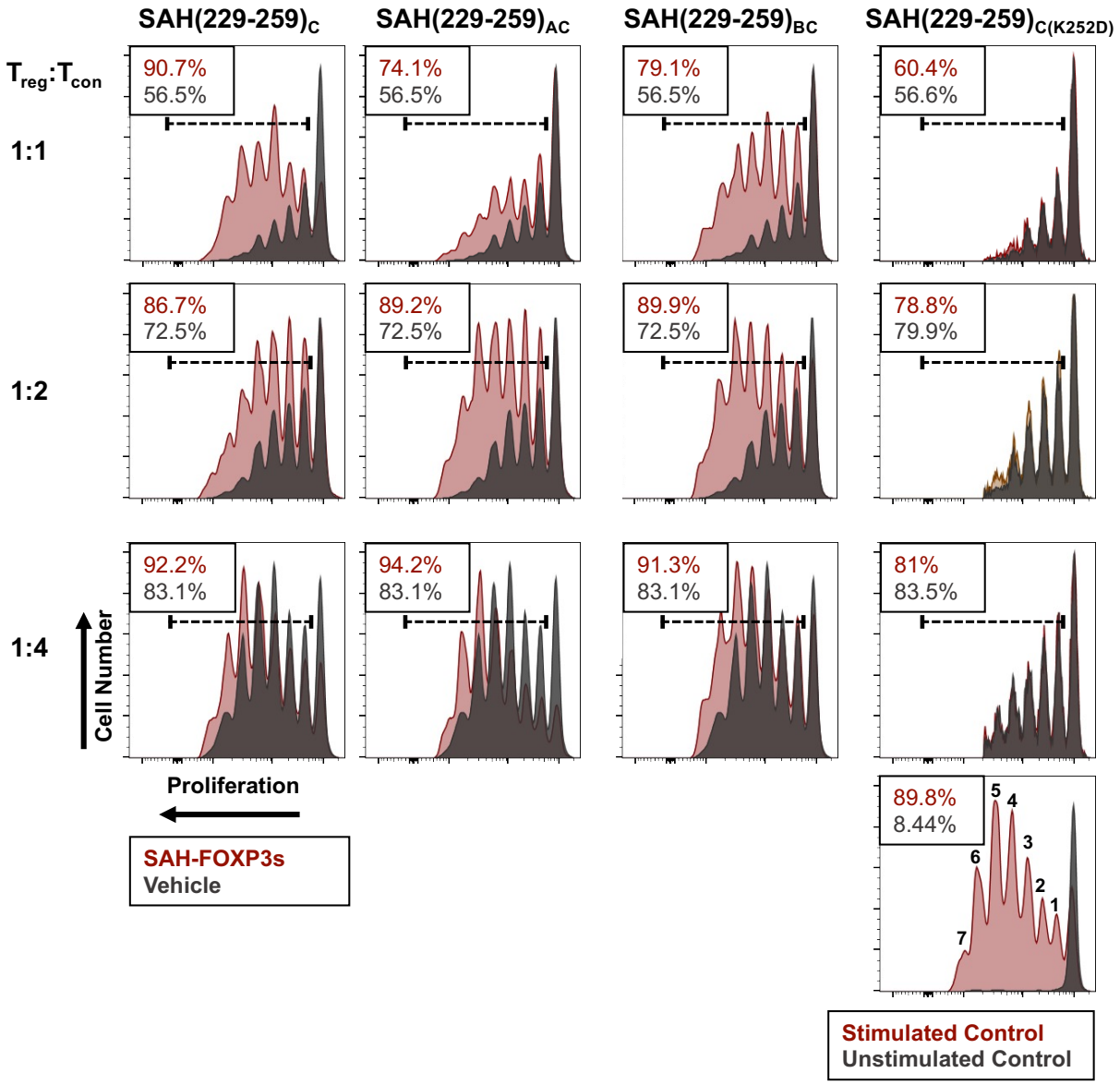

Figure 3.15: **SAH(229-259)$_C$ results in greater dampening of Treg-mediated immune suppression compared to double stapled SAHs** *Ex-vivo* suppression assays demonstrate dampened suppressive capacity of Tregs treated with SAHs (maroon) compared to vehicle (black) to inhibit target cell proliferation at a series of cell titrations. SAH(229-259)$_{C(K252D)}$ had no effect on Treg suppressive function. Respective Tcon target proliferation is listed in top corner of each plot. Stimulated and unstimulated target cell controls with numbered generations of cells are shown in the bottom right histogram.

3.8 SAH(229-259)$_C$ alters Treg mRNA expression *in vivo*

Based on correlation between target binding, genetic and protein alterations, intracellular localization, and functional Treg inhibition, we next tested the ability of SAH(229-259)$_C$ to alter Treg and Tcon expression patterns *in vivo*. Mice were treated with 4 daily intraperitoneal (i.p.) injections of SAH(229-259)$_C$ (Figure 3.16a). Twenty-four hours following the final dose, Tregs and Tcons were sorted and subjected to comprehensive transcriptional profiling. Gene set enrichment analysis (GSEA) found that Tregs from SAH(229-259)$_C$ treated animals had expression profiles that mirrored murine Foxp3-deficient hybridomas (211) (Figure 3.16b). Further, GSEA also indicated that the transcriptional profiles of Tregs from SAH(229-259)$_C$ treated animals were more similar to induced rather than natural Tregs (51), Tcons rather than Tregs (212), and activated Tcons as opposed to activated Tregs (51). Collectively, these data demonstrated SAH(229-259) $_C$ induced transcriptional changes in Tregs that made them inherently less like natural, thymic-derived Tregs and more like Tcons. Interestingly, Tcons isolated from SAH(229-259)$_C$ - treated animals had enrichment of gene sets corresponding to pro-inflammatory responses and T cell activation ((213), Biocarta, Hallmark) (Figure 3.16c). These expression patterns support that treatment with stapled peptides targeting FOXP3 are capable of inducing transcriptional reprogramming in Tregs, at least in the short-term, which may, in turn, induce a bystander T cell pro-inflammatory state as has been measured in patients with Treg dysfunction.

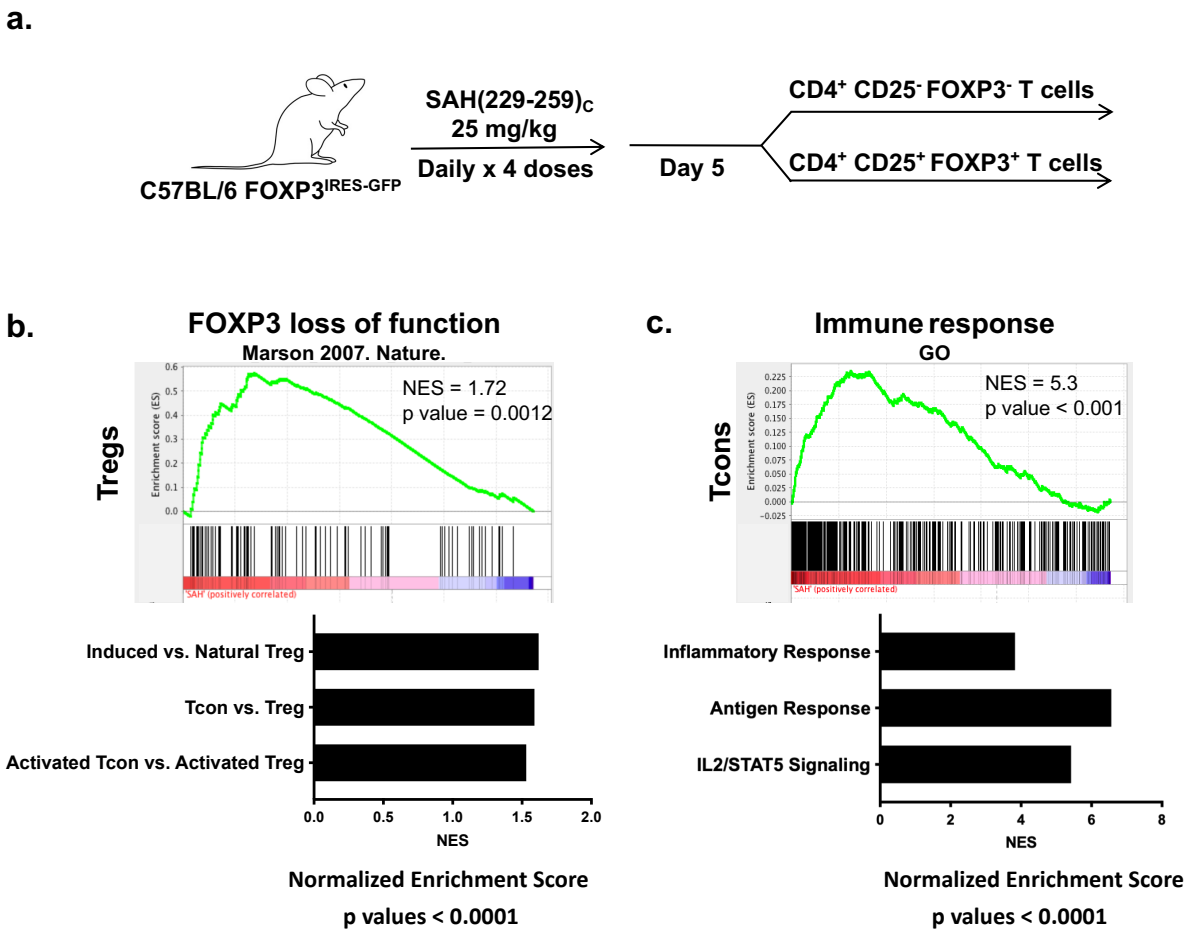

Figure 3.16: **SAH(229-259)$_C$ alters Treg mRNA expression *in vivo*** (a) Treatment and isolation strategy of C57/BL6$^{FOXP3-IRES-GFP}$ mice with SAH(229-259)$_C$ in preparation for RNA sequencing. Treatments of SAH(229-259)$_C$ altered global gene expression programs in (b) Tregs and (c) Tcons with p values < 0.0001. Following RNA-seq analysis and subsequent GSEA, Treg gene expression mimicked gene sets corresponding to FOXP3 loss, among others. Tcon gene expression alterations mimicked gene sets corresponding to increased inflammatory responses, among others.

CHAPTER 4

DISCUSSION

4.1 Conclusions

Despite great interest in the therapeutic targeting of Tregs as a modality to improve anti-tumor immunity, major barriers have prevented effective clinical use of a number of compounds targeting molecules associated with Treg function (214). Challenges have included a combination of hurdles such as a lack of specificity for Tregs, compensation by other inhibitory molecules and inhibitory cytokines expressed by Tregs, and off-target cellular toxicity in non-Treg T cells (102). Furthermore, many theoretical ideal targets include large PPIs which current small molecule approaches have been extremely difficult to target due to their more complex topographies and geographies (215; 216).

Perhaps an ideal therapeutic target due to its specificity and non-redundant role, an understanding of the FOXP3:FOXP3 interaction itself gives even more promise toward the capacity for targeting this interaction. The interface accessible surface area of the FOXP3 coiled-coil is 966Å2 (16% of total), compared to the average of 1492Å2 in other similar protein dimers, highly suggestive of a transient interaction (114; 199). Additionally, empty space of approximately 260Å3 in this interface leads to large packing holes. Non-hydrophobic core residues lead to further dimerization instability. Such flexibility and accessibility suggest that the FOXP3 coiled-coil interaction is dynamic and transient, thus, highly targetable by peptide interference.

Previous work targeting a separate FOXP3 PPI, that between FOXP3 and NFAT, demonstrated that non-structured peptides spanning a loop domain and the Wing1 region of the FKH domain of FOXP3 (FOXP3 393–403) could partially inhibit FOXP3:NFAT and decrease tumor burden in mice coincidentally treated with chemotherapy or a tumor adjuvant vaccine (217). While encouraging, this peptide was not cell permeable and required plasmid

transfection for cellular introduction. In another study, the same group utilized phage display to identify a random 15-mer peptide, P60, able to putatively bind somewhere within the contiguous FOXP3 ZF-LZ helix (a.a.177-331) (218). While P60 showed some efficacy at doses greater than an order of magnitude above doses used here (100µM), treated cells had indicators of apoptosis with observably higher cytoplasm:nucleus ratios and condensed chromatin. P60 underwent alanine scanning to further optimize its sequence. Treatment of mice with murine colon carcinoma with a cyclized version of the peptide emulsified in Freund adjuvant showed efficacy in a fraction of mice (219). We believe that the SAHs described in this study provide several promising advancements beyond this previous work, including inhibition of a new PPI, identification of specific binding location, improvement on required *ex vivo* dosage, and conclusive evidence of impacted FOXP3-mediated transcription.

In the present study, hydrocarbon stapling created stabilized α-helical peptide mimetics targeting the FOXP3 homodimer. Interestingly, while double-stapled SAHs may confer biophysical advantages in other systems including reduced proteolytic degradation and helical stability compared to single-stapled peptides, our data suggests that increased rigidity may be detrimental depending upon the native PPI. In the case of FOXP3:FOXP3, the coiled-coil appears to be best recapitulated through mimicry with a more flexible SAH. Whether such SAHs would result in ideal *in vivo* bioavailability is currently unclear and an area of active study.

The findings of this current study warrant further biochemical and cellular studies in order to elucidate how these SAHs perturb other signaling pathways and identify their downstream mechanism(s) of action. SAHs targeting FOXP3:FOXP3 represent active pre-clinical probes of FOXP3 programs which have been demonstrated to reduce Treg suppressive function and alter global transcriptional profiles, reprogramming the immune system toward immune activation and away from suppression. These mimetics will enable future studies of FOXP3 domain-specific and protein partner-specific control of expression programs, many of which

have not been fully elucidated.

We have shown that designing peptide mimetics after known FOXP3 PPI crystal structures provides a promising starting point for development of future transcription factor inhibitors, a class of drug targets that have largely been considered 'undruggable' to date. Similarly designed mimetics will enable studies of signaling pathways in normal and disease states that have thus far gone uninterrogated, opening exciting new doors to subsequent discoveries utilizing these approaches.

4.2 Future Directions

4.2.1 In vivo anti-tumor efficacy studies

Additional studies exploring anti-tumor efficacy in pre-clinical models would provide further justification for the continued development and exploration of SAHs targeting FOXP3 as a therapeutic to amplify anti-tumor immunity. As has been discovered across a wide variety of targets and cancer types, Treg cell-targeted therapy alone may not be effective against all tumors, particularly those with low neoantigen loads and otherwise lacking immunogenicity. This has been identified in murine models, where tumors derived from certain cell lines did not regress following T cell depletion (93). A necessary corollary will be in identifying biomarkers of tumors in which Tregs play an essential role in dampening anti-tumor immunity in order to identify models where we can more reasonably expect success utilizing a Treg-targeting therapy. This will involve vetting SAHs in a number of tumor types, including tumors originating from different tissues as the specific tissue environment has been found to influence tissue-resident immune cell function through release of soluble molecules and interaction with tissue-specific stromal cells. As with many other therapeutic strategies, rational combination regimens are likely to be another reasonable approach, perhaps in this case, the combination of FOXP3 SAHs with immune checkpoint blockade or tumor cell

vaccination strategies to provide non-redundant means of amplifying anti-tumor immunity.

We intend to begin evaluating the anti-tumor effects of our FOXP3-targeting SAHs in murine models of melanoma with a known tumor-specific antigen (*e.g.* B16-OVA) to determine whether Tregs in the TME become dysfunctional in SAH-treated mice, and if we can observe patterns suggestive of a more inflamed environment, such as infiltration of OVA-specific $CD8^+$ cytotoxic T cells, or an increase in the ratio of $CD8^+$ T cells to Tregs. We have performed initial pilot experiments in this model, treating mice with intratumoral injections of SAHS at two concentrations. Though these experiments need to be expanded, we observed dose-dependent increased infiltration of OVA specific $CD8^+$ T cells. FOXP3 expression remains stable, necessitating future studies of Treg dysfunction of Tregs in the TME. To understand distinct effects of SAHs targeting Tregs in the TME, we'll plan to sort intratumoral Tregs to perform *ex vivo* suppression assays and perform multiplexed cytokine analysis to glean a more thorough glimpse of Treg functional changes following SAH treatment in the tumor. Preliminary *ex vivo* suppression assays performed from mice treated with SAHs under homeostatic conditions have shown decreased Treg suppressive capacity, we have yet to determine whether this will hold in tumor-bearing mice.

4.2.2 Iterating SAHs targeting FOXP3

Peptide mimetics are designed after their native structure. In the case of the FOXP3 homodimer, binding is mediated between two identical homodimers; as a result, we expect there is a high likelihood that two SAHs would be able to bind to each other (much like the native structure), muting their potential effect by roughly two-fold. To overcome this obstacle, we've designed new iterations based on our initial SAH(229-259)$_C$ structure, still encompassing residues that have been identified to be most crucial for binding to FOXP3, while shortening the overall length of the SAHs to ensure that the SAHs are non-overlapping and would presumably be less likely to homodimerize either in solution or within treated

cells (Figure 4.1). These next generation of SAHs still need to be tested for bioactivity, but we're optimistic that they will be more efficacious due to decreased self-dimerization and overall increased efficiency of cellular penetration and binding. An additional advantage to generating shorter iterations is the likely improvement in quantity of SAH we're able to synthesize; yield following synthesis and purification has been an ongoing challenge (only approximately 30% yield is reached with our longer SAHs) and is inversely correlated to length of SAH.

In addition to developing shorter non-overlapping mimetics, we intend to develop SAHs with (i, i+4) staples. Our work has shown that an increased degree of flexibility was beneficial in design of SAHs targeting FOXP3 towards ultimate bioactivity. In this vein, a hydrocarbon staple spanning only one turn of the helix would likely have increased flexibility and should be vetted as an additional strategic approach in further iterations.

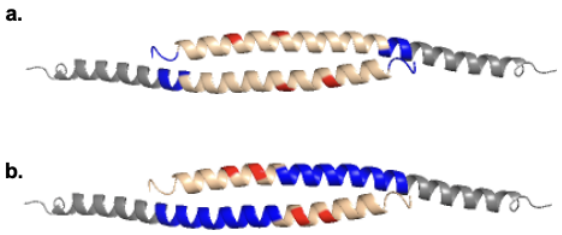

Figure 4.1: **SAHs designed in the likeness of FOXP3 may dimerize, muting their potential activity** (a) SAH(229-259)$_C$ (shown in tan) is likely able to bind a complementary SAH through molecular mimicry. (b) Shortening the sequence of the SAH (shown in tan) would confer two potential benefits: reducing the capacity for homodimerization, effectively improving effectiveness, and providing for higher yield in the peptide synthesis and purification processes. Representative shorterned iteration shown.

4.2.3 Improving pharmacokinetic properties and cell permeability of SAHs

Current challenges that will need to be overcome include determining appropriate delivery mechanisms and application of medicinal chemistry approaches to improve pharmacokinetic

properties of our existing SAHs. These challenges are not unique to SAHs; small molecule hits often have poor initial affinity, often in the micromolar range. Structure-based optimization can often improve these affinities by orders of magnitude. It is reasonable to expect that similar medicinal chemistry approaches could also improve SAH affinity. This has precedent, based on the evolution of SAHs targeting p53 (190; 220; 221). Following subsequent iterations, SAHs targeting p53 have entered several Phase 1 and 2 clinical trials in both adult and pediatric cancer patients (NCT02264613, NCT02909972, NCT03654716, NCT03725436, NCT04022876).

Several approaches exist that can be taken to improve cell permeability including addition of charged amino acids or targeting domains like Transactivating activator of transcription (TAT) sequences. Negatively-charged SAHs rarely cross cellular membranes; SAHs with charges that range from 0 to +2 have been shown to penetrate cells. Charge can be increased through either substitution of anionic amino acids to their neutral counterparts, for example glutamate to glutamine, or through addition of positively charged residues like lysine to either the N- or C- termini (180). Which of these two approaches should be selected will largely be dependent upon where anionic amino acids are positioned within in the binding interface of the PPI being interrogated. TAT, a polycationic protein, was identified to pass through cell membranes (222; 223) after being found to be part of the essential machinery for HIV pathogenicity. This protein or a shortened peptide sequence variant of it can be covalently bound to SAHs in order to facilitate cellular uptake. However, while such manipulations may improve solubility, we have also found that there exist trade-offs that may ultimately reduce target affinity (195).

To further comfirm permeability, we intend to check for endosomal compartmentalization of these peptides. If SAHs are trapped in the endosome, strategies can be utilized to enable endosomal escape, preventing degradation and sequestration of SAHs prior to their ability to act upon any PPI of interest.

Other members of the lab have worked to develop biodegradable, biocompatible polymersomes capable of endosomal escape. These amphiphilic diblock copolymers can be packaged with a variety of therapeutics, including small molecules and stapled peptides. To aid in targeted drug delivery, Fabs can be attached to these polymersomes. Work in the lab to date has included packaging BH3 mimetics and a p53-reactivating stapled peptide to target diffuse large B cell lymphoma (DLBCL) tumor-bearing mice by targeting CD19, an endocytic receptor specific to B cells. Performing *in vivo* experiments in tumor-bearing mice treated with SAHs has been an ongoing challenge in part due to the poor solubility of our FOXP3-targeting SAHs. We hope to leverage this polymersome approach to improve deliverability of our SAHs. Unlike B cells, Tregs don't express specific endocytic receptors, possibly limiting the usefulness of the nanoparticle approach, though we still expect an overall improvement in cellular uptake and hope to at minimum bring a greater bolus of peptide in close proximity to our Treg targets. The observed enhanced permeability and retention effect in dysregulated vasculature may allow for a greater accumulation of SAHs in the TME, often known to have greater vasculature. Packaging SAHs or improving cellular uptake in general will allow for larger animal studies by reducing the overall amount of compound necessary to be synthesized. One final possible value-add in using the nanoparticle approach is to either use single or a combination of Fabs that more specifically target intratumoral Tregs, possible proteins known to be upregulated on the surface of intratumoral Tregs like 4-1BB, CD25, CTLA-4, GITR, inducible T cell co-stimulator (ICOS), LAG-3, programmed death protein 1 (PD-1), T cell immunoreceptor with Ig and ITIM domains (TIGIT), and T cell immunoglobulin and mucin protein 3 (TIM-3).

4.2.4 SAH specificity for the FOXP3 homodimer and additional PPI targets

FOXP3 does not exist solely as a homodimer, thus it is also reasonable to focus our efforts on resultant transcriptional changes due to reduced or inhibited FOXP3, both as a homodimer or in interactions with other binding partners. One such PPI that should be interrogated further is the FOXP1:FOXP3 heterodimer, which binds in a similar location (FOXP3 LZDD). It is conceivable that our SAHs could also disrupt this heterodimer, obscuring our understanding of domain-specific transcriptional regulation if we're unable to parse out the individual roles of each separate PPI. It should be straightforward to identify whether we're targeting multiple PPIs. Co-immunoprecipitations (Co-IPs) where FITC- or biotin-labeled SAHs are pulled down and probed for both FOXP1 and FOXP3 binding partners can provide preliminary evidence suggesting either alternative. If SAHs are confirmed to bind both FOXP1 and FOXP3 we'll have to assess the possibility of any off-target effects due to possible binding of FOXP1. Recent work has suggested that FOXP1 and FOXP3 share a large number of FOXP3-bound genomic sites in Tregs; FOXP1 largely acts in a non-redundant role to stabilize FOXP3 binding in Tregs (224). Despite this additional layer of complexity, SAHs potentially blocking FOXP1:FOXP3 binding in addition to FOXP3:FOXP3 may in fact be a net positive from a therapeutic perspective; further reduction of FOXP3 stabilization could improve our ability to dysregulating Treg suppressive function.

In addition to interrogating bystander targeting of other FOXP3 PPIs with our current SAHs, there is remaining opportunity to develop SAHs targeting other PPIs important for Treg function including the FOXP3:NFAT heterodimer. This heterodimer has been implicated as required for Treg suppressive function in a nonredundant manner to FOXP3:FOXP3 (23; 225). To this end, we've developed SAHs in the likeness of FOXP3 intended to bind NFAT by molecular mimicry. After performing a staple walk, where each iteration had an i, (i+7) staple placed one residue down the helix across the entirety of the sequence, we

observed that there was large variability in cellular uptake measured through two separate assays, one measuring increasing fluorescence over time of adherent cells treated with FITC-labeled SAH and the other using confocal to visualize uptake in iTregs (Figure 4.2). This indicates to us that staple position, much like in our studies of SAHs targeting the FOXP3 homodimer, is key to screening SAHs for good bioactivity.

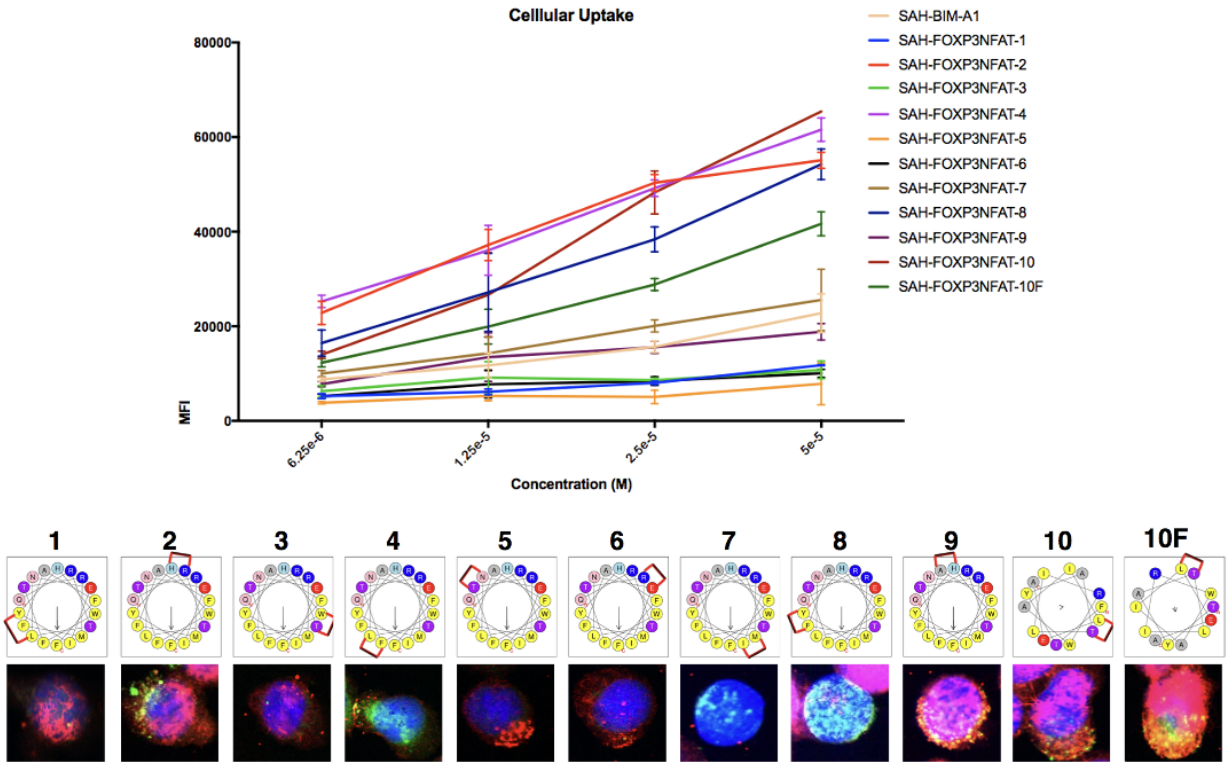

Figure 4.2: **SAHs targeting the FOXP3:NFAT heterodimer are variably cell permeable dependent upon staple position** An array of SAHs targeting FOXP3:NFAT were synthesized across the same sequence. SAHs were synthesized in a staple walk, where each i, $(i+7)$ staple was placed one sequential residue down the helix. Depending upon the staple position, FITC-labeled SAHs were variably able to penetrate cells, measured in two assays: cellular uptake measuring fluorescence increases over time (top) and in confocal microscopy (bottom), both of which correlated highly with each other.

While these studies are still in pilot stages, our preliminary data suggests that targeting the FOXP3:NFAT heterodimer raises an additional layer of complexity in that binding NFAT may have unexpected consequences on Tcon function, and this particular set of SAHs may not have the desired specificity to Tregs. Further evaluation is essential to identify the consequences of inhibiting NFAT in separate cell types. Aside from designing SAHs with the intent of therapeutic application, these peptides can be designed to enable better understanding of domain-specific functions of PPIs.

Our SAHs targeting the FOXP3 homodimer can be assessed in ATACseq to confirm chromatin accessibility changes as a result of SAH-mediated inhibition of this PPI. Separately, several other PPIs of FOXP3 are much less well-classified, including FOXP3:EOS. SAHs designed against such PPIs can be used to understand and identify unique and redundant transcriptional regulation occurring as a result of dimerization at these particular sites. SAHs can also be used in this context to better understand functional consequences of IPEX mutations leading to Treg hypofunctionality. Outside of Tregs, many PPIs are composed of α-helical protein-protein interaction interfaces; development of SAHs provide a unique opportunity to probe molecular mechanisms and consequences of abrogating them in a highly specific manner.

4.2.5 Predictive modeling to inform SAH design and identify new target PPIs

Complementary computational techniques can be used to assess druggability and identify PPIs and binding regions amenable to disruption by either small molecules or peptide mimetics. Dr. PIAS (226) and similar software identify shared homology in binding interfaces to known PPI inhibitors and targets. The ANCHOR system has also been used as a tool to identify putative hotspot residues involved in the burial of solvent accessible surface area (227; 228). Groups have also utilized secondary and tertiary structure elements to inspire

rational design; databases of these structures at PPI interfaces have been created and paired with docking and pharmacophore-based searching (229) to enable mimicry of α-helices, β-strands, and helix dimers essential for maintenance of an array of PPIs (230; 231). These approaches provide the opportunity for more high throughput screening of PPIs and remain a promising next step in the development of our mimetics targeting PPIs associated with Treg function. Despite these advances, one outstanding complication remains in that these approaches are less suitable for proteins that experience conformational changes. Several groups have worked to overcome this by generating druggability algorithms for snapshots of molecular dynamics in time (232), though ultimately these are still incomplete. All in all, pairing these tools can be used to computationally predict SAH-protein affinity and avoid trial and error approaches to expedite development and testing of therapeutics targeting PPIs.

4.3 Considerations

Our approach and therapeutic design is predicated on the fact that Treg dysfunction or depletion within the tumor microenvironment would lead to improved tumor regression as a result of amplified endogenous anti-tumor immunity. However, there is a growing body of literature suggestive that outcomes following Treg depletion are perhaps more context-dependent than initially thought, with the potential for depletion to instead be tumor promoting both in mice (233; 234) and humans (235). Furthermore, studies have shown that specific point mutations in Foxp3, specifically some IPEX mutations, have variable functional consequences, with inconsistent degrees of observed Treg hypofunctionality. This has major implications for any new therapies developed, along with existing immunotherapies like ICB. Agonistic targets in preclinical studies like anti-OX40 and anti-GITR, and trafficking inhibitors like anti-CCR8 have been shown to promote intratumoral Treg depletion (236; 237; 238), specifically depending upon the Fc region of each targeting antibody. This is reminiscent

of the observation that *in vivo* administration of anti-CTLA-4 antibodies depleted Tregs in an antibody-dependent cellular cytotoxicity (ADCC) dependent manner where later work demonstrated that the activity of these antibodies was dependent upon the ability of the Fc region to bind activating Fc receptors. These findings necessitate the deeper understanding of mechanism of action of developed immunotherapies, elucidation of whether targeting intratumoral Tregs is harmful or beneficial in patients, and finally clarifying whether any established trends exist or if response persistently varies at the level of each individual patient. While we have a high degree of confidence that our FOXP3-targeting SAHs would not cause intratumoral Treg depletion, and have preliminary data in support, this is clearly something that should be confirmed in larger studies. Regardless, even altering Treg functional states may be more dependent on local environments than anticipated and will require thorough analysis to maintain confidence that our therapeutic would be a clinically viable approach to altering the immune landscape in a meaningful way.

We surmise that targeting intratumoral Tregs would be advantageous over targeting bulk Tregs from a specificity point of view. As of yet, we have not developed a means to specifically target intratumoral Tregs, leading to the possibility that Tregs in the periphery and residing in lymph nodes may also be targeted by our SAHs. An obvious concern here is that excess destabilization of Tregs may lead to autoimmunity (239). While we are optimistic that the transient on/off binding that characterizes our SAHs likely provides the opportunity for transient destabilization without incurring autoimmune consequences, this is an area that we have yet to confirm.

It'll be imperative to better understand differential effects of our SAHs on heterogenous populations of Tregs including induced vs. thymic-derived Tregs. Additionally, tissue-specific Treg functions and the impacts of local vs systemic suppression of anti-tumor immunity remain largely unknown in the context of immunotherapy resistance and ultimate metastasis. To this end, growing evidence demonstrates that organs are largely populated with

their unique tissue-adapted immune cells; organ-specific mechanisms not only direct local anti-tumor immunity, but also can exert influence on distant sites, particularly metastases (240; 241). Tregs have been connected to metastatic disease as they've been thought to promote tumor metastatic disease by enabling immune evasion and facilitating tumor cell dissemination (242). Tissue-specific inputs like oxygen and pressure changes in the lungs, changes in the gut microbiome, neuronal signals, and tissue regeneration in the liver can all impact Treg function (72). Safe targeting of Tregs involved in promoting metastases will require identification of unique cell surface receptors and other local mediators; locoregional approaches may also be a viable strategy but will likely involve crafting novel delivery strategies, which to date has been less successful. All of these nuances will need to be taken into account to understand tumor-intrinsic or extrinsic resistance pathways in an effort to continue to improve immunotherapy design.

While immunotherapies continue to gain traction and represent an exciting area of research with high potential, currently approved therapies like ICB are unfortunately only able to change the course of disease for a minority of patients. As has been observed throughout history, disease onset and continuance is complicated and highly heterogenous even at the level of an individual patient. To this end, we are interested in leveraging the crucial role of PPIs in impacting discrete downstream cellular functions to develop inhibitors that are highly specific. We've generated stapled-peptide inhibitors of the FOXP3 homodimer, specifically targeting Tregs and dysregulating their suppressive capacity. While this alone may not ultimately be enough to yield a therapeutic effect, we are optimistic that this approach can be used in combination with other therapies with the intent of bolstering anti-tumor immunity and providing inherent usefulness in developing tool compounds to interrogate and understand highly specific domain-dependent or PPI-specific roles of transcription factors. This work has yielded proof-of-concept data suggesting that not only is it possible to specifically target a T cell compartment where previous attempts have been rife with off-target

effects, but that we are able to gain a functional readout through observed decrease in Treg suppressive capacity, and *in vivo* transcriptional reprogramming.

REFERENCES

[1] J. Janeway, C. A. and R. Medzhitov, "Innate immune recognition," *Annu Rev Immunol*, vol. 20, pp. 197–216, 2002.

[2] D. Jung and F. W. Alt, "Unraveling v(d)j recombination; insights into gene regulation," *Cell*, vol. 116, no. 2, pp. 299–311, 2004.

[3] T. K. Starr, S. C. Jameson, and K. A. Hogquist, "Positive and negative selection of t cells," *Annu Rev Immunol*, vol. 21, pp. 139–76, 2003.

[4] G. L. Stritesky, S. C. Jameson, and K. A. Hogquist, "Selection of self-reactive t cells in the thymus," *Annu Rev Immunol*, vol. 30, pp. 95–114, 2012.

[5] P. A. Savage, D. E. J. Klawon, and C. H. Miller, "Regulatory t cell development," *Annu Rev Immunol*, vol. 38, pp. 421–453, 2020.

[6] K. R. McIntire, S. Sell, and J. F. Miller, "Pathogenesis of the post-neonatal thymectomy wasting syndrome," *Nature*, vol. 204, pp. 151–5, 1964.

[7] S. Sakaguchi, N. Sakaguchi, M. Asano, M. Itoh, and M. Toda, "Immunologic self-tolerance maintained by activated t cells expressing il-2 receptor alpha-chains (cd25). breakdown of a single mechanism of self-tolerance causes various autoimmune diseases," *J Immunol*, vol. 155, no. 3, pp. 1151–64, 1995.

[8] T. A. Chatila, F. Blaeser, N. Ho, H. M. Lederman, C. Voulgaropoulos, C. Helms, and A. M. Bowcock, "Jm2, encoding a fork head-related protein, is mutated in x-linked autoimmunity-allergic disregulation syndrome," *J Clin Invest*, vol. 106, no. 12, pp. R75–81, 2000.

[9] M. E. Brunkow, E. W. Jeffery, K. A. Hjerrild, B. Paeper, L. B. Clark, S. A. Yasayko, J. E. Wilkinson, D. Galas, S. F. Ziegler, and F. Ramsdell, "Disruption of a new forkhead/winged-helix protein, scurfin, results in the fatal lymphoproliferative disorder of the scurfy mouse," *Nat Genet*, vol. 27, no. 1, pp. 68–73, 2001.

[10] R. S. Wildin, F. Ramsdell, J. Peake, F. Faravelli, J. L. Casanova, N. Buist, E. Levy-Lahad, M. Mazzella, O. Goulet, L. Perroni, F. D. Bricarelli, G. Byrne, M. McEuen, S. Proll, M. Appleby, and M. E. Brunkow, "X-linked neonatal diabetes mellitus, enteropathy and endocrinopathy syndrome is the human equivalent of mouse scurfy," *Nat Genet*, vol. 27, no. 1, pp. 18–20, 2001.

[11] J. D. Fontenot, M. A. Gavin, and A. Y. Rudensky, "Foxp3 programs the development and function of cd4+cd25+ regulatory t cells," *Nat Immunol*, vol. 4, no. 4, pp. 330–6, 2003.

[12] S. Hori, T. Nomura, and S. Sakaguchi, "Control of regulatory t cell development by the transcription factor foxp3," *Science*, vol. 299, no. 5609, pp. 1057–61, 2003.

[13] R. Khattri, T. Cox, S. A. Yasayko, and F. Ramsdell, "An essential role for scurfin in cd4+cd25+ t regulatory cells," *Nat Immunol*, vol. 4, no. 4, pp. 337–42, 2003.

[14] C. L. Bennett, J. Christie, F. Ramsdell, M. E. Brunkow, P. J. Ferguson, L. Whitesell, T. E. Kelly, F. T. Saulsbury, P. F. Chance, and H. D. Ochs, "The immune dysregulation, polyendocrinopathy, enteropathy, x-linked syndrome (ipex) is caused by mutations of foxp3," *Nat Genet*, vol. 27, no. 1, pp. 20–1, 2001.

[15] J. D. Fontenot, J. P. Rasmussen, L. M. Williams, J. L. Dooley, A. G. Farr, and A. Y. Rudensky, "Regulatory t cell lineage specification by the forkhead transcription factor foxp3," *Immunity*, vol. 22, no. 3, pp. 329–41, 2005.

[16] R. Pacholczyk, J. Kern, N. Singh, M. Iwashima, P. Kraj, and L. Ignatowicz, "Nonself-antigens are the cognate specificities of foxp3+ regulatory t cells," *Immunity*, vol. 27, no. 3, pp. 493–504, 2007.

[17] Y. P. Rubtsov, R. E. Niec, S. Josefowicz, L. Li, J. Darce, D. Mathis, C. Benoist, and A. Y. Rudensky, "Stability of the regulatory t cell lineage in vivo," *Science*, vol. 329, no. 5999, pp. 1667–71, 2010.

[18] M. R. Walker, D. J. Kasprowicz, V. H. Gersuk, A. Benard, M. Van Landeghen, J. H. Buckner, and S. F. Ziegler, "Induction of foxp3 and acquisition of t regulatory activity by stimulated human cd4+cd25- t cells," *J Clin Invest*, vol. 112, no. 9, pp. 1437–43, 2003.

[19] Y. Feng, A. Arvey, T. Chinen, J. van der Veeken, G. Gasteiger, and A. Y. Rudensky, "Control of the inheritance of regulatory t cell identity by a cis element in the foxp3 locus," *Cell*, vol. 158, no. 4, pp. 749–763, 2014.

[20] Y. Zheng, S. Josefowicz, A. Chaudhry, X. P. Peng, K. Forbush, and A. Y. Rudensky, "Role of conserved non-coding dna elements in the foxp3 gene in regulatory t-cell fate," *Nature*, vol. 463, no. 7282, pp. 808–12, 2010.

[21] J. Du, C. Huang, B. Zhou, and S. F. Ziegler, "Isoform-specific inhibition of ror alpha-mediated transcriptional activation by human foxp3," *J Immunol*, vol. 180, no. 7, pp. 4785–92, 2008.

[22] E. Bettelli, M. Dastrange, and M. Oukka, "Foxp3 interacts with nuclear factor of activated t cells and nf-kappa b to repress cytokine gene expression and effector functions of t helper cells," *Proc Natl Acad Sci U S A*, vol. 102, no. 14, pp. 5138–43, 2005.

[23] J. E. Lopes, T. R. Torgerson, L. A. Schubert, S. D. Anover, E. L. Ocheltree, H. D. Ochs, and S. F. Ziegler, "Analysis of foxp3 reveals multiple domains required for its function as a transcriptional repressor," *J Immunol*, vol. 177, no. 5, pp. 3133–42, 2006.

[24] H. Yagi, T. Nomura, K. Nakamura, S. Yamazaki, T. Kitawaki, S. Hori, M. Maeda, M. Onodera, T. Uchiyama, S. Fujii, and S. Sakaguchi, "Crucial role of foxp3 in the

development and function of human cd25+cd4+ regulatory t cells," *Int Immunol*, vol. 16, no. 11, pp. 1643–56, 2004.

[25] S. E. Allan, L. Passerini, R. Bacchetta, N. Crellin, M. Dai, P. C. Orban, S. F. Ziegler, M. G. Roncarolo, and M. K. Levings, "The role of 2 foxp3 isoforms in the generation of human cd4+ tregs," *J Clin Invest*, vol. 115, no. 11, pp. 3276–84, 2005.

[26] C. Cozzo Picca, D. M. Simons, S. Oh, M. Aitken, O. A. Perng, C. Mergenthaler, E. Kropf, J. Erikson, and A. J. Caton, "Cd4(+)cd25(+)foxp3(+) regulatory t cell formation requires more specific recognition of a self-peptide than thymocyte deletion," *Proc Natl Acad Sci U S A*, vol. 108, no. 36, pp. 14890–5, 2011.

[27] S. Sakaguchi, T. Yamaguchi, T. Nomura, and M. Ono, "Regulatory t cells and immune tolerance," *Cell*, vol. 133, no. 5, pp. 775–87, 2008.

[28] G. C. Furtado, M. A. Curotto de Lafaille, N. Kutchukhidze, and J. J. Lafaille, "Interleukin 2 signaling is required for cd4(+) regulatory t cell function," *J Exp Med*, vol. 196, no. 6, pp. 851–7, 2002.

[29] T. R. Malek, A. Yu, V. Vincek, P. Scibelli, and L. Kong, "Cd4 regulatory t cells prevent lethal autoimmunity in il-2rbeta-deficient mice. implications for the nonredundant function of il-2," *Immunity*, vol. 17, no. 2, pp. 167–78, 2002.

[30] N. Watanabe, S. Hanabuchi, V. Soumelis, W. Yuan, S. Ho, R. de Waal Malefyt, and Y. J. Liu, "Human thymic stromal lymphopoietin promotes dendritic cell-mediated cd4+ t cell homeostatic expansion," *Nat Immunol*, vol. 5, no. 4, pp. 426–34, 2004.

[31] S. Hanabuchi, T. Ito, W. R. Park, N. Watanabe, J. L. Shaw, E. Roman, K. Arima, Y. H. Wang, K. S. Voo, W. Cao, and Y. J. Liu, "Thymic stromal lymphopoietin-activated plasmacytoid dendritic cells induce the generation of foxp3+ regulatory t cells in human thymus," *J Immunol*, vol. 184, no. 6, pp. 2999–3007, 2010.

[32] I. Apostolou and H. von Boehmer, "In vivo instruction of suppressor commitment in naive t cells," *J Exp Med*, vol. 199, no. 10, pp. 1401–8, 2004.

[33] K. Kretschmer, I. Apostolou, D. Hawiger, K. Khazaie, M. C. Nussenzweig, and H. von Boehmer, "Inducing and expanding regulatory t cell populations by foreign antigen," *Nat Immunol*, vol. 6, no. 12, pp. 1219–27, 2005.

[34] C. A. Finney, M. D. Taylor, M. S. Wilson, and R. M. Maizels, "Expansion and activation of cd4(+)cd25(+) regulatory t cells in heligmosomoides polygyrus infection," *Eur J Immunol*, vol. 37, no. 7, pp. 1874–86, 2007.

[35] K. Atarashi, T. Tanoue, T. Shima, A. Imaoka, T. Kuwahara, Y. Momose, G. Cheng, S. Yamasaki, T. Saito, Y. Ohba, T. Taniguchi, K. Takeda, S. Hori, I. Ivanov, Y. Umesaki, K. Itoh, and K. Honda, "Induction of colonic regulatory t cells by indigenous clostridium species," *Science*, vol. 331, no. 6015, pp. 337–41, 2011.

[36] S. K. Lathrop, S. M. Bloom, S. M. Rao, K. Nutsch, C. W. Lio, N. Santacruz, D. A. Peterson, T. S. Stappenbeck, and C. S. Hsieh, "Peripheral education of the immune system by colonic commensal microbiota," *Nature*, vol. 478, no. 7368, pp. 250–4, 2011.

[37] C. S. Hsieh, Y. Liang, A. J. Tyznik, S. G. Self, D. Liggitt, and A. Y. Rudensky, "Recognition of the peripheral self by naturally arising cd25+ cd4+ t cell receptors," *Immunity*, vol. 21, no. 2, pp. 267–77, 2004.

[38] J. Wong, R. Obst, M. Correia-Neves, G. Losyev, D. Mathis, and C. Benoist, "Adaptation of tcr repertoires to self-peptides in regulatory and nonregulatory cd4+ t cells," *J Immunol*, vol. 178, no. 11, pp. 7032–41, 2007.

[39] J. Wong, D. Mathis, and C. Benoist, "Tcr-based lineage tracing: no evidence for conversion of conventional into regulatory t cells in response to a natural self-antigen in pancreatic islets," *J Exp Med*, vol. 204, no. 9, pp. 2039–45, 2007.

[40] Y. Peng, Y. Laouar, M. O. Li, E. A. Green, and R. A. Flavell, "Tgf-beta regulates in vivo expansion of foxp3-expressing cd4+cd25+ regulatory t cells responsible for protection against diabetes," *Proc Natl Acad Sci U S A*, vol. 101, no. 13, pp. 4572–7, 2004.

[41] W. Chen, W. Jin, N. Hardegen, K. J. Lei, L. Li, N. Marinos, G. McGrady, and S. M. Wahl, "Conversion of peripheral cd4+cd25- naive t cells to cd4+cd25+ regulatory t cells by tgf-beta induction of transcription factor foxp3," *J Exp Med*, vol. 198, no. 12, pp. 1875–86, 2003.

[42] M. C. Fantini, C. Becker, G. Monteleone, F. Pallone, P. R. Galle, and M. F. Neurath, "Cutting edge: Tgf-beta induces a regulatory phenotype in cd4+cd25- t cells through foxp3 induction and down-regulation of smad7," *J Immunol*, vol. 172, no. 9, pp. 5149–53, 2004.

[43] J. A. Hall, J. L. Cannons, J. R. Grainger, L. M. Dos Santos, T. W. Hand, S. Naik, E. A. Wohlfert, D. B. Chou, G. Oldenhove, M. Robinson, M. E. Grigg, R. Kastenmayer, P. L. Schwartzberg, and Y. Belkaid, "Essential role for retinoic acid in the promotion of cd4(+) t cell effector responses via retinoic acid receptor alpha," *Immunity*, vol. 34, no. 3, pp. 435–47, 2011.

[44] T. S. Davidson, R. J. DiPaolo, J. Andersson, and E. M. Shevach, "Cutting edge: Il-2 is essential for tgf-beta-mediated induction of foxp3+ t regulatory cells," *J Immunol*, vol. 178, no. 7, pp. 4022–6, 2007.

[45] S. Floess, J. Freyer, C. Siewert, U. Baron, S. Olek, J. Polansky, K. Schlawe, H. D. Chang, T. Bopp, E. Schmitt, S. Klein-Hessling, E. Serfling, A. Hamann, and J. Huehn, "Epigenetic control of the foxp3 locus in regulatory t cells," *PLoS Biol*, vol. 5, no. 2, p. e38, 2007.

[46] J. A. Bluestone and A. K. Abbas, "Natural versus adaptive regulatory t cells," *Nat Rev Immunol*, vol. 3, no. 3, pp. 253–7, 2003.

[47] A. M. Thornton, P. E. Korty, D. Q. Tran, E. A. Wohlfert, P. E. Murray, Y. Belkaid, and E. M. Shevach, "Expression of helios, an ikaros transcription factor family member, differentiates thymic-derived from peripherally induced foxp3+ t regulatory cells," *J Immunol*, vol. 184, no. 7, pp. 3433–41, 2010.

[48] J. Verhagen and D. C. Wraith, "Comment on "expression of helios, an ikaros transcription factor family member, differentiates thymic-derived from peripherally induced foxp3+ t regulatory cells"," *J Immunol*, vol. 185, no. 12, p. 7129; author reply 7130, 2010.

[49] J. Darce, D. Rudra, L. Li, J. Nishio, D. Cipolletta, A. Y. Rudensky, D. Mathis, and C. Benoist, "An n-terminal mutation of the foxp3 transcription factor alleviates arthritis but exacerbates diabetes," *Immunity*, vol. 36, no. 5, pp. 731–41, 2012.

[50] R. A. Gottschalk, E. Corse, and J. P. Allison, "Expression of helios in peripherally induced foxp3+ regulatory t cells," *J Immunol*, vol. 188, no. 3, pp. 976–80, 2012.

[51] D. Haribhai, W. Lin, B. Edwards, J. Ziegelbauer, N. H. Salzman, M. R. Carlson, S. H. Li, P. M. Simpson, T. A. Chatila, and C. B. Williams, "A central role for induced regulatory t cells in tolerance induction in experimental colitis," *J Immunol*, vol. 182, no. 6, pp. 3461–8, 2009.

[52] M. Feuerer, J. A. Hill, K. Kretschmer, H. von Boehmer, D. Mathis, and C. Benoist, "Genomic definition of multiple ex vivo regulatory t cell subphenotypes," *Proc Natl Acad Sci U S A*, vol. 107, no. 13, pp. 5919–24, 2010.

[53] D. Valmori, A. Merlo, N. E. Souleimanian, C. S. Hesdorffer, and M. Ayyoub, "A peripheral circulating compartment of natural naive cd4 tregs," *J Clin Invest*, vol. 115, no. 7, pp. 1953–62, 2005.

[54] T. Korn, J. Reddy, W. Gao, E. Bettelli, A. Awasthi, T. R. Petersen, B. T. Backstrom, R. A. Sobel, K. W. Wucherpfennig, T. B. Strom, M. Oukka, and V. K. Kuchroo, "Myelin-specific regulatory t cells accumulate in the cns but fail to control autoimmune inflammation," *Nat Med*, vol. 13, no. 4, pp. 423–31, 2007.

[55] X. Liu, P. Nguyen, W. Liu, C. Cheng, M. Steeves, J. C. Obenauer, J. Ma, and T. L. Geiger, "T cell receptor cdr3 sequence but not recognition characteristics distinguish autoreactive effector and foxp3(+) regulatory t cells," *Immunity*, vol. 31, no. 6, pp. 909–20, 2009.

[56] W. Liu, A. L. Putnam, Z. Xu-Yu, G. L. Szot, M. R. Lee, S. Zhu, P. A. Gottlieb, P. Kapranov, T. R. Gingeras, B. Fazekas de St Groth, C. Clayberger, D. M. Soper, S. F. Ziegler, and J. A. Bluestone, "Cd127 expression inversely correlates with foxp3 and suppressive function of human cd4+ t reg cells," *J Exp Med*, vol. 203, no. 7, pp. 1701–11, 2006.

[57] S. Fisson, G. Darrasse-Jeze, E. Litvinova, F. Septier, D. Klatzmann, R. Liblau, and B. L. Salomon, "Continuous activation of autoreactive cd4+ cd25+ regulatory t cells in the steady state," *J Exp Med*, vol. 198, no. 5, pp. 737–46, 2003.

[58] M. Miyara, Y. Yoshioka, A. Kitoh, T. Shima, K. Wing, A. Niwa, C. Parizot, C. Taflin, T. Heike, D. Valeyre, A. Mathian, T. Nakahata, T. Yamaguchi, T. Nomura, M. Ono, Z. Amoura, G. Gorochov, and S. Sakaguchi, "Functional delineation and differentiation dynamics of human cd4+ t cells expressing the foxp3 transcription factor," *Immunity*, vol. 30, no. 6, pp. 899–911, 2009.

[59] T. Ito, S. Hanabuchi, Y. H. Wang, W. R. Park, K. Arima, L. Bover, F. X. Qin, M. Gilliet, and Y. J. Liu, "Two functional subsets of foxp3+ regulatory t cells in human thymus and periphery," *Immunity*, vol. 28, no. 6, pp. 870–80, 2008.

[60] N. Seddiki, B. Santner-Nanan, S. G. Tangye, S. I. Alexander, M. Solomon, S. Lee, R. Nanan, and B. Fazekas de Saint Groth, "Persistence of naive cd45ra+ regulatory t cells in adult life," *Blood*, vol. 107, no. 7, pp. 2830–8, 2006.

[61] M. Vukmanovic-Stejic, Y. Zhang, J. E. Cook, J. M. Fletcher, A. McQuaid, J. E. Masters, M. H. Rustin, L. S. Taams, P. C. Beverley, D. C. Macallan, and A. N. Akbar, "Human cd4+ cd25hi foxp3+ regulatory t cells are derived by rapid turnover of memory populations in vivo," *J Clin Invest*, vol. 116, no. 9, pp. 2423–33, 2006.

[62] K. Wing, Y. Onishi, P. Prieto-Martin, T. Yamaguchi, M. Miyara, Z. Fehervari, T. Nomura, and S. Sakaguchi, "Ctla-4 control over foxp3+ regulatory t cell function," *Science*, vol. 322, no. 5899, pp. 271–5, 2008.

[63] S. Paust, L. Lu, N. McCarty, and H. Cantor, "Engagement of b7 on effector t cells by regulatory t cells prevents autoimmune disease," *Proc Natl Acad Sci U S A*, vol. 101, no. 28, pp. 10398–403, 2004.

[64] B. Liang, C. Workman, J. Lee, C. Chew, B. M. Dale, L. Colonna, M. Flores, N. Li, E. Schweighoffer, S. Greenberg, V. Tybulewicz, D. Vignali, and R. Clynes, "Regulatory t cells inhibit dendritic cells by lymphocyte activation gene-3 engagement of mhc class ii," *J Immunol*, vol. 180, no. 9, pp. 5916–26, 2008.

[65] S. Deaglio, K. M. Dwyer, W. Gao, D. Friedman, A. Usheva, A. Erat, J. F. Chen, K. Enjyoji, J. Linden, M. Oukka, V. K. Kuchroo, T. B. Strom, and S. C. Robson, "Adenosine generation catalyzed by cd39 and cd73 expressed on regulatory t cells mediates immune suppression," *J Exp Med*, vol. 204, no. 6, pp. 1257–65, 2007.

[66] X. Cao, S. F. Cai, T. A. Fehniger, J. Song, L. I. Collins, D. R. Piwnica-Worms, and T. J. Ley, "Granzyme b and perforin are important for regulatory t cell-mediated suppression of tumor clearance," *Immunity*, vol. 27, no. 4, pp. 635–46, 2007.

[67] D. A. Vignali, L. W. Collison, and C. J. Workman, "How regulatory t cells work," *Nat Rev Immunol*, vol. 8, no. 7, pp. 523–32, 2008.

[68] G. Oldenhove, N. Bouladoux, E. A. Wohlfert, J. A. Hall, D. Chou, L. Dos Santos, S. O'Brien, R. Blank, E. Lamb, S. Natarajan, R. Kastenmayer, C. Hunter, M. E. Grigg, and Y. Belkaid, "Decrease of foxp3+ treg cell number and acquisition of effector cell phenotype during lethal infection," *Immunity*, vol. 31, no. 5, pp. 772–86, 2009.

[69] Y. Zheng, A. Chaudhry, A. Kas, P. deRoos, J. M. Kim, T. T. Chu, L. Corcoran, P. Treuting, U. Klein, and A. Y. Rudensky, "Regulatory t-cell suppressor program co-opts transcription factor irf4 to control t(h)2 responses," *Nature*, vol. 458, no. 7236, pp. 351–6, 2009.

[70] A. Chaudhry, D. Rudra, P. Treuting, R. M. Samstein, Y. Liang, A. Kas, and A. Y. Rudensky, "Cd4+ regulatory t cells control th17 responses in a stat3-dependent manner," *Science*, vol. 326, no. 5955, pp. 986–91, 2009.

[71] C. Benoist and D. Mathis, "Treg cells, life history, and diversity," *Cold Spring Harb Perspect Biol*, vol. 4, no. 9, p. a007021, 2012.

[72] L. A. Huppert, M. D. Green, L. Kim, C. Chow, Y. Leyfman, A. I. Daud, and J. C. Lee, "Tissue-specific tregs in cancer metastasis: opportunities for precision immunotherapy," *Cell Mol Immunol*, vol. 19, no. 1, pp. 33–45, 2022.

[73] A. N. Mathur, B. Zirak, I. C. Boothby, M. Tan, J. N. Cohen, T. M. Mauro, P. Mehta, M. M. Lowe, A. K. Abbas, N. Ali, and M. D. Rosenblum, "Treg-cell control of a cxcl5-il-17 inflammatory axis promotes hair-follicle-stem-cell differentiation during skin-barrier repair," *Immunity*, vol. 50, no. 3, pp. 655–667 e4, 2019.

[74] E. Haertel, N. Joshi, P. Hiebert, M. Kopf, and S. Werner, "Regulatory t cells are required for normal and activin-promoted wound repair in mice," *Eur J Immunol*, vol. 48, no. 6, pp. 1001–1013, 2018.

[75] D. Burzyn, W. Kuswanto, D. Kolodin, J. L. Shadrach, M. Cerletti, Y. Jang, E. Sefik, T. G. Tan, A. J. Wagers, C. Benoist, and D. Mathis, "A special population of regulatory t cells potentiates muscle repair," *Cell*, vol. 155, no. 6, pp. 1282–95, 2013.

[76] G. P. Dunn, L. J. Old, and R. D. Schreiber, "The immunobiology of cancer immunosurveillance and immunoediting," *Immunity*, vol. 21, no. 2, pp. 137–48, 2004.

[77] Z. Shen, S. Zhou, Y. Wang, R. L. Li, C. Zhong, C. Liang, and Y. Sun, "Higher intratumoral infiltrated foxp3+ treg numbers and foxp3+/cd8+ ratio are associated with adverse prognosis in resectable gastric cancer," *J Cancer Res Clin Oncol*, vol. 136, no. 10, pp. 1585–95, 2010.

[78] R. P. Petersen, M. J. Campa, J. Sperlazza, D. Conlon, M. B. Joshi, J. Harpole, D. H., and J. Patz, E. F., "Tumor infiltrating foxp3+ regulatory t-cells are associated with recurrence in pathologic stage i nsclc patients," *Cancer*, vol. 107, no. 12, pp. 2866–72, 2006.

[79] J. Fu, D. Xu, Z. Liu, M. Shi, P. Zhao, B. Fu, Z. Zhang, H. Yang, H. Zhang, C. Zhou, J. Yao, L. Jin, H. Wang, Y. Yang, Y. X. Fu, and F. S. Wang, "Increased regulatory t cells correlate with cd8 t-cell impairment and poor survival in hepatocellular carcinoma patients," *Gastroenterology*, vol. 132, no. 7, pp. 2328–39, 2007.

[80] T. Saito, H. Nishikawa, H. Wada, Y. Nagano, D. Sugiyama, K. Atarashi, Y. Maeda, M. Hamaguchi, N. Ohkura, E. Sato, H. Nagase, J. Nishimura, H. Yamamoto, S. Takiguchi, T. Tanoue, W. Suda, H. Morita, M. Hattori, K. Honda, M. Mori, Y. Doki, and S. Sakaguchi, "Two foxp3(+)cd4(+) t cell subpopulations distinctly control the prognosis of colorectal cancers," *Nat Med*, vol. 22, no. 6, pp. 679–84, 2016.

[81] A. Martens, K. Wistuba-Hamprecht, M. Geukes Foppen, J. Yuan, M. A. Postow, P. Wong, E. Romano, A. Khammari, B. Dreno, M. Capone, P. A. Ascierto, A. M. Di Giacomo, M. Maio, B. Schilling, A. Sucker, D. Schadendorf, J. C. Hassel, T. K. Eigentler, P. Martus, J. D. Wolchok, C. Blank, G. Pawelec, C. Garbe, and B. Weide, "Baseline peripheral blood biomarkers associated with clinical outcome of advanced melanoma patients treated with ipilimumab," *Clin Cancer Res*, vol. 22, no. 12, pp. 2908–18, 2016.

[82] S. P. Wu, R. Q. Liao, H. Y. Tu, W. J. Wang, Z. Y. Dong, S. M. Huang, W. B. Guo, L. Y. Gou, H. W. Sun, Q. Zhang, Z. Xie, L. X. Yan, J. Su, J. J. Yang, W. Z. Zhong, X. C. Zhang, and Y. L. Wu, "Stromal pd-l1-positive regulatory t cells and pd-1-positive cd8-positive t cells define the response of different subsets of non-small cell lung cancer to pd-1/pd-l1 blockade immunotherapy," *J Thorac Oncol*, vol. 13, no. 4, pp. 521–532, 2018.

[83] L. Ren, Y. Yu, L. Wang, Z. Zhu, R. Lu, and Z. Yao, "Hypoxia-induced ccl28 promotes recruitment of regulatory t cells and tumor growth in liver cancer," *Oncotarget*, vol. 7, no. 46, pp. 75763–75773, 2016.

[84] Z. W. Xia, L. Q. Xu, W. W. Zhong, J. J. Wei, N. L. Li, J. Shao, Y. Z. Li, S. C. Yu, and Z. L. Zhang, "Heme oxygenase-1 attenuates ovalbumin-induced airway inflammation by up-regulation of foxp3 t-regulatory cells, interleukin-10, and membrane-bound transforming growth factor- 1," *Am J Pathol*, vol. 171, no. 6, pp. 1904–14, 2007.

[85] D. Hanahan and R. A. Weinberg, "Hallmarks of cancer: the next generation," *Cell*, vol. 144, no. 5, pp. 646–74, 2011.

[86] M. D. Buck, R. T. Sowell, S. M. Kaech, and E. L. Pearce, "Metabolic instruction of immunity," *Cell*, vol. 169, no. 4, pp. 570–586, 2017.

[87] L. Berod, C. Friedrich, A. Nandan, J. Freitag, S. Hagemann, K. Harmrolfs, A. Sandouk, C. Hesse, C. N. Castro, H. Bahre, S. K. Tschirner, N. Gorinski, M. Gohmert, C. T. Mayer, J. Huehn, E. Ponimaskin, W. R. Abraham, R. Muller, M. Lochner, and T. Sparwasser, "De novo fatty acid synthesis controls the fate between regulatory t and t helper 17 cells," *Nat Med*, vol. 20, no. 11, pp. 1327–33, 2014.

[88] A. Angelin, L. Gil-de Gomez, S. Dahiya, J. Jiao, L. Guo, M. H. Levine, Z. Wang, r. Quinn, W. J., P. K. Kopinski, L. Wang, T. Akimova, Y. Liu, T. R. Bhatti, R. Han, B. L. Laskin, J. A. Baur, I. A. Blair, D. C. Wallace, W. W. Hancock, and U. H. Beier, "Foxp3 reprograms t cell metabolism to function in low-glucose, high-lactate environments," *Cell Metab*, vol. 25, no. 6, pp. 1282–1293 e7, 2017.

[89] T. N. Schumacher and R. D. Schreiber, "Neoantigens in cancer immunotherapy," *Science*, vol. 348, no. 6230, pp. 69–74, 2015.

[90] J. Larkin, V. Chiarion-Sileni, R. Gonzalez, J. J. Grob, P. Rutkowski, C. D. Lao, C. L. Cowey, D. Schadendorf, J. Wagstaff, R. Dummer, P. F. Ferrucci, M. Smylie, D. Hogg, A. Hill, I. Marquez-Rodas, J. Haanen, M. Guidoboni, M. Maio, P. Schoffski, M. S. Carlino, C. Lebbe, G. McArthur, P. A. Ascierto, G. A. Daniels, G. V. Long, L. Bastholt, J. I. Rizzo, A. Balogh, A. Moshyk, F. S. Hodi, and J. D. Wolchok, "Five-year survival with combined nivolumab and ipilimumab in advanced melanoma," *N Engl J Med*, vol. 381, no. 16, pp. 1535–1546, 2019.

[91] M. J. Overman, S. Lonardi, K. Y. M. Wong, H. J. Lenz, F. Gelsomino, M. Aglietta, M. A. Morse, E. Van Cutsem, R. McDermott, A. Hill, M. B. Sawyer, A. Hendlisz, B. Neyns, M. Svrcek, R. A. Moss, J. M. Ledeine, Z. A. Cao, S. Kamble, S. Kopetz, and T. Andre, "Durable clinical benefit with nivolumab plus ipilimumab in dna mismatch repair-deficient/microsatellite instability-high metastatic colorectal cancer," *J Clin Oncol*, vol. 36, no. 8, pp. 773–779, 2018.

[92] A. Haslam and V. Prasad, "Estimation of the percentage of us patients with cancer who are eligible for and respond to checkpoint inhibitor immunotherapy drugs," *JAMA Netw Open*, vol. 2, no. 5, p. e192535, 2019.

[93] S. Onizuka, I. Tawara, J. Shimizu, S. Sakaguchi, T. Fujita, and E. Nakayama, "Tumor rejection by in vivo administration of anti-cd25 (interleukin-2 receptor alpha) monoclonal antibody," *Cancer Res*, vol. 59, no. 13, pp. 3128–33, 1999.

[94] T. J. Curiel, G. Coukos, L. Zou, X. Alvarez, P. Cheng, P. Mottram, M. Evdemon-Hogan, J. R. Conejo-Garcia, L. Zhang, M. Burow, Y. Zhu, S. Wei, I. Kryczek, B. Daniel, A. Gordon, L. Myers, A. Lackner, M. L. Disis, K. L. Knutson, L. Chen, and W. Zou, "Specific recruitment of regulatory t cells in ovarian carcinoma fosters immune privilege and predicts reduced survival," *Nat Med*, vol. 10, no. 9, pp. 942–9, 2004.

[95] D. Sugiyama, H. Nishikawa, Y. Maeda, M. Nishioka, A. Tanemura, I. Katayama, S. Ezoe, Y. Kanakura, E. Sato, Y. Fukumori, J. Karbach, E. Jager, and S. Sakaguchi, "Anti-ccr4 mab selectively depletes effector-type foxp3+cd4+ regulatory t cells, evoking antitumor immune responses in humans," *Proc Natl Acad Sci U S A*, vol. 110, no. 44, pp. 17945–50, 2013.

[96] G. L. Beatty, P. J. O'Dwyer, J. Clark, J. G. Shi, K. J. Bowman, P. A. Scherle, R. C. Newton, R. Schaub, J. Maleski, L. Leopold, and T. F. Gajewski, "First-in-human phase i study of the oral inhibitor of indoleamine 2,3-dioxygenase-1 epacadostat (incb024360) in patients with advanced solid malignancies," *Clin Cancer Res*, vol. 23, no. 13, pp. 3269–3276, 2017.

[97] D. H. Munn and A. L. Mellor, "Ido in the tumor microenvironment: Inflammation, counter-regulation, and tolerance," *Trends Immunol*, vol. 37, no. 3, pp. 193–207, 2016.

[98] T. R. Simpson, F. Li, W. Montalvo-Ortiz, M. A. Sepulveda, K. Bergerhoff, F. Arce, C. Roddie, J. Y. Henry, H. Yagita, J. D. Wolchok, K. S. Peggs, J. V. Ravetch, J. P. Allison, and S. A. Quezada, "Fc-dependent depletion of tumor-infiltrating regulatory t cells co-defines the efficacy of anti-ctla-4 therapy against melanoma," *J Exp Med*, vol. 210, no. 9, pp. 1695–710, 2013.

[99] A. Sharma, S. K. Subudhi, J. Blando, L. Vence, J. Wargo, J. P. Allison, A. Ribas, and P. Sharma, "Anti-ctla-4 immunotherapy does not deplete foxp3(+) regulatory t cells (tregs) in human cancers-response," *Clin Cancer Res*, vol. 25, no. 11, pp. 3469–3470, 2019.

[100] A. J. Rech, R. Mick, S. Martin, A. Recio, N. A. Aqui, J. Powell, D. J., T. A. Colligon, J. A. Trosko, L. I. Leinbach, C. H. Pletcher, C. K. Tweed, A. DeMichele, K. R. Fox, S. M. Domchek, J. L. Riley, and R. H. Vonderheide, "Cd25 blockade depletes and selectively reprograms regulatory t cells in concert with immunotherapy in cancer patients," *Sci Transl Med*, vol. 4, no. 134, p. 134ra62, 2012.

[101] K. Mahnke, K. Schonfeld, S. Fondel, S. Ring, S. Karakhanova, K. Wiedemeyer, T. Bedke, T. S. Johnson, V. Storn, S. Schallenberg, and A. H. Enk, "Depletion of cd4+cd25+ human regulatory t cells in vivo: kinetics of treg depletion and alterations in immune functions in vivo and in vitro," *Int J Cancer*, vol. 120, no. 12, pp. 2723–33, 2007.

[102] A. B. Avarbock, A. W. Loren, J. Y. Park, J. M. Junkins-Hopkins, J. Choi, L. A. Litzky, and A. H. Rook, "Lethal vascular leak syndrome after denileukin diftitox administration to a patient with cutaneous gamma/delta t-cell lymphoma and occult cirrhosis," *Am J Hematol*, vol. 83, no. 7, pp. 593–5, 2008.

[103] L. S. Cheung, J. Fu, P. Kumar, A. Kumar, M. E. Urbanowski, E. A. Ihms, S. Parveen, C. K. Bullen, G. J. Patrick, R. Harrison, J. R. Murphy, D. M. Pardoll, and W. R. Bishai, "Second-generation il-2 receptor-targeted diphtheria fusion toxin exhibits anti-tumor activity and synergy with anti-pd-1 in melanoma," *Proc Natl Acad Sci U S A*, vol. 116, no. 8, pp. 3100–3105, 2019.

[104] C. T. Luo and M. O. Li, "Transcriptional control of regulatory t cell development and function," *Trends Immunol*, vol. 34, no. 11, pp. 531–9, 2013.

[105] X. Xie, M. J. Stubbington, J. K. Nissen, K. G. Andersen, D. Hebenstreit, S. A. Teichmann, and A. G. Betz, "The regulatory t cell lineage factor foxp3 regulates gene expression through several distinct mechanisms mostly independent of direct dna binding," *PLoS Genet*, vol. 11, no. 6, p. e1005251, 2015.

[106] C. Devaud, P. K. Darcy, and M. H. Kershaw, "Foxp3 expression in t regulatory cells and other cell lineages," *Cancer Immunol Immunother*, vol. 63, no. 9, pp. 869–76, 2014.

[107] A. Balandina, S. Lecart, P. Dartevelle, A. Saoudi, and S. Berrih-Aknin, "Functional defect of regulatory cd4(+)cd25+ t cells in the thymus of patients with autoimmune myasthenia gravis," *Blood*, vol. 105, no. 2, pp. 735–41, 2005.

[108] Y. Miura, C. J. Thoburn, E. C. Bright, M. L. Phelps, T. Shin, E. C. Matsui, W. H. Matsui, S. Arai, E. J. Fuchs, G. B. Vogelsang, R. J. Jones, and A. D. Hess, "Association of foxp3 regulatory gene expression with graft-versus-host disease," *Blood*, vol. 104, no. 7, pp. 2187–93, 2004.

[109] Y. Y. Wan and R. A. Flavell, "Regulatory t-cell functions are subverted and converted owing to attenuated foxp3 expression," *Nature*, vol. 445, no. 7129, pp. 766–70, 2007.

[110] E. d'Hennezel, K. Bin Dhuban, T. Torgerson, and C. A. Piccirillo, "The immunogenetics of immune dysregulation, polyendocrinopathy, enteropathy, x linked (ipex) syndrome," *J Med Genet*, vol. 49, no. 5, pp. 291–302, 2012.

[111] A. Arvey, J. van der Veeken, G. Plitas, S. S. Rich, P. Concannon, and A. Y. Rudensky, "Genetic and epigenetic variation in the lineage specification of regulatory t cells," *Elife*, vol. 4, p. e07571, 2015.

[112] K. Bolzer, T. Kaser, A. Saalmuller, and S. E. Hammer, "Molecular characterisation of porcine forkhead-box p3 (foxp3)," *Vet Immunol Immunopathol*, vol. 132, no. 2-4, pp. 275–81, 2009.

[113] H. S. Bandukwala, Y. Wu, M. Feuerer, Y. Chen, B. Barboza, S. Ghosh, J. C. Stroud, C. Benoist, D. Mathis, A. Rao, and L. Chen, "Structure of a domain-swapped foxp3 dimer on dna and its function in regulatory t cells," *Immunity*, vol. 34, no. 4, pp. 479–91, 2011.

[114] X. Song, B. Li, Y. Xiao, C. Chen, Q. Wang, Y. Liu, A. Berezov, C. Xu, Y. Gao, Z. Li, S. L. Wu, Z. Cai, H. Zhang, B. L. Karger, W. W. Hancock, A. D. Wells, Z. Zhou, and M. I. Greene, "Structural and biological features of foxp3 dimerization relevant to regulatory t cell function," *Cell Rep*, vol. 1, no. 6, pp. 665–75, 2012.

[115] L. M. Charbonnier, Y. Cui, E. Stephen-Victor, H. Harb, D. Lopez, J. J. Bleesing, M. I. Garcia-Lloret, K. Chen, A. Ozen, P. Carmeliet, M. O. Li, M. Pellegrini, and T. A. Chatila, "Functional reprogramming of regulatory t cells in the absence of foxp3," *Nat Immunol*, vol. 20, no. 9, pp. 1208–1219, 2019.

[116] J. Dannull, Z. Su, D. Rizzieri, B. K. Yang, D. Coleman, D. Yancey, A. Zhang, P. Dahm, N. Chao, E. Gilboa, and J. Vieweg, "Enhancement of vaccine-mediated antitumor immunity in cancer patients after depletion of regulatory t cells," *J Clin Invest*, vol. 115, no. 12, pp. 3623–33, 2005.

[117] K. Lahl, C. Loddenkemper, C. Drouin, J. Freyer, J. Arnason, G. Eberl, A. Hamann, H. Wagner, J. Huehn, and T. Sparwasser, "Selective depletion of foxp3+ regulatory t cells induces a scurfy-like disease," *J Exp Med*, vol. 204, no. 1, pp. 57–63, 2007.

[118] S. Jones and J. M. Thornton, "Principles of protein-protein interactions," *Proc Natl Acad Sci U S A*, vol. 93, no. 1, pp. 13–20, 1996.

[119] S. Miller, "The structure of interfaces between subunits of dimeric and tetrameric proteins," *Protein Eng*, vol. 3, no. 2, pp. 77–83, 1989.

[120] T. A. Larsen, A. J. Olson, and D. S. Goodsell, "Morphology of protein-protein interfaces," *Structure*, vol. 6, no. 4, pp. 421–7, 1998.

[121] D. E. Scott, A. R. Bayly, C. Abell, and J. Skidmore, "Small molecules, big targets: drug discovery faces the protein-protein interaction challenge," *Nat Rev Drug Discov*, vol. 15, no. 8, pp. 533–50, 2016.

[122] T. L. Blundell, B. L. Sibanda, R. W. Montalvao, S. Brewerton, V. Chelliah, C. L. Worth, N. J. Harmer, O. Davies, and D. Burke, "Structural biology and bioinformatics in drug design: opportunities and challenges for target identification and lead discovery," *Philos Trans R Soc Lond B Biol Sci*, vol. 361, no. 1467, pp. 413–23, 2006.

[123] B. Lehner and A. G. Fraser, "A first-draft human protein-interaction map," *Genome Biol*, vol. 5, no. 9, p. R63, 2004.

[124] Q. C. Zhang, D. Petrey, L. Deng, L. Qiang, Y. Shi, C. A. Thu, B. Bisikirska, C. Lefebvre, D. Accili, T. Hunter, T. Maniatis, A. Califano, and B. Honig, "Structure-based prediction of protein-protein interactions on a genome-wide scale," *Nature*, vol. 490, no. 7421, pp. 556–60, 2012.

[125] D. Szklarczyk, A. Franceschini, M. Kuhn, M. Simonovic, A. Roth, P. Minguez, T. Doerks, M. Stark, J. Muller, P. Bork, L. J. Jensen, and C. von Mering, "The string database in 2011: functional interaction networks of proteins, globally integrated and scored," *Nucleic Acids Res*, vol. 39, no. Database issue, pp. D561–8, 2011.

[126] A. P. Higueruelo, A. Schreyer, G. R. Bickerton, W. R. Pitt, C. R. Groom, and T. L. Blundell, "Atomic interactions and profile of small molecules disrupting protein-protein interfaces: the timbal database," *Chem Biol Drug Des*, vol. 74, no. 5, pp. 457–67, 2009.

[127] G. R. Bickerton, A. P. Higueruelo, and T. L. Blundell, "Comprehensive, atomic-level characterization of structurally characterized protein-protein interactions: the piccolo database," *BMC Bioinformatics*, vol. 12, p. 313, 2011.

[128] A. Ciulli, G. Williams, A. G. Smith, T. L. Blundell, and C. Abell, "Probing hot spots at protein-ligand binding sites: a fragment-based approach using biophysical methods," *J Med Chem*, vol. 49, no. 16, pp. 4992–5000, 2006.

[129] P. J. Hajduk and J. Greer, "A decade of fragment-based drug design: strategic advances and lessons learned," *Nat Rev Drug Discov*, vol. 6, no. 3, pp. 211–9, 2007.

[130] M. C. Lo, A. Aulabaugh, G. Jin, R. Cowling, J. Bard, M. Malamas, and G. Ellestad, "Evaluation of fluorescence-based thermal shift assays for hit identification in drug discovery," *Anal Biochem*, vol. 332, no. 1, pp. 153–9, 2004.

[131] I. Navratilova and A. L. Hopkins, "Emerging role of surface plasmon resonance in fragment-based drug discovery," *Future Med Chem*, vol. 3, no. 14, pp. 1809–20, 2011.

[132] T. G. Davies and I. J. Tickle, "Fragment screening using x-ray crystallography," *Top Curr Chem*, vol. 317, pp. 33–59, 2012.

[133] F. Barabe, J. A. Kennedy, K. J. Hope, and J. E. Dick, "Modeling the initiation and progression of human acute leukemia in mice," *Science*, vol. 316, no. 5824, pp. 600–4, 2007.

[134] A. V. Krivtsov, D. Twomey, Z. Feng, M. C. Stubbs, Y. Wang, J. Faber, J. E. Levine, J. Wang, W. C. Hahn, D. G. Gilliland, T. R. Golub, and S. A. Armstrong, "Transformation from committed progenitor to leukaemia stem cell initiated by mll-af9," *Nature*, vol. 442, no. 7104, pp. 818–22, 2006.

[135] Y. H. Kuo, S. F. Landrette, S. A. Heilman, P. N. Perrat, L. Garrett, P. P. Liu, M. M. Le Beau, S. C. Kogan, and L. H. Castilla, "Cbf beta-smmhc induces distinct abnormal myeloid progenitors able to develop acute myeloid leukemia," *Cancer Cell*, vol. 9, no. 1, pp. 57–68, 2006.

[136] R. J. Bell, H. T. Rube, A. Kreig, A. Mancini, S. D. Fouse, R. P. Nagarajan, S. Choi, C. Hong, D. He, M. Pekmezci, J. K. Wiencke, M. R. Wrensch, S. M. Chang, K. M. Walsh, S. Myong, J. S. Song, and J. F. Costello, "Cancer. the transcription factor gabp selectively binds and activates the mutant tert promoter in cancer," *Science*, vol. 348, no. 6238, pp. 1036–9, 2015.

[137] M. M. Makowski, E. Willems, J. Fang, J. Choi, T. Zhang, P. W. Jansen, K. M. Brown, and M. Vermeulen, "An interaction proteomics survey of transcription factor binding at recurrent tert promoter mutations," *Proteomics*, vol. 16, no. 3, pp. 417–26, 2016.

[138] A. Ptasinska, S. A. Assi, D. Mannari, S. R. James, D. Williamson, J. Dunne, M. Hoogenkamp, M. Wu, M. Care, H. McNeill, P. Cauchy, M. Cullen, R. M. Tooze, D. G. Tenen, B. D. Young, P. N. Cockerill, D. R. Westhead, O. Heidenreich, and C. Bonifer, "Depletion of runx1/eto in t(8;21) aml cells leads to genome-wide changes in chromatin structure and transcription factor binding," *Leukemia*, vol. 26, no. 8, pp. 1829–41, 2012.

[139] H. Zhang, L. Liu, Y. Wang, G. Zhao, R. Xie, C. Liu, X. Xiao, K. Wu, Y. Nie, H. Zhang, and D. Fan, "Klf8 involves in tgf-beta-induced emt and promotes invasion and migration in gastric cancer cells," *J Cancer Res Clin Oncol*, vol. 139, no. 6, pp. 1033–42, 2013.

[140] D. S. Micalizzi, K. L. Christensen, P. Jedlicka, R. D. Coletta, A. E. Baron, J. C. Harrell, K. B. Horwitz, D. Billheimer, K. A. Heichman, A. L. Welm, W. P. Schiemann, and H. L. Ford, "The six1 homeoprotein induces human mammary carcinoma cells to undergo epithelial-mesenchymal transition and metastasis in mice through increasing tgf-beta signaling," *J Clin Invest*, vol. 119, no. 9, pp. 2678–90, 2009.

[141] H. de The, P. P. Pandolfi, and Z. Chen, "Acute promyelocytic leukemia: A paradigm for oncoprotein-targeted cure," *Cancer Cell*, vol. 32, no. 5, pp. 552–560, 2017.

[142] S. Matkar, P. Sharma, S. Gao, B. Gurung, B. W. Katona, J. Liao, A. B. Muhammad, X. C. Kong, L. Wang, G. Jin, C. V. Dang, and X. Hua, "An epigenetic pathway regulates sensitivity of breast cancer cells to her2 inhibition via foxo/c-myc axis," *Cancer Cell*, vol. 28, no. 4, pp. 472–485, 2015.

[143] T. Hirade, M. Abe, C. Onishi, T. Taketani, S. Yamaguchi, and S. Fukuda, "Internal tandem duplication of flt3 deregulates proliferation and differentiation and confers resistance to the flt3 inhibitor ac220 by up-regulating runx1 expression in hematopoietic cells," *Int J Hematol*, vol. 103, no. 1, pp. 95–106, 2016.

[144] T. Sanda, L. N. Lawton, M. I. Barrasa, Z. P. Fan, H. Kohlhammer, A. Gutierrez, W. Ma, J. Tatarek, Y. Ahn, M. A. Kelliher, C. H. Jamieson, L. M. Staudt, R. A. Young, and A. T. Look, "Core transcriptional regulatory circuit controlled by the tal1 complex in human t cell acute lymphoblastic leukemia," *Cancer Cell*, vol. 22, no. 2, pp. 209–21, 2012.

[145] K. Morita, M. Noura, C. Tokushige, S. Maeda, H. Kiyose, G. Kashiwazaki, J. Taniguchi, T. Bando, K. Yoshida, T. Ozaki, H. Matsuo, S. Ogawa, P. P. Liu, T. Nakahata, H. Sugiyama, S. Adachi, and Y. Kamikubo, "Autonomous feedback loop of runx1-p53-cbfb in acute myeloid leukemia cells," *Sci Rep*, vol. 7, no. 1, p. 16604, 2017.

[146] K. Rakhra, P. Bachireddy, T. Zabuawala, R. Zeiser, L. Xu, A. Kopelman, A. C. Fan, Q. Yang, L. Braunstein, E. Crosby, S. Ryeom, and D. W. Felsher, "Cd4(+) t cells contribute to the remodeling of the microenvironment required for sustained tumor regression upon oncogene inactivation," *Cancer Cell*, vol. 18, no. 5, pp. 485–98, 2010.

[147] M. Cerezo, R. Guemiri, S. Druillennec, I. Girault, H. Malka-Mahieu, S. Shen, D. Allard, S. Martineau, C. Welsch, S. Agoussi, C. Estrada, J. Adam, C. Libenciuc, E. Routier, S. Roy, L. Desaubry, A. M. Eggermont, N. Sonenberg, J. Y. Scoazec, A. Eychene, S. Vagner, and C. Robert, "Translational control of tumor immune escape via the eif4f-stat1-pd-l1 axis in melanoma," *Nat Med*, vol. 24, no. 12, pp. 1877–1886, 2018.

[148] A. T. Look, "Oncogenic transcription factors in the human acute leukemias," *Science*, vol. 278, no. 5340, pp. 1059–64, 1997.

[149] C. J. Scheitz, T. S. Lee, D. J. McDermitt, and T. Tumbar, "Defining a tissue stem cell-driven runx1/stat3 signalling axis in epithelial cancer," *EMBO J*, vol. 31, no. 21, pp. 4124–39, 2012.

[150] J. Jane-Valbuena, H. R. Widlund, S. Perner, L. A. Johnson, A. C. Dibner, W. M. Lin, A. C. Baker, R. M. Nazarian, K. G. Vijayendran, W. R. Sellers, W. C. Hahn, L. M. Duncan, M. A. Rubin, D. E. Fisher, and L. A. Garraway, "An oncogenic role for etv1 in melanoma," *Cancer Res*, vol. 70, no. 5, pp. 2075–84, 2010.

[151] S. A. Tomlins, A. Bjartell, A. M. Chinnaiyan, G. Jenster, R. K. Nam, M. A. Rubin, and J. A. Schalken, "Ets gene fusions in prostate cancer: from discovery to daily clinical practice," *Eur Urol*, vol. 56, no. 2, pp. 275–86, 2009.

[152] M. J. Henley and A. N. Koehler, "Advances in targeting 'undruggable' transcription factors with small molecules," *Nat Rev Drug Discov*, vol. 20, no. 9, pp. 669–688, 2021.

[153] A. K. Mapp, R. Pricer, and S. Sturlis, "Targeting transcription is no longer a quixotic quest," *Nat Chem Biol*, vol. 11, no. 12, pp. 891–4, 2015.

[154] F. Fontaine, J. Overman, and M. Francois, "Pharmacological manipulation of transcription factor protein-protein interactions: opportunities and obstacles," *Cell Regen*, vol. 4, no. 1, p. 2, 2015.

[155] L. Caboni and D. G. Lloyd, "Beyond the ligand-binding pocket: targeting alternate sites in nuclear receptors," *Med Res Rev*, vol. 33, no. 5, pp. 1081–118, 2013.

[156] T. P. Burris, L. A. Solt, Y. Wang, C. Crumbley, S. Banerjee, K. Griffett, T. Lundasen, T. Hughes, and D. J. Kojetin, "Nuclear receptors and their selective pharmacologic modulators," *Pharmacol Rev*, vol. 65, no. 2, pp. 710–78, 2013.

[157] H. de The, "Differentiation therapy revisited," *Nat Rev Cancer*, vol. 18, no. 2, pp. 117–127, 2018.

[158] P. B. Dervan, "Molecular recognition of dna by small molecules," *Bioorg Med Chem*, vol. 9, no. 9, pp. 2215–35, 2001.

[159] G. P. Mognol, E. Gonzalez-Avalos, S. Ghosh, R. Spreafico, A. Gudlur, A. Rao, R. Damoiseaux, and P. G. Hogan, "Targeting the nfat:ap-1 transcriptional complex on dna with a small-molecule inhibitor," *Proc Natl Acad Sci U S A*, vol. 116, no. 20, pp. 9959–9968, 2019.

[160] F. Geng, S. Wenzel, and W. P. Tansey, "Ubiquitin and proteasomes in transcription," *Annu Rev Biochem*, vol. 81, pp. 177–201, 2012.

[161] S. Venkatachalam, Y. P. Shi, S. N. Jones, H. Vogel, A. Bradley, D. Pinkel, and L. A. Donehower, "Retention of wild-type p53 in tumors from p53 heterozygous mice: reduction of p53 dosage can promote cancer formation," *EMBO J*, vol. 17, no. 16, pp. 4657–67, 1998.

[162] Y. Xie, M. L. Koch, X. Zhang, M. J. Hamblen, F. J. Godinho, Y. Fujiwara, H. Xie, J. H. Klusmann, S. H. Orkin, and Z. Li, "Reduced erg dosage impairs survival of hematopoietic stem and progenitor cells," *Stem Cells*, vol. 35, no. 7, pp. 1773–1785, 2017.

[163] X. Xu, S. G. Brodie, X. Yang, Y. H. Im, W. T. Parks, L. Chen, Y. X. Zhou, M. Weinstein, S. J. Kim, and C. X. Deng, "Haploid loss of the tumor suppressor smad4/dpc4 initiates gastric polyposis and cancer in mice," *Oncogene*, vol. 19, no. 15, pp. 1868–74, 2000.

[164] G. Lu, R. E. Middleton, H. Sun, M. Naniong, C. J. Ott, C. S. Mitsiades, K. K. Wong, J. E. Bradner, and J. Kaelin, W. G., "The myeloma drug lenalidomide promotes the cereblon-dependent destruction of ikaros proteins," *Science*, vol. 343, no. 6168, pp. 305–9, 2014.

[165] A. C. Lai, M. Toure, D. Hellerschmied, J. Salami, S. Jaime-Figueroa, E. Ko, J. Hines, and C. M. Crews, "Modular protac design for the degradation of oncogenic bcr-abl," *Angew Chem Int Ed Engl*, vol. 55, no. 2, pp. 807–10, 2016.

[166] D. P. Bondeson, A. Mares, I. E. Smith, E. Ko, S. Campos, A. H. Miah, K. E. Mulholland, N. Routly, D. L. Buckley, J. L. Gustafson, N. Zinn, P. Grandi, S. Shimamura, G. Bergamini, M. Faelth-Savitski, M. Bantscheff, C. Cox, D. A. Gordon, R. R. Willard, J. J. Flanagan, L. N. Casillas, B. J. Votta, W. den Besten, K. Famm, L. Kruidenier, P. S. Carter, J. D. Harling, I. Churcher, and C. M. Crews, "Catalytic in vivo protein knockdown by small-molecule protacs," *Nat Chem Biol*, vol. 11, no. 8, pp. 611–7, 2015.

[167] G. E. Winter, D. L. Buckley, J. Paulk, J. M. Roberts, A. Souza, S. Dhe-Paganon, and J. E. Bradner, "Drug development. phthalimide conjugation as a strategy for in vivo target protein degradation," *Science*, vol. 348, no. 6241, pp. 1376–81, 2015.

[168] H. Lu, Q. Zhou, J. He, Z. Jiang, C. Peng, R. Tong, and J. Shi, "Recent advances in the development of protein-protein interactions modulators: mechanisms and clinical trials," *Signal Transduct Target Ther*, vol. 5, no. 1, p. 213, 2020.

[169] J. H. Bushweller, "Targeting transcription factors in cancer - from undruggable to reality," *Nat Rev Cancer*, vol. 19, no. 11, pp. 611–624, 2019.

[170] P. Buchwald, "Small-molecule protein-protein interaction inhibitors: therapeutic potential in light of molecular size, chemical space, and ligand binding efficiency considerations," *IUBMB Life*, vol. 62, no. 10, pp. 724–31, 2010.

[171] M. C. Smith and J. E. Gestwicki, "Features of protein-protein interactions that translate into potent inhibitors: topology, surface area and affinity," *Expert Rev Mol Med*, vol. 14, p. e16, 2012.

[172] P. Chakrabarti and J. Janin, "Dissecting protein-protein recognition sites," *Proteins*, vol. 47, no. 3, pp. 334–43, 2002.

[173] A. A. Ivanov, F. R. Khuri, and H. Fu, "Targeting protein-protein interactions as an anticancer strategy," *Trends Pharmacol Sci*, vol. 34, no. 7, pp. 393–400, 2013.

[174] A. C. Cheng, R. G. Coleman, K. T. Smyth, Q. Cao, P. Soulard, D. R. Caffrey, A. C. Salzberg, and E. S. Huang, "Structure-based maximal affinity model predicts small-molecule druggability," *Nat Biotechnol*, vol. 25, no. 1, pp. 71–5, 2007.

[175] M. J. de Vega, M. Martin-Martinez, and R. Gonzalez-Muniz, "Modulation of protein-protein interactions by stabilizing/mimicking protein secondary structure elements," *Curr Top Med Chem*, vol. 7, no. 1, pp. 33–62, 2007.

[176] I. S. Moreira, P. A. Fernandes, and M. J. Ramos, "Hot spots–a review of the protein-protein interface determinant amino-acid residues," *Proteins*, vol. 68, no. 4, pp. 803–12, 2007.

[177] T. Clackson and J. A. Wells, "A hot spot of binding energy in a hormone-receptor interface," *Science*, vol. 267, no. 5196, pp. 383–6, 1995.

[178] A. A. Bogan and K. S. Thorn, "Anatomy of hot spots in protein interfaces," *J Mol Biol*, vol. 280, no. 1, pp. 1–9, 1998.

[179] O. Keskin, B. Ma, and R. Nussinov, "Hot regions in protein–protein interactions: the organization and contribution of structurally conserved hot spot residues," *J Mol Biol*, vol. 345, no. 5, pp. 1281–94, 2005.

[180] M. Moiola, M. G. Memeo, and P. Quadrelli, "Stapled peptides-a useful improvement for peptide-based drugs," *Molecules*, vol. 24, no. 20, 2019.

[181] G. H. Bird, E. Gavathiotis, J. L. LaBelle, S. G. Katz, and L. D. Walensky, "Distinct bimbh3 (bimsahb) stapled peptides for structural and cellular studies," *ACS Chem Biol*, vol. 9, no. 3, pp. 831–7, 2014.

[182] P. Wojcik and L. Berlicki, "Peptide-based inhibitors of protein-protein interactions," *Bioorg Med Chem Lett*, vol. 26, no. 3, pp. 707–713, 2016.

[183] J. L. LaBelle, S. G. Katz, G. H. Bird, E. Gavathiotis, M. L. Stewart, C. Lawrence, J. K. Fisher, M. Godes, K. Pitter, A. L. Kung, and L. D. Walensky, "A stapled bim peptide overcomes apoptotic resistance in hematologic cancers," *J Clin Invest*, vol. 122, no. 6, pp. 2018–31, 2012.

[184] G. H. Bird, N. Madani, A. F. Perry, A. M. Princiotto, J. G. Supko, X. He, E. Gavathiotis, J. G. Sodroski, and L. D. Walensky, "Hydrocarbon double-stapling remedies the proteolytic instability of a lengthy peptide therapeutic," *Proc Natl Acad Sci U S A*, vol. 107, no. 32, pp. 14093–8, 2010.

[185] A. Hadji, G. K. Schmitt, M. R. Schnorenberg, L. Roach, C. M. Hickey, L. B. Leak, M. V. Tirrell, and J. L. LaBelle, "Preferential targeting of mcl-1 by a hydrocarbon-stapled bim bh3 peptide," *Oncotarget*, vol. 10, no. 58, pp. 6219–6233, 2019.

[186] R. E. Moellering, M. Cornejo, T. N. Davis, C. Del Bianco, J. C. Aster, S. C. Blacklow, A. L. Kung, D. G. Gilliland, G. L. Verdine, and J. E. Bradner, "Direct inhibition of the notch transcription factor complex," *Nature*, vol. 462, no. 7270, pp. 182–8, 2009.

[187] J. A. Kritzer, "Stapled peptides: Magic bullets in nature's arsenal," *Nat Chem Biol*, vol. 6, no. 8, pp. 566–7, 2010.

[188] J. L. Yap, H. Wang, A. Hu, J. Chauhan, K. Y. Jung, R. B. Gharavi, E. V. Prochownik, and S. Fletcher, "Pharmacophore identification of c-myc inhibitor 10074-g5," *Bioorg Med Chem Lett*, vol. 23, no. 1, pp. 370–4, 2013.

[189] H. Yin, G. I. Lee, K. A. Sedey, O. Kutzki, H. S. Park, B. P. Orner, J. T. Ernst, H. G. Wang, S. M. Sebti, and A. D. Hamilton, "Terphenyl-based bak bh3 alpha-helical proteomimetics as low-molecular-weight antagonists of bcl-xl," *J Am Chem Soc*, vol. 127, no. 29, pp. 10191–6, 2005.

[190] F. Bernal, A. F. Tyler, S. J. Korsmeyer, L. D. Walensky, and G. L. Verdine, "Reactivation of the p53 tumor suppressor pathway by a stapled p53 peptide," *J Am Chem Soc*, vol. 129, no. 9, pp. 2456–7, 2007.

[191] A. L. Jochim and P. S. Arora, "Systematic analysis of helical protein interfaces reveals targets for synthetic inhibitors," *ACS Chem Biol*, vol. 5, no. 10, pp. 919–23, 2010.

[192] L. D. Walensky, A. L. Kung, I. Escher, T. J. Malia, S. Barbuto, R. D. Wright, G. Wagner, G. L. Verdine, and S. J. Korsmeyer, "Activation of apoptosis in vivo by a hydrocarbon-stapled bh3 helix," *Science*, vol. 305, no. 5689, pp. 1466–70, 2004.

[193] L. A. Carvajal, D. B. Neriah, A. Senecal, L. Benard, V. Thiruthuvanathan, T. Yatsenko, S. R. Narayanagari, J. C. Wheat, T. I. Todorova, K. Mitchell, C. Kenworthy, V. Guerlavais, D. A. Annis, B. Bartholdy, B. Will, J. D. Anampa, I. Mantzaris, M. Aivado, R. H. Singer, R. A. Coleman, A. Verma, and U. Steidl, "Dual inhibition of mdmx and mdm2 as a therapeutic strategy in leukemia," *Sci Transl Med*, vol. 10, no. 436, 2018.

[194] M. J. Reilley, A. Bailey, V. Subbiah, F. Janku, A. Naing, G. Falchook, D. Karp, S. Piha-Paul, A. Tsimberidou, S. Fu, J. Lim, S. Bean, A. Bass, S. Montez, L. Vence, P. Sharma, J. Allison, F. Meric-Bernstam, and D. S. Hong, "Phase i clinical trial of combination imatinib and ipilimumab in patients with advanced malignancies," *J Immunother Cancer*, vol. 5, p. 35, 2017.

[195] M. R. Schnorenberg, J. A. Bellairs, R. Samaeekia, H. Acar, M. V. Tirrell, and J. L. LaBelle, "Activating the intrinsic pathway of apoptosis using bim bh3 peptides delivered by peptide amphiphiles with endosomal release," *Materials (Basel)*, vol. 12, no. 16, 2019.

[196] K. P. Koh, M. S. Sundrud, and A. Rao, "Domain requirements and sequence specificity of dna binding for the forkhead transcription factor foxp3," *PLoS One*, vol. 4, no. 12, p. e8109, 2009.

[197] W. J. Chae, O. Henegariu, S. K. Lee, and A. L. Bothwell, "The mutant leucine-zipper domain impairs both dimerization and suppressive function of foxp3 in t cells," *Proc Natl Acad Sci U S A*, vol. 103, no. 25, pp. 9631–6, 2006.

[198] B. Li, A. Samanta, X. Song, K. Furuuchi, K. T. Iacono, S. Kennedy, M. Katsumata, S. J. Saouaf, and M. I. Greene, "Foxp3 ensembles in t-cell regulation," *Immunol Rev*, vol. 212, pp. 99–113, 2006.

[199] C. Reynolds, D. Damerell, and S. Jones, "Protorp: a protein-protein interaction analysis server," *Bioinformatics*, vol. 25, no. 3, pp. 413–4, 2009.

[200] Y. H. Lau, P. de Andrade, Y. Wu, and D. R. Spring, "Peptide stapling techniques based on different macrocyclisation chemistries," *Chem Soc Rev*, vol. 44, no. 1, pp. 91–102, 2015.

[201] N. J. Greenfield, "Using circular dichroism spectra to estimate protein secondary structure," *Nat Protoc*, vol. 1, no. 6, pp. 2876–90, 2006.

[202] A. L. Edwards, D. H. Meijer, R. M. Guerra, R. J. Molenaar, J. A. Alberta, F. Bernal, G. H. Bird, C. D. Stiles, and L. D. Walensky, "Challenges in targeting a basic helix-loop-helix transcription factor with hydrocarbon-stapled peptides," *ACS Chem Biol*, vol. 11, no. 11, pp. 3146–3153, 2016.

[203] N. J. Greenfield, G. V. Swapna, Y. Huang, T. Palm, S. Graboski, G. T. Montelione, and S. E. Hitchcock-DeGregori, "The structure of the carboxyl terminus of striated alpha-tropomyosin in solution reveals an unusual parallel arrangement of interacting alpha-helices," *Biochemistry*, vol. 42, no. 3, pp. 614–9, 2003.

[204] A. Singh and S. E. Hitchcock-DeGregori, "Dual requirement for flexibility and specificity for binding of the coiled-coil tropomyosin to its target, actin," *Structure*, vol. 14, no. 1, pp. 43–50, 2006.

[205] L. Truebestein and T. A. Leonard, "Coiled-coils: The long and short of it," *Bioessays*, vol. 38, no. 9, pp. 903–16, 2016.

[206] G. H. Bird, E. Mazzola, K. Opoku-Nsiah, M. A. Lammert, M. Godes, D. S. Neuberg, and L. D. Walensky, "Biophysical determinants for cellular uptake of hydrocarbon-stapled peptide helices," *Nat Chem Biol*, vol. 12, no. 10, pp. 845–52, 2016.

[207] L. D. Walensky and G. H. Bird, "Hydrocarbon-stapled peptides: principles, practice, and progress," *J Med Chem*, vol. 57, no. 15, pp. 6275–88, 2014.

[208] A. D. Bautista, J. S. Appelbaum, C. J. Craig, J. Michel, and A. Schepartz, "Bridged beta(3)-peptide inhibitors of p53-hdm2 complexation: correlation between affinity and cell permeability," *J Am Chem Soc*, vol. 132, no. 9, pp. 2904–6, 2010.

[209] W. W. Hancock and E. Ozkaynak, "Three distinct domains contribute to nuclear transport of murine foxp3," *PLoS One*, vol. 4, no. 11, p. e7890, 2009.

[210] F. Birzele, T. Fauti, H. Stahl, M. C. Lenter, E. Simon, D. Knebel, A. Weith, T. Hildebrandt, and D. Mennerich, "Next-generation insights into regulatory t cells: expression profiling and foxp3 occupancy in human," *Nucleic Acids Res*, vol. 39, no. 18, pp. 7946–60, 2011.

[211] A. Marson, K. Kretschmer, G. M. Frampton, E. S. Jacobsen, J. K. Polansky, K. D. MacIsaac, S. S. Levine, E. Fraenkel, H. von Boehmer, and R. A. Young, "Foxp3 occupancy and regulation of key target genes during t-cell stimulation," *Nature*, vol. 445, no. 7130, pp. 931–5, 2007.

[212] J. A. Hill, M. Feuerer, K. Tash, S. Haxhinasto, J. Perez, R. Melamed, D. Mathis, and C. Benoist, "Foxp3 transcription-factor-dependent and -independent regulation of the regulatory t cell transcriptional signature," *Immunity*, vol. 27, no. 5, pp. 786–800, 2007.

[213] A. W. Goldrath, C. J. Luckey, R. Park, C. Benoist, and D. Mathis, "The molecular program induced in t cells undergoing homeostatic proliferation," *Proc Natl Acad Sci U S A*, vol. 101, no. 48, pp. 16885–90, 2004.

[214] B. J. Chen, J. W. Zhao, D. H. Zhang, A. H. Zheng, and G. Q. Wu, "Immunotherapy of cancer by targeting regulatory t cells," *Int Immunopharmacol*, vol. 104, p. 108469, 2022.

[215] Y. Xiao, B. Li, Z. Zhou, W. W. Hancock, H. Zhang, and M. I. Greene, "Histone acetyltransferase mediated regulation of foxp3 acetylation and treg function," *Curr Opin Immunol*, vol. 22, no. 5, pp. 583–91, 2010.

[216] D. Rudra, P. deRoos, A. Chaudhry, R. E. Niec, A. Arvey, R. M. Samstein, C. Leslie, S. A. Shaffer, D. R. Goodlett, and A. Y. Rudensky, "Transcription factor foxp3 and its protein partners form a complex regulatory network," *Nat Immunol*, vol. 13, no. 10, pp. 1010–9, 2012.

[217] T. Lozano, L. Villanueva, M. Durantez, M. Gorraiz, M. Ruiz, V. Belsue, J. I. Riezu-Boj, S. Hervas-Stubbs, J. Oyarzabal, H. Bandukwala, A. R. Lourenco, P. J. Coffer, P. Sarobe, J. Prieto, N. Casares, and J. J. Lasarte, "Inhibition of foxp3/nfat interaction enhances t cell function after tcr stimulation," *J Immunol*, vol. 195, no. 7, pp. 3180–9, 2015.

[218] N. Casares, F. Rudilla, L. Arribillaga, D. Llopiz, J. I. Riezu-Boj, T. Lozano, J. Lopez-Sagaseta, L. Guembe, P. Sarobe, J. Prieto, F. Borras-Cuesta, and J. J. Lasarte, "A peptide inhibitor of foxp3 impairs regulatory t cell activity and improves vaccine efficacy in mice," *J Immunol*, vol. 185, no. 9, pp. 5150–9, 2010.

[219] T. Lozano, M. Gorraiz, A. Lasarte-Cia, M. Ruiz, O. Rabal, J. Oyarzabal, S. Hervas-Stubbs, D. Llopiz, P. Sarobe, J. Prieto, N. Casares, and J. J. Lasarte, "Blockage of foxp3 transcription factor dimerization and foxp3/aml1 interaction inhibits t regulatory cell activity: sequence optimization of a peptide inhibitor," *Oncotarget*, vol. 8, no. 42, pp. 71709–71724, 2017.

[220] F. Bernal, M. Wade, M. Godes, T. N. Davis, D. G. Whitehead, A. L. Kung, G. M. Wahl, and L. D. Walensky, "A stapled p53 helix overcomes hdmx-mediated suppression of p53," *Cancer Cell*, vol. 18, no. 5, pp. 411–22, 2010.

[221] Y. S. Chang, B. Graves, V. Guerlavais, C. Tovar, K. Packman, K. H. To, K. A. Olson, K. Kesavan, P. Gangurde, A. Mukherjee, T. Baker, K. Darlak, C. Elkin, Z. Filipovic, F. Z. Qureshi, H. Cai, P. Berry, E. Feyfant, X. E. Shi, J. Horstick, D. A. Annis, A. M. Manning, N. Fotouhi, H. Nash, L. T. Vassilev, and T. K. Sawyer, "Stapled alpha-helical peptide drug development: a potent dual inhibitor of mdm2 and mdmx for p53-dependent cancer therapy," *Proc Natl Acad Sci U S A*, vol. 110, no. 36, pp. E3445–54, 2013.

[222] M. Green and P. M. Loewenstein, "Autonomous functional domains of chemically synthesized human immunodeficiency virus tat trans-activator protein," *Cell*, vol. 55, no. 6, pp. 1179–88, 1988.

[223] A. D. Frankel and C. O. Pabo, "Cellular uptake of the tat protein from human immunodeficiency virus," *Cell*, vol. 55, no. 6, pp. 1189–93, 1988.

[224] C. Konopacki, Y. Pritykin, Y. Rubtsov, C. S. Leslie, and A. Y. Rudensky, "Transcription factor foxp1 regulates foxp3 chromatin binding and coordinates regulatory t cell function," *Nat Immunol*, vol. 20, no. 2, pp. 232–242, 2019.

[225] Y. Wu, M. Borde, V. Heissmeyer, M. Feuerer, A. D. Lapan, J. C. Stroud, D. L. Bates, L. Guo, A. Han, S. F. Ziegler, D. Mathis, C. Benoist, L. Chen, and A. Rao, "Foxp3 controls regulatory t cell function through cooperation with nfat," *Cell*, vol. 126, no. 2, pp. 375–87, 2006.

[226] N. Sugaya and T. Furuya, "Dr. pias: an integrative system for assessing the druggability of protein-protein interactions," *BMC Bioinformatics*, vol. 12, p. 50, 2011.

[227] L. M. Meireles, A. S. Domling, and C. J. Camacho, "Anchor: a web server and database for analysis of protein-protein interaction binding pockets for drug discovery," *Nucleic Acids Res*, vol. 38, no. Web Server issue, pp. W407–11, 2010.

[228] J. C. Fuller, N. J. Burgoyne, and R. M. Jackson, "Predicting druggable binding sites at the protein-protein interface," *Drug Discov Today*, vol. 14, no. 3-4, pp. 155–61, 2009.

[229] F. Falchi, F. Caporuscio, and M. Recanatini, "Structure-based design of small-molecule protein-protein interaction modulators: the story so far," *Future Med Chem*, vol. 6, no. 3, pp. 343–57, 2014.

[230] N. Sawyer, A. M. Watkins, and P. S. Arora, "Protein domain mimics as modulators of protein-protein interactions," *Acc Chem Res*, vol. 50, no. 6, pp. 1313–1322, 2017.

[231] R. J. Bienstock, "Computational drug design targeting protein-protein interactions," *Curr Pharm Des*, vol. 18, no. 9, pp. 1240–54, 2012.

[232] P. J. Hajduk, J. R. Huth, and S. W. Fesik, "Druggability indices for protein targets derived from nmr-based screening data," *J Med Chem*, vol. 48, no. 7, pp. 2518–25, 2005.

[233] W. Tan, W. Zhang, A. Strasner, S. Grivennikov, J. Q. Cheng, R. M. Hoffman, and M. Karin, "Tumour-infiltrating regulatory t cells stimulate mammary cancer metastasis through rankl-rank signalling," *Nature*, vol. 470, no. 7335, pp. 548–53, 2011.

[234] Y. Zhang, J. Lazarus, N. G. Steele, W. Yan, H. J. Lee, Z. C. Nwosu, C. J. Halbrook, R. E. Menjivar, S. B. Kemp, V. R. Sirihorachai, A. Velez-Delgado, K. Donahue, E. S. Carpenter, K. L. Brown, V. Irizarry-Negron, A. C. Nevison, A. Vinta, M. A. Anderson, H. C. Crawford, C. A. Lyssiotis, T. L. Frankel, F. Bednar, and M. Pasca di Magliano, "Regulatory t-cell depletion alters the tumor microenvironment and accelerates pancreatic carcinogenesis," *Cancer Discov*, vol. 10, no. 3, pp. 422–439, 2020.

[235] S. Kato, A. Goodman, V. Walavalkar, D. A. Barkauskas, A. Sharabi, and R. Kurzrock, "Hyperprogressors after immunotherapy: Analysis of genomic alterations associated with accelerated growth rate," *Clin Cancer Res*, vol. 23, no. 15, pp. 4242–4250, 2017.

[236] D. Coe, S. Begom, C. Addey, M. White, J. Dyson, and J. G. Chai, "Depletion of regulatory t cells by anti-gitr mab as a novel mechanism for cancer immunotherapy," *Cancer Immunol Immunother*, vol. 59, no. 9, pp. 1367–77, 2010.

[237] A. J. Furness, F. A. Vargas, K. S. Peggs, and S. A. Quezada, "Impact of tumour microenvironment and fc receptors on the activity of immunomodulatory antibodies," *Trends Immunol*, vol. 35, no. 7, pp. 290–8, 2014.

[238] J. R. Campbell, B. R. McDonald, P. B. Mesko, N. O. Siemers, P. B. Singh, M. Selby, T. W. Sproul, A. J. Korman, L. M. Vlach, J. Houser, S. Sambanthamoorthy, K. Lu, S. V. Hatcher, J. Lohre, R. Jain, and R. Y. Lan, "Fc-optimized anti-ccr8 antibody depletes regulatory t cells in human tumor models," *Cancer Res*, vol. 81, no. 11, pp. 2983–2994, 2021.

[239] J. M. Kim, J. P. Rasmussen, and A. Y. Rudensky, "Regulatory t cells prevent catastrophic autoimmunity throughout the lifespan of mice," *Nat Immunol*, vol. 8, no. 2, pp. 191–7, 2007.

[240] A. J. Oliver, S. P. Keam, B. von Scheidt, D. J. Zanker, A. J. Harrison, D. G. Tantalo, P. K. Darcy, M. H. Kershaw, and C. Y. Slaney, "Primary and metastatic breast tumors cross-talk to influence immunotherapy responses," *Oncoimmunology*, vol. 9, no. 1, p. 1802979, 2020.

[241] J. C. Lee, S. Mehdizadeh, J. Smith, A. Young, I. A. Mufazalov, C. T. Mowery, A. Daud, and J. A. Bluestone, "Regulatory t cell control of systemic immunity and immunotherapy response in liver metastasis," *Sci Immunol*, vol. 5, no. 52, 2020.

[242] E. C. Halvorsen, S. M. Mahmoud, and K. L. Bennewith, "Emerging roles of regulatory t cells in tumour progression and metastasis," *Cancer Metastasis Rev*, vol. 33, no. 4, pp. 1025–41, 2014.